

Rochester Institute of Technology

RIT Digital Institutional Repository

Theses

4-26-2019

Multiscale Fluid-Structure Interaction Models Development and Applications to the 3D Elements of a Human Cardiovascular System

Yogesh Karnam
yk2359@rit.edu

Follow this and additional works at: <https://repository.rit.edu/theses>

Recommended Citation

Karnam, Yogesh, "Multiscale Fluid-Structure Interaction Models Development and Applications to the 3D Elements of a Human Cardiovascular System" (2019). Thesis. Rochester Institute of Technology. Accessed from

This Thesis is brought to you for free and open access by the RIT Libraries. For more information, please contact repository@rit.edu.

Multiscale Fluid-Structure Interaction Models Development and Applications to the 3D Elements of a Human Cardiovascular System

Submitted by

Yogesh Karnam

A Thesis Presented in Partial Fulfillment of the Requirements for
the Degree of *Master of Science in Mechanical Engineering*

Approved by:

Dr. Alexander Liberson

Department of Mechanical Engineering

(Thesis Advisor)

Dr. Hany Ghoneim

Department of Mechanical Engineering

(Committee Member)

Dr. Ali Ogut

Department of Mechanical Engineering

(Committee Member)

Dr. Michael Schrlau

Department of Mechanical Engineering

(Department Representative)

Rochester Institute of Technology
Kate Gleason College of Engineering
Department of Mechanical Engineering

Rochester, NY

April 26, 2019

Abstract

Cardiovascular diseases (CVD) are the number one cause of death of humans in the United States and worldwide. Accurate, non-invasive, and cheaper diagnosis methods have always been on demand as cardiovascular monitoring increase in prevalence. The primary causes of the various forms of these CVDs are atherosclerosis and aneurysms in the blood vessels. Current noninvasive methods (i.e., statistical/medical) permit fairly accurate detection of the disease once clinical symptoms are suggestive of the existence of hemodynamic disorders. Therefore, the recent surge of hemodynamics models facilitated the prediction of cardiovascular conditions.

The hemodynamic modeling of a human circulatory system involves varying levels of complexity which must be accounted for and resolved. Pulse-wave propagation effects and high aspect-ratio segments of the vasculature are represented using a quasi-one-dimensional (1D), non-steady, averaged over the cross-section models. However, these reduced 1D models do not account for the blood flow patterns (recirculation zones), vessel wall shear stresses and quantification of repetitive mechanical stresses which helps to predict a vessel life. Even a whole three-dimensional (3D) modeling of the vasculature is computationally intensive and do not fit the timeline of practical use. Thus the intertwining of a quasi 1D global vasculature model with a specific/risk-prone 3D local vessel ones is imperative.

This research forms part of a multiphysics project that aims to improve the detailed understanding of the hemodynamics by investigating a computational model of fluid-structure interaction (FSI) of in vivo blood flow. First idealized computational a 3D FSI artery model is configured and executed in ANSYS Workbench, forming an implicit coupling of the blood flow and vessel walls. Then the thesis focuses on an approach developed to employ commercial tools rather than in-house mathematical models in achieving multiscale simulations. A robust algorithm is constructed to combine stabilization techniques to simultaneously overcome the added-mass effect in 3D FSI simulation and mathematical difficulties such as the assignment of boundary conditions at the interface between the 3D-1D coupling. Applications can be of numerical examples evaluating the change of hemodynamic parameters and diagnosis of an abdominal aneurysm, deep vein thrombosis, and bifurcation areas.

Acknowledgments

First of all, I would like to offer thankful gratitude to my advisor, Dr. Alexander Liberson, who allowed me to work on his team and introduced me to the fascinating field of cardiovascular modeling. For supporting me by offering a research/teaching assistantship, for having much patience with my work and making sure I had all the resources needed. I would never have followed the path I am on without his trust, thanks again for letting me go on a co-op.

A special thanks go to my co-advisor Yashar S Vehedein, who is most responsible for sharing his learnings, literature and helping me understand the cardiovascular dynamics as well as the challenging research that lies behind it. Yashar has been a friend and mentor. He had confidence in me when I doubted myself, and brought out the good ideas in me.

Besides my advisors, I would like to thank my committee members: Dr. Hany Ghoneim, Dr. Ali Ogut, and Dr. Michael Scharlau. I truly appreciate their comments, suggestions, time, encouragement, and for evaluating this thesis. I extend my deepest thanks to department staff especially William Finch, Diane Selleck, and Jill Ehmann for being very accommodative with all my questions and requests.

Last, but not least, I thank my family: my parents, for unconditional support and encouragement to pursue my interests; and my dear friend, for listening to my complaints and frustrations, and for believing in me.

Table of Contents

Abstract.....	2
Acknowledgments.....	3
LIST OF FIGURES	6
LIST OF TABLES.....	8
1 PROBLEM INTRODUCTION.....	9
1.1 Cardiovascular System.....	11
1.2 Blood Flow, Vessels & their Dynamic Properties	12
1.3 Arterial diseases	17
1.4 Hemodynamics	19
1.5 Engineering Approach: Computational Modeling.....	21
2 RESEARCH QUESTION.....	2
3 LITERATURE REVIEW	26
4 OBJECTIVES	26
5 METHODOLOGY	32
5.1 Fluid Domain: Newtonian Blood.....	33
5.2 Structure Domain: The Artery Wall.....	36
5.3 Fluid-Structure Interaction Theory	38
5.4 Arbitrary Lagrangian-Eulerian (ALE) Method.....	39
5.5 FSI Modeling.....	40
5.6 In-house 1D Code	44
5.7 Geometrical Multiscale Approach: 3D-1D Coupling	45
5.8 Artificial Boundaries.....	46
5.9 In-house 3D-1D Coupling Formulation.....	47
5.10 Coupling Implementation using ANSYS & MATLAB.....	48
6 IMPLEMENTATION & RESULTS	51
6.1 3D FSI Model	51
6.1.1 Blood Domain: Geometry.....	51
6.1.2 Blood Domain: Material behavior and boundary conditions.....	53
6.1.3 Blood Domain: Mesh Generation	55
6.1.4 Blood Domain: Solver settings and solution behavior	56
6.1.5 Structural Domain: Geometry & Mesh.....	57
6.1.6 Structural Domain: Material	57

6.1.7 Structural Domain: Boundary and initial conditions	58
6.1.8 Structural Domain: Solution method	58
6.1.9 FSI set-up & analysis	58
6.1.10 Results	61
6.2 3D-1D Coupling.....	68
6.3 1D-3D-1D Coupling	75
7 CONCLUSION & FUTURE WORK.....	78
8 SOCIETAL CONTEXT.....	80
9 REFERENCES	78

LIST OF FIGURES

Figure 1.1 Cardiovascular System	10
Figure 1.2 Blood & Vessel Components	11
Figure 1.3 Blood flow profile	12
Figure 1.4 Laminar vs. Turbulent flow circulation.....	13
Figure 1.5 Artery Composition.....	14
Figure 1.6 Plaque formation in an artery	15
Figure 1.7 Dilation of an artery.....	16
Figure 1.8 Forces exerted by blood flow on an arterial wall	18
Figure 1.9 Plaque build-up leading to Atherosclerosis on the left; Dilation leading to Aneurysm on right.....	19
Figure 1.10 Computation model of an arterial bifurcation	20
Figure 5.2.1 Non-linear elastic response due to cyclic pressure loads	34
Figure 5.3.1 Transfer of forces & displacements between an arbitrary mapped fluid & structural mesh face	36
Figure 5.4.1 FSI governing equations	37
Figure 5.5.1 Biomedical computational models demand a fully coupled FSI.....	38
Figure 5.5.2 Advantages of two-way FSI.....	39
Figure 5.5.3 FSI iterative loops	39
Figure 5.5.4 FSI process	40
Figure 5.6.1 Sectional view of coupling a 3D model exit (downstream) with a reduced 1D model	42
Figure 5.8.1 Artificial Boundaries	44
Figure 5.9.1 Coupling a 3D & a 1D model requires an interface formulation	45
Figure 5.10.1 Variables needed to facilitate coupling	46
Figure 5.10.2 Coupling implementation scheme	47
Figure 5.10.3 A multiscale coupling process employing ANSYS & MATLAB	48
Figure 6.1.1 Carotid artery bifurcation Perktold et al [49,51]	50
Figure 6.1.2 Blood domain boundaries	51
Figure 6.1.3 Inlet Velocity Jasanova et al. [105]	52

Figure 6.1.4 Structural boundaries.....	55
Figure 6.1.5 Acceleration & deceleration phases in a cardiac cycle	60
Figure 6.1.6 Axial velocity on axial slices.....	60
Figure 6.1.7 Axial velocity contours in normal plane view for CFD on the left and FSI on the right silghtly tilted towards left	61
Figure 6.1.8 Perktold et al [49,51]	61
Figure 6.1.9 Velocity magnitude contours and recirculation zones in carotid sinus 0.08s-0.4s(top- bottom) verified with experiments conducted by Ku. et al [30].....	62
Figure 6.1.10 Peak systole wall shear stress (WSS); CFD on the top in Pa & FSI in the bottom in N/mm ²	63
Figure 6.1.11 WSS on Carotid sinus curvature at maximum diameter	64
Figure 6.1.12 WSS on bifurcation curvature	64
Figure 6.1.13 Velocity in internal carotid artery compared to Josanova et al. [105]	65
Figure 6.2.1 Aneurysm geometry (Units in mm) extracted from Mix et al. [112]	66
Figure 6.2.2 3D & 1D boundaries (3D Structural on the left & 3D Fluid on the right)	66
Figure 6.2.3 Inlet velocity at 3D inlet	67
Figure 6.2.4 3D-1D coupling representation	67
Figure 6.2.5 Velocity plot at 3D-1D interface (3D outlet connected to 1D inlet)	70
Figure 6.2.6 Pressure plot at 3D-1D interface (3D outlet connected to 1D inlet)	70
Figure 6.2.7 Wall shear stress (WSS)	71
Figure 6.2.8 Velocity magnitude contours and recirculation zones in aneurysm	72
Figure 6.2.9 Validation on 3D-1D with total 3D model	73
Figure 6.3.1 Two 1D segments connected to a 3D cylinder model	73
Figure 6.3.2 Velocity & Pressure plots at 1D-3D interface on top and 3D-1D interface in bottom	74
Figure 6.3.3 Time varying velocity plots at center cross-section in three models.....	75

LIST OF TABLES

Table 1 Geometry Specifications	50
Table 2 ANSYS Fluent UDF Macros	53
Table 3 ANSYS Fluent Solver Settings	54
Table 4 Computation time for a FSI case	58
Table 5 Dynamic Mesh & System Coupling Settings	59

NOMENCLATURE

CVD – Cardiovascular Disease

1D – One-Dimensional

3D – Three-Dimensional

CFD – Computational Fluid Dynamics

FSI – Fluid-Structure Interaction

u – Velocity of the blood

R – Radius of the artery

P – Pressure in the artery

μ – Kinematic viscosity of the blood

L – Length of the artery

Q – Flow rate of the blood

σ – Normal stress on the artery

τ – Tangential stress of the artery

Re – Reynolds number of the blood

α – Womersly number of the blood

T – Time period of the pulse

ρ_f – Density of the blood

E – Young's modulus of the artery

ε – Poisson's ratio of the artery

η – Displacement of the artery

ρ_w – Density of the artery

A – Cross-sectional area of the blood/artery

WSS – Wall Shear Stress

RBC – Red Blood Cells

LDV – Laser Doppler Velocimetry

PIV – Particle Image Velocimetry

WSSG – Wall Shear Stress Gradient

OSI – Oscillatory Shear Index

DOF – Degrees Of Freedom

FEM – Finite Element Method

FVM – Finite Volume Method

RMS – Root Mean Square

PWV – Pulse Wave Velocity

CCA – Common Carotid Artery

ICA – Internal Carotid Artery

ECA – External Carotid Artery

BC – Boundary Condition

UDF – User Defined Function

1 PROBLEM INTRODUCTION

Cardiovascular diseases (CVDs) are the number 1 cause of death globally: more people die annually from CVDs than from any other cause. An estimated 17.9 million people died from CVDs in 2016, representing 31% of all global deaths[1]. These diseases are listed as the underlying cause of death, accounted for 840,678 deaths in the US in 2016, approximately 1 of every three deaths. Between 2013 and 2016, 121.5 million American adults had some form of CVDs. Between 2014 and 2015, direct and indirect costs of total cardiovascular diseases and stroke were \$351.2 billion (\$213.8 billion in direct costs and \$137.4 billion in lost productivity/mortality)[2]. It is rather tragic, if not cynical, the fact that the prime cause of death in our advanced civilization are phenomena like blockage, thinning, hardening and dilations of the blood vessels causing cardiovascular accidents. Having a comprehensive understanding of the cardiovascular physiology will enable the early diagnosis and treatment of these diseases, based on a patient-specific process, replacing the traditional method of diagnosing an already diseased condition and developing a treatment plan based on population means.

1.1 Cardiovascular System

The *cardiovascular system* shown in Fig 1.1 is a major system in the human body, consisting of the heart and blood vessels, whose purpose is to move blood through the body. The heart muscle acts as a pump in the system, expanding and contracting to receive and send blood, respectively. The blood vessels, including arteries, arterioles, capillaries, venules, and veins, are the piping components that allow for distribution of the blood through the body [3]. Two major circulation paths make up the cardiovascular system – pulmonary circulation, which carries blood between the heart and lungs, and systemic circulation, which carries blood from the heart through the body and back again. The purpose of the pulmonary circulation system is to take deoxygenated blood from the heart to the lungs, where carbon dioxide is released, and oxygen is added, and return the blood to the heart. The systemic circulatory system begins in the left atrium, which receives oxygenated blood from the pulmonary veins. The blood then moves from the left atrium to the left ventricle where it is pumped into the aorta, the largest artery in the body. From the aorta, the blood travels through the arteries into the capillaries and returns to the right atrium through the veins.

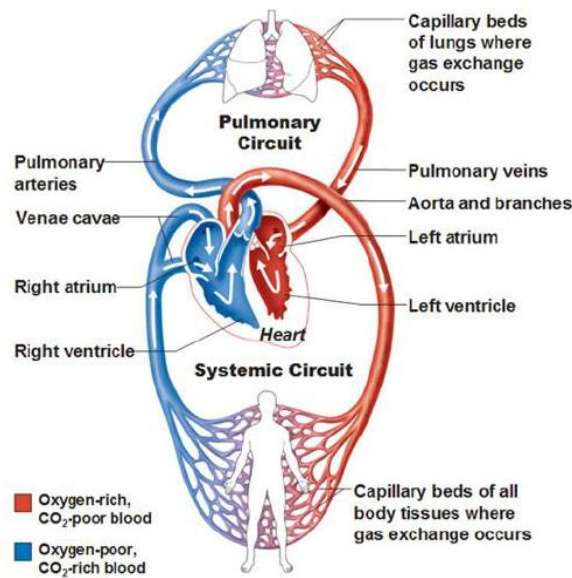


Figure 1.1 Cardiovascular System

The heart is continually expanding or contracting. This motion creates pulsatile blood flow, which moves the blood as pressure waves through the body. One complete cardiac cycle occurs during every heartbeat. Two important terms describe the motion of the heart chambers during the cycle – systole and diastole. Systole is the contraction of a chamber, while diastole is the relaxation of a chamber [3].

1.2 Blood Flow, Vessels & their Dynamic Properties

Blood is a suspension of red blood cells, white blood cells, and platelets in plasma illustrated in Fig 1.2. The viscoelastic fluid behavior of blood is associated with the elastic properties of the red cell membrane and the viscosity of internal and external fluids. Red blood cells constitute more than 99 percent of the particulate matter in blood and 40 to 45 percent of the blood by volume (hematocrit). The material properties of the red blood cell membrane and the fluidity of its internal contents make it easy for the cell to deform into a variety of shapes. However, the deformation of red blood cells in vitro or in vivo in circulation occurs at an essentially constant area, which can be attributed to the relatively high dilatational modulus of the cell membrane. After red blood cells, white blood cells are the largest in number. However, they constitute less than 1 percent of the

total volume of blood cells in normal human blood and exert little influence on the bulk rheological properties of blood. White blood cells are much less deformable than red blood cells.

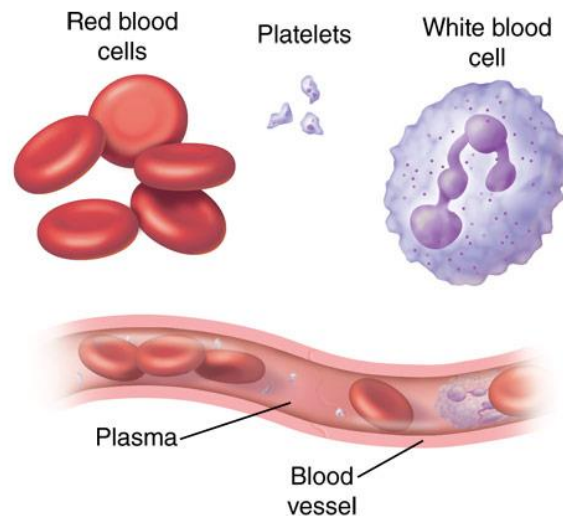


Figure 1.2 Blood & Vessel Components

White blood cells have a viscoelastic interior that makes them several orders of magnitude stiffer than red blood cells under rapid deformations. The stress required to cause the deformation of white blood cells is much greater than for red blood cells. This indicates that white blood cells are more viscous compared to red blood cells. Platelets occupy even less of blood volume than white blood cells. They play an important role in blood clotting, but they are rheologically unimportant to consider for the normal blood simulation. Adhesion of both red blood cells and white blood cells to blood-vessel walls increases the apparent viscosity. Since one must consider different viscosities for both red and white blood cells, blood is considered a non-Newtonian fluid.

The nature and behavior of blood are not only dependent on the fluid properties, but also other mechanical factors, including the forces, exerted on the fluid, the fluid motion, and the boundary conditions of the arterial geometry. Moreover, blood viscosity also dictates its behavior. According to these features, the blood flow may be characterized as steady or pulsatile, Newtonian or non-Newtonian, and laminar or turbulent. Fully developed flows are described by velocity and pressure fields, with all kinematic quantities independent from the axial coordinate, but this ideal behavior is never achieved in the vascular system. Two important particular cases are the steady flow, governed by the Poiseuille solution, and the time-periodic flow, governed by the Womersley solution. In most of the arterial system, blood flow has pulsatile behavior, that varies in different

sites of the arterial tree, due to the repeated, rhythmic mechanical pumping of the heart [4]. It means that the blood flow is an unsteady flow and because of that, the time dependence should not be neglected.

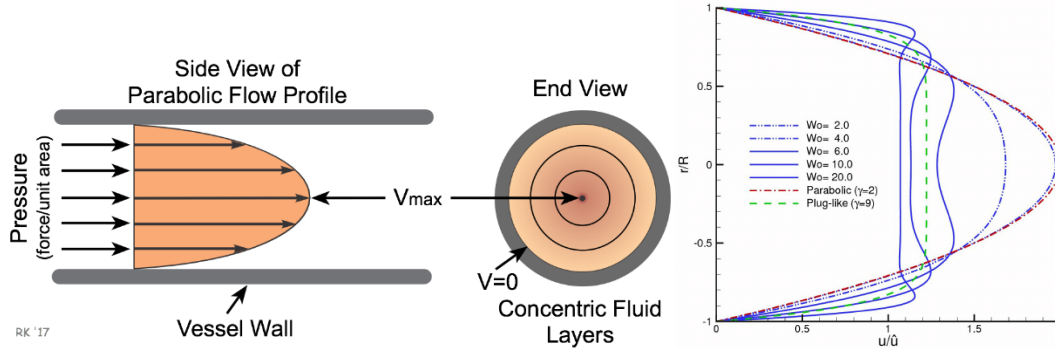


Figure 1.3 Blood flow profile

The Womersley solution for pulsatile flow Fig 1.3 in straight or tapered cylinders is a reasonable approximation to model blood flow in the arterial network [5]. In this case, the flow rate at the inlet regularly varies with time, and at sufficient distance from the inlet, the velocity only has an axial component, the function of radius. Generally, the Womersley velocity profile is not parabolic and, even though the total volume flow always remains positive, there is a boundary layer of reversed flow close to the wall. This inversion is vital in the characterization of pulsatile flow and is featured in the blood flow when the viscous traction forces are opposed to the dominant flow direction [6]. Even so, the blood flow is often considered in a steady state, depending only on the spatial position, since an unsteady flow is usually much more complicated than a steady one. In this case, the blood flow is approximated by the Poiseuille solution for steady flow and the velocity profile is parabolic, with a flow direction parallel to the vessel wall. It is a simplification and does not correspond to the general physiological situation, however, in an extended circular cylinder after a reasonable distance the fluid tends to be parabolic, and in small arteries, sufficiently distant from the heart, the flow is predominantly steady. The parabolic velocity profile of steady flow shown in Fig 1.3 is given by

$$u(r) = u_0 \left[1 - \left(\frac{r}{R} \right)^2 \right] \quad 0 \leq r \leq R \quad (1)$$

where u_0 is the velocity of the central layer and R is the luminal vessel radius. The Poiseuille law

establishes the relation between steady flow and pressure gradient, in which L is the vessel length, Q is the flow rate, and μ is the fluid viscosity.

$$\Delta P = \frac{8\mu QL}{\pi R^4} \quad (2)$$

$$Q = \pi R^2 \frac{u_0}{2} \quad (3)$$

Generally, blood velocity field has a laminar regime flowing parallel to the vessel centerline but under conditions of high flow during the systole period of the cardiac cycle, particularly in the ascending aorta and in stenotic or aneurysmal arteries, the flow can be disrupted and acquire turbulent features, that may include recirculation sites, also known as vortices. Curves and branches across the vascular network also generate secondary flows. Laminar flow has a parabolic velocity profile, and turbulence occurs when fluctuating velocity components are found in both the axial and nonaxial directions [7]. Pulsatile flows become turbulent for Reynolds numbers larger than 2000, especially during decelerating systole or near the end of systole flow perfuses/splits into smaller vessels as shown in Fig 1.4 [8]. Over one cardiac cycle, the maximum value of this parameter can range from 6000 to 10,000, in transport from the heart to the periphery [9].

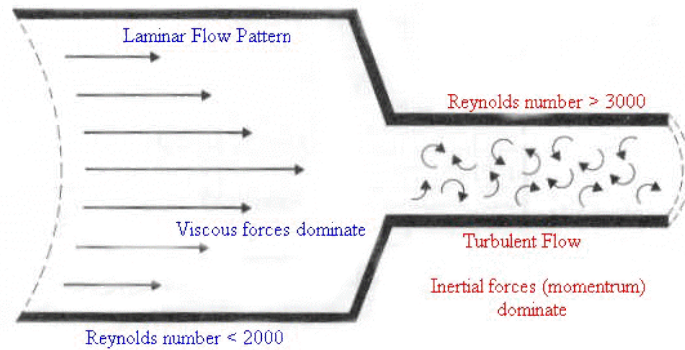


Figure 1.4 Laminar vs. Turbulent flow circulation

Two significant differences exist between blood vessel walls in the vasculature and more traditional engineering pipe materials. Unlike pipes, which are generally rigid, blood vessel walls are both elastic and porous. The consequence of this is that, as blood travels through the blood vessels, the walls expand and contract. Also, nutrients can be transferred to the surrounding tissues through the pores in the blood vessel walls. These pores are selectively permeable, allowing nutrient transfer while preventing red blood cells from leaving the vessels [10]. As most common CVDs mainly incept in arteries, the current study considers purely elastic arterial vessels only.

However, their mechanical behavior is not purely elastic but slightly viscoelastic. *Arteries* are muscular vessels that carry blood away from the heart. They are contrasted with veins, which carry blood toward the heart. Arteries can be subdivided into several groups with ascending diameter: arterioles ($10 - 100 \mu\text{m}$), muscular arteries (diameter $> 0.1 \text{ mm}$), and elastic arteries (diameter $> 5 \text{ mm}$), such as the aorta, the carotid arteries, coronary arteries, etc.

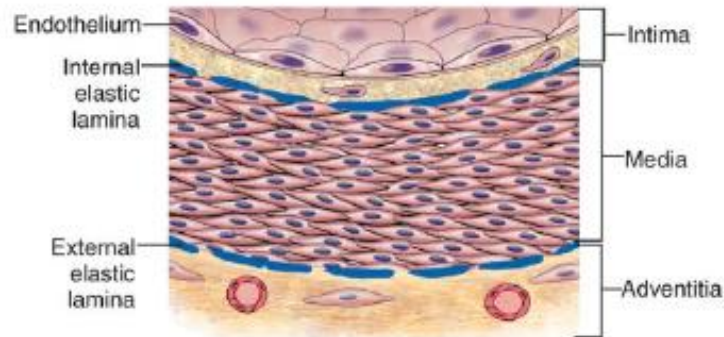


Figure 1.5 Artery Composition

The main constituents shown in Fig 1.5 of arteries are collagen, elastin, and smooth muscle. The intima mainly consists of elastin; the media consists of collagen smooth muscle and some elastin, and the adventitia mainly consists of collagen. To understand the *mechanical behavior of arteries*, it is necessary to know the mechanical properties [11] of these constituents. *Collagen* is the main protein of connective tissue in animals and the most abundant protein in mammals. It is tough and inextensible, having great tensile strength. It is responsible for skin strength and elasticity, and its degradation leads to wrinkles that accompany aging. It strengthens blood vessels and plays a role in tissue development. Due to its waviness, tissue stiffness is low at small strains and the stiffness increases once the fibers are fully stretched. A typical Young's modulus of collagen is approximately 500 MPa. *Elastin* is a protein in connective tissue, which is elastic and allows many tissues in the body to resume their shape after stretching or contracting. It also helps the skin to return to its original position when it is poked or pinched. It has an almost linear stress-strain relationship, with Young's modulus of approximately 500 KPa. *The smooth muscle* which constitutes 40% of the media is used to move matter within the body via contraction and has Young's modulus of 100 kPa in the deactivated state whereas in the activated state it increases to 200 KPa making the vessel stiffer.

Since the focus of current research is not related to the mechanical properties of the arteries, only a brief discussion is presented. As mentioned above, the arterial wall has a layered structure making the wall anisotropic. The elastin in the media bears most of the pressure load at small strains, and the collagen fiber network in the adventitia limits the radial deformability at higher blood pressures and causes the steep rise in wall stiffness at higher strains, making the material nonlinear [12].

1.3 Arterial diseases

Atherosclerosis, a common cause of a CVD, is a chronic artery disease that affects millions of people worldwide which is a condition that primarily affects the aorta, and large- and medium-sized arteries, particularly the coronary and cerebral arteries, where disturbed flow patterns occur.

It refers to a process where the arterial walls thicken and harden due to a gradual build-up of intracellular or extracellular fatty deposits, such as lipids and cholesterol and proliferation of smooth muscle cells shown in Fig 1.6. In general, atherosclerosis occurs when one passes the age of thirty, and its existence increases with age. Apart from these purely temporal reasons, lifestyle also seems to play an important role. Occlusion (thrombosis/embolic blockages) of the artery lumen can cause a substantial decrease in blood supply to the myocardium, giving rise to chest pains or transient ischemic attack (temporary blockage of the blood supply to the brain). If the hardened inner layer of the artery ruptures, thrombus may form inside the artery lumen, leading to stroke (sudden death of brain cells).

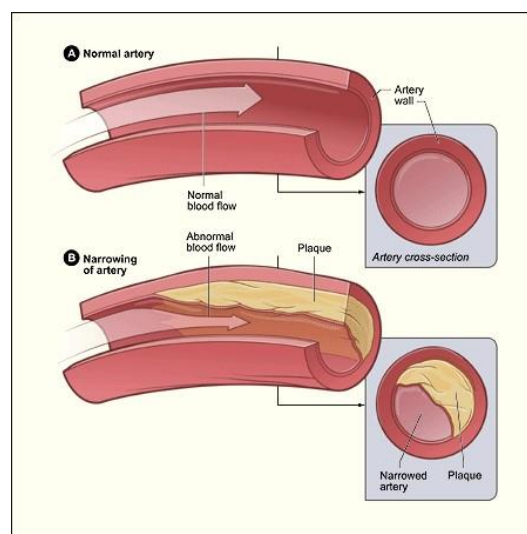


Figure 1.6 Plaque formation in an artery

Atherosclerosis develops inside the walls of vessels so that the genesis is challenging to observe and test directly in vivo. The evolution of atherosclerosis is prolonged; disease progression may span decades, which makes experiments to reproduce and study its pathogenesis very difficult. Because of these characteristics, most information about the disease has come from clinical observations and autopsies that indicated the high-frequency localizations of lesions in the vascular system, the categorization of lesions, and the relative importance of various risk factors.

Aneurysm ruptures are among the other reasons causing hemorrhagic strokes, which, in the majority of the cases, and unlike most medical conditions, is a sudden event, with no warning signs. Nowadays, aneurysms still represent a frightening and devastating silent threat, not only due to their association with high prevalence and mortality rates but also because they are the greatest cause of long-term disabilities. Thus, aneurysms have a significant impact on cost and the overall state of health care, and the understanding of the fundamental aspects of their pathophysiology and treatment is a subject of great importance, both nationally and globally, highly contributing to the progress of the modulation of the complex phenomena associated with these pathologies.

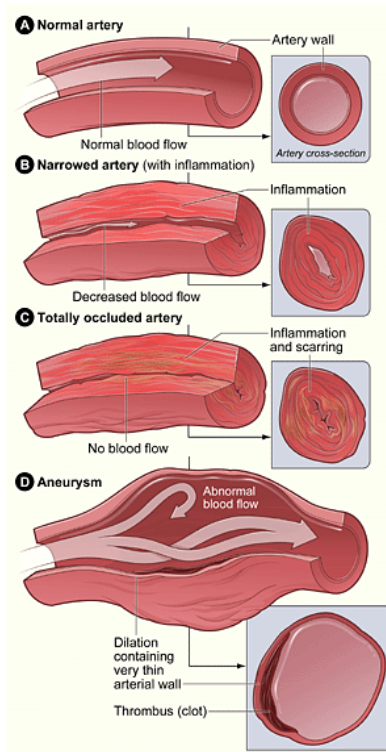


Figure 1.7 Dilation of an artery

Generally, an aneurysm is a localized pathological dilation of the wall of a blood vessel shown in Fig 1.7, due to the congenital or acquired structural weakening of the wall media, and potentially results in severe complications, or even sudden death, through pressing on adjacent structures, thrombus formation or rupturing causing massive hemorrhage [13]. The natural history of this pathology is far from being fully understood, mainly because of the paucity of temporal investigations, which is related to the fact that aneurysms are rarely detected before rupture. A possible cause for these incidents is the involvement of hemodynamics, the basis for the current research activity.

1.4 Hemodynamics

Hemodynamics or blood dynamics is the study of the properties and flow of blood. Hemodynamic factors that have been suggested to be important in plaque formations and arterial dilations are derived from the blood pressures, velocity fields and involve several different forms, such as flow separation and vortex formation [14,15].

The red blood cells transport oxygen and waste products by flowing through the blood vessels. Blood flows through the vessels by blood pressure. Just as water flows through pipes from areas of higher pressure to lesser, blood flows through the body from areas of higher pressure to areas of lower pressure. Blood pressure is measured both as the heart contracts, which is called systole, and as it relaxes, which is called diastole. A systolic blood pressure of 120 millimeters of mercury is considered right in the middle of the range of normal blood pressures, as is a diastolic pressure of 80 mm of mercury. Normal blood pressure is essential for proper blood flow to the body's organs and tissues. Each heartbeat forces blood to the rest of the body. The force of the blood on the walls of the arteries is called blood pressure. Blood pressure moves from high pressure near the heart to low pressure away from the heart. Blood pressure depends on many factors, including the amount of blood pumped by the heart. The diameter of the arteries through which blood is pumped is also an essential factor. Generally, blood pressure is higher when more blood is pumped by the heart, and the diameter of an artery is narrow. Stressful situations can result in a temporary increase in blood pressure. If an individual were to have a consistent blood pressure reading of 140 over 90, he would be evaluated for having high blood pressure. If left untreated, high blood pressure can damage vital organs, such as the brain and kidneys as well as lead to a stroke.

However, the specific mechanism whereby blood flow patterns influence the development of arterial disease remains a challenging topic in bioengineering. A considerable amount of evidence shows that the hemodynamics and the genesis of arterial diseases are believed to be reasonably related through the action of mechanical parameters on and near the vessel wall, such as Wall Shear Stress (WSS) and its derivatives. Details of the pressure and shear stress distributions on the walls of a bend or bifurcation are of interest in the study of atherogenesis because it appears that the localization of plaque is related to local flow patterns. Besides that, aneurysms are usually located at high WSS sites, like bifurcations, and can be created in animals through systemic hypertension and high-flow blood.

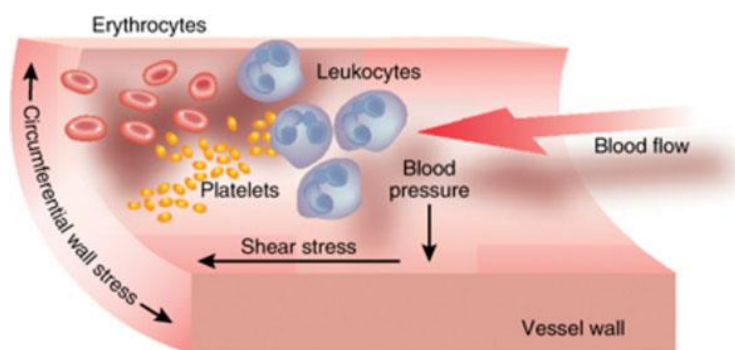


Figure 1.8 Forces exerted by blood flow on an arterial wall

As shown in Fig 1.8, In vivo, the pulsatile blood flow through the branched tubular array of the arterial vasculature generates three types of hemodynamic forces: (1)WSS, a tangential frictional drag force due to blood viscosity; (2) transmural pressure, a perpendicular cyclic force due to blood pressure; (3) mechanical stretch, a cyclic tensile stress of pulsatile flow.

Among these hemodynamic forces, the influences of WSS on the pathogenesis of atherosclerosis have been extensively investigated and well understood. WSS plays a significant role in the pathogenesis of the atherosclerotic plaque, particularly when laminar blood flow is disturbed with low or oscillatory WSS. The combination of altered arterial hemodynamics around atherosclerosis-prone sites (e.g., curvatures, bifurcations), where secondary flows occur Fig 1.9, and systemic risk factors promote atherosclerotic lesion initiation, the progression of atherosclerotic plaques.

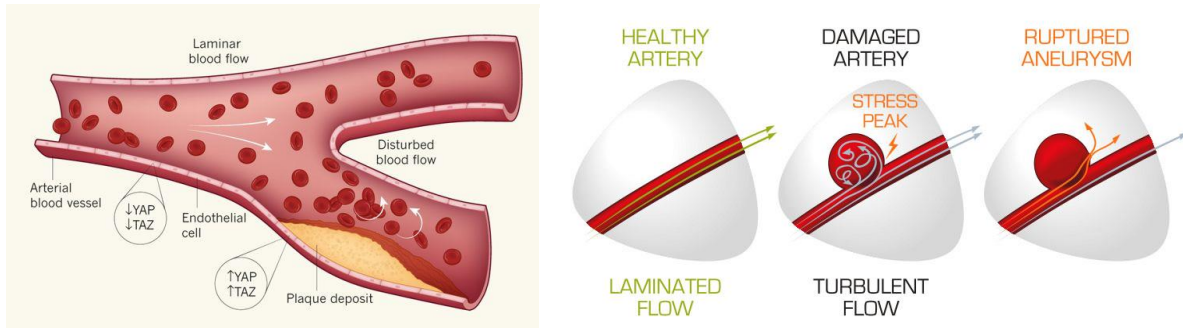


Figure 1.9 Plaque build-up leading to Atherosclerosis on the left; Dilation leading to Aneurysm on right

Despite the continuous progress in the medical research field and the wide range of studies on the pathogenesis of aneurysms, the exact developmental stages are far from being thoroughly comprehended. Because of the scarcity of studies with a significant amount of patients and longterm follow-up [16], mostly due to the fact that the majority of aneurysms are only detected in an advanced stage. How and why these pathologies first develop is intimately related to interaction between the biological processes of the arterial wall and high-flow hemodynamic forces [17]. Like platelets and RBC, endothelial cells discriminate among different types of flow patterns and are physiologically stimulated by stress, i.e. blood pressure acting normal to the cell surface and WSS acting tangentially. Endothelial cells respond to stress through an active adaptive process that leads to modifications in their morphology and function [18, 19]. Moreover, WSS promotes the elongation and alignment of endothelial cells nuclei in the direction of the local flow pattern [19] causing destructive remodeling that leads to a disturbance of the equilibrium between the blood pressure forces and the internal wall stress forces, resulting in the progressive dilation of the wall.

1.5 Engineering Approach: Computational Modeling

Currently, the investigations use a variety of methodologies, from in vitro to in vivo models, but a great percentage is based on mathematical modeling and numerical simulations of blood flow, since it is now well established that blood flow dynamics shown in Fig 1.10 play a major role in the development of cardiovascular pathologies, like atherosclerosis & aneurysms. At a macroscopic level, the arterial wall is a complex multi-layer structure that deforms under pressure forces.

In the past, hemodynamic computations have often been performed using rigid geometries, which forms a subset of computational fluid dynamics (CFD). CFD can present results with high

resolution if the boundary condition information is correct; therefore, the geometrical data and boundary velocity data that come from in vivo measurements are necessary for realistic modeling of blood flow in the artery. Medical imaging techniques can supply these data. From CFD solutions, it is straightforward to present velocity distributions for blood flows and to extract WSS and other important hemodynamic factors. However, CFD models do not account for arterial wall distensibility.

The physical process of the oxygen supply to the human brain and various organs provided by blood flow in vessels in a cardiovascular system resembles a flow of an incompressible fluid in a compliant tube. Even though constitutive equations have been proposed for the structural behavior of the vessel wall, its elastic characteristics in vivo are still very difficult to determine. This is a case where the influence of the displacements of a structure has a significant effect on the flow and pressure of the fluid.

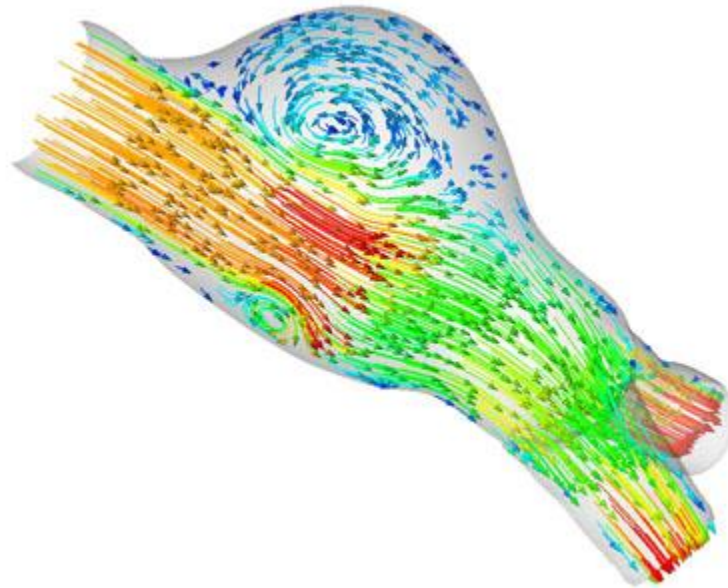


Figure 1.10 Computation model of an arterial bifurcation

Fluid-structure interaction (FSI) scenarios are those that involve the coupling of fluid mechanics and structural mechanics problems. FSI plays an important role in several different types of applications such as biomedical, material processing, automotive, aeronautical, and civil engineering. The solutions of structural and fluid mechanics problems can be considered a relatively mature technology. Commercial codes have been available from the mid-70s for structural mechanics and from the mid-80s for fluid mechanics. However, the coupling of the two

problems brings up new algorithmic issues, such as impulsive starts, velocity coupling, added mass, coupling of Lagrangian and Eulerian approaches, large mesh movements, contact, change in topology, etc.

In recent years, the study of FSI effects in biomechanics has intensified, especially in the field of arterial blood flow. Other examples of application of FSI analysis in cardiovascular research is the modeling of blood flow through the left ventricle [20] and the aortic valve [21]. A three-dimensional model of the natural heart with moving valves [22] was simulated using the immersed boundary method, which was specifically developed for the study of FSI problems in the cardiovascular system.

As mentioned previously, arteries differ in size considerably. Large arteries, in general, are very elastic. Due to their large deformations they can store and release elastic energy, making the blood flow more regular than if they were rigid. Smaller arteries are more rigid when compared to larger arteries. In the past, all numerical models used idealized geometries of large- and medium-sized arteries that simulate the hemodynamic quantities - pressure, velocity, wall displacement, and wall shear stresses; in a generalized way but these methods fell short since, ultimately, each aneurysm is a unique case, with a singular geometry, location, relationship with the surrounding environment, and hemodynamic behavior, which is heavily dependent not only on its own geometry but also the parent vessel.

The realistic simulation of the local and global events, that have such a significant influence on the blood flow behavior and cardiovascular pathologies, represents a computational challenge because of the diversity and intricacy of the human arterial system, not only in terms of its geometry but also the functional interactions that take place between several entities. The use of coupled mathematical models and numerical simulations, is still a very challenging task and a field of active research [17]. The aim of this research was to develop these coupled engineering modeling tools to describe complex blood flow patterns, thereby helping to determine the link between blood flow patterns and arterial disease. A powerful way to achieve this long term goal is to correlate patient-specific hemodynamic patterns with patient-specific spatial distributions of artery disease. This, in turn, requires tools for quantifying artery hemodynamics, which forms the major focus of this study.

2 RESEARCH QUESTION

People with CVDs or who are at high cardiovascular risk (due to the presence of one or more risk factors such as hypertension, diabetes, or already established disease) caused by modifiable or non-modifiable risk factors need early detection and monitoring management, as appropriate.

In recent years, the number of publications in the area of modeling and simulation of the cardiovascular circulatory system is growing exponentially. Regarding three-dimensional modeling, typical approach is mainly based on the classical CFD analysis of an incompressible hemodynamic flow within a rigid wall flow path. One of the objectives of the present investigation is to create a 3D model, accounting for the fluid-structure interaction between a Newtonian viscous fluid and a compliant arterial wall in typical 3D model of a circulatory system such as bifurcated branches and an artery with an aneurysm. Wall shear stress distributions and locations and extension of circulatory zones obtained based on a FSI model and a classical CFD are compared and conclusions made.

Geometric multiscale model is an approach for modeling the circulatory system including reciprocal coupling of a 1D FSI model with a total 3D FSI approach. It allows to save significantly time of circulatory system modeling compared to the fully 3D simulation. The propagating nature of a hemodynamic flow requires an appropriate technique to avoid artificial wave reflections and spurious oscillations at the interphases connecting 3D to the 1D model. This approach leads to the nontrivial problems at mechanical, mathematical and numerical levels.

The boundary conditions applied in this work are based on a 3D -1D FSI variational principle, complemented by the compatibility relations on outgoing characteristics. Interactions between the commercial ANSYS/FLUENT 3D simulation model and the CardioFAN - an in-house quasi 1D nonsteady FSI circulatory system modeling computer code, is provided by implementing the User-defined functions (UDFs), allowing the reciprocal exchange of information between the commercial “black box” system and the in-house code. Obtained results are validated against total 3D ANSYS based FSI modeling of an aortic aneurysm affecting the human arterial system.

This study is motivated by the prospect of implementing multi-scale models for the human cardiovascular system instead of a total 3D simulation. It is clear that a realistic, detailed numerical simulation of the flow in a segment of an artery (like, for instance, the carotid bifurcation or an abdominal aorta) may not be fully accomplished without accounting for the interactions with the

remaining part of the cardiovascular system. One possibility to this direction is ordered by the leveraging previous studies on unique set of coupling boundary conditions at an interface between 3D FSI model of the idealized large arterial vessel and a quasi-1D FSI artery segment. Hemodynamics are obtained and analyzed to gain insight into the complexity of the unsteady flow in that region and also to evaluate the computational requirements for an accurate representation of the phenomena.

3 LITERATURE REVIEW

The latest computing technologies have demonstrated an increasing influence upon medical health care, and biomedical engineers have become intimately involved in developing computer-aided medical tools such as image processing, biomaterials and biosensors. To review current relevant research progress, particularly significant amount of work and related publications due to the continued widespread incidence of CVDs, especially arteriosclerosis and identify interesting areas in this field, a preliminary literature review is presented here.

According to statistics reported by the American Heart Association for adults of age above 20, the prevalence of stroke in 2005 was as high as 6.5 million; and each year, approximately 795,000 cardiac patients experience a new or recurrent stroke[25]. Of all strokes, 87% are ischemic, 10% are intra-cerebral hemorrhage, and 3% is a subarachnoid hemorrhage.

The causative factors that contribute to the formation of atherosclerotic lesions have been studied extensively[26,27]. Hemodynamic factors are important determinants of the local distribution of atherosclerosis and the development of vascular plaques. The presence of atherosclerotic plaques has been shown to be closely related to the vessel geometry[28,29]. And typically occur in arterial regions that display complex geometry resulting in ‘disturbed’ blood flow behavior[30,31].

The history of blood flow measurement started from the mid of 19th century when Dokunin et al.[32] the ends of a known volume airtight U-tube was connected to a blood vessel to measure the rate of arterial blood flow according to the Poiseuille formula. After decades of evaluation, a variety of techniques are routinely employed for the measurement of beat-to-beat cardiac output nowadays. Currently, the most widely applied methods for in vivo blood flow measurement or the local arterial flow field include Doppler[33,34], magnetic resonance imaging flowmetry[35], and ultrasonic transit-time flow sensors[36]. Whereas, WSS is calculated from velocities close to the wall, or is measured directly with an electromechanical technique.

In vivo methods as mentioned above have the potential to provide the most realistic flow field data with limited spatial and temporal resolution[37,38], which limits the representation of the real physiological boundary conditions such as vessel geometry, blood and tissue properties. However, the complex etiology of atherosclerosis is not fully understood due to unknown relationships between hemodynamics, mechanical factors and atherosclerotic changes of the arterial wall.

Although WSS has been implicated in inducing endothelial wall cell responses[39], identifying WSS from flow patterns and mechanical forces in vivo is difficult[40].

An alternative to vivo measurements is Laser Doppler Velocimetry (LDV), or Particle Image Velocimetry (PIV) experiments using laboratory models representing the interested arterial geometries. These models are either reconstructed from patient-specific arteries or summarized based on population averaged data built by optically transparent materials. Therefore, the experiments can be of various degrees of complexity, including steady[41] and pulsatile flow conditions[30,42], and patient specific geometries[43,44].

The initial research conducted on the physics of atherosclerosis incorporated mostly experimental techniques into visualizing the flow through a tube, partially occluded or otherwise, referred to as hemodynamics. Variations made as to the occlusion shape and severity, location and the fluid flowing through the vessel to determine the flow characteristics such as the pressure, shear stress and flow velocity. Several local 3D in vitro and computational flow models have been applied, revealing the complex flow structure in the sinus district of carotid artery bifurcation.

Bharadvaj et al.[45,46] defined a standard geometry of the carotid bifurcation (an average over 57 actual geometries from different subjects) and conducted stationary studies of the internal carotid blood flow. They found a region of low velocities near the non-dividing wall that extend with increasing Reynolds number. Conversely, the opposite region showed substantial axial velocities and shear stresses. These results were confirmed by Rindt et al.[47] using experimental and computational stationary models. This method is limited, however, by the preparation required before running the equipment; a complicated process susceptible to limitations of accuracy in the angle of the lasers and attenuation as a result of the tube and fluid material. Some flow characteristics, such as the WSS are challenging and even the more advanced experimental methods can provide poor results near the wall region. Although a considerable amount of in vitro experimental studies have been conducted, the majority of them are focused on flow velocity measurements, while one of the most important hemodynamic parameters, WSS, is not accessible due to the relatively low spatial resolution of the visualized flow field.

Anayiotos et al.[48] compared WSS distribution in rigid and compliant models of a carotid bifurcation using laser Doppler velocimetry. Their results indicated that vessel compliance reduced the mean wall shear rate level by about 30% at most locations. The effect of compliance was more

significant on the instantaneous maximum and minimum shear stresses, which could be reduced by as much as 100% in the compliant model in some locations.

Similarly, in computer simulations, a 25% decrease of WSS was reported in a compliant model of the carotid bifurcation[49]. Plenty of evidence implicates the mechanical forces and intravascular hemodynamics that result from blood flow [e.g., high circumferential tensile stress and low WSS (WSS)] and can chronically affect and regulate blood vessel structure[50]. Perktod and Resch[51] investigated the effects of artery geometric factors, such as the shape of the carotid sinus and the branch angle, in carotid bifurcation under pulsatile flow conditions. They concluded that the most physiologically relevant flow variable is WSS and its temporal variation, which is in agreement with previous in vitro results. Following this, numerous numerical studies were conducted in a variety of arterial models, predominantly artery bends and bifurcations like WSS research[52,53], and related indices such as oscillatory shear index (OSI)[54], WSS gradients (WSSG)[55,56].

The first numerical study of pulsatile blood flow in aneurysms[57] demonstrated the presence of a vortex that varied in size and intensity during the cardiac cycle. Perktold et al.[58] represented pulsatile flow patterns with velocity vectors and particle paths through axisymmetric aneurysm models in carotid artery bifurcation. Finol et al.[59] numerically simulated pulsatile flow, providing flow patterns and their effect on WSSs and pressure distributions.

In the cases above, blood was assumed to be a Newtonian fluid. It has been demonstrated that assigning Newtonian behavior to blood is only valid when it has shear rates more than 100s^{-1} , which tends to occur in larger arteries[59]. In most cases, though, non-Newtonian blood models would provide a more accurate representation of blood flow behavior within the arteries of interest, particularly for stenosed conditions. In some diseased conditions, blood flow is non-Newtonian regardless. Direct numerical simulations of non-Newtonian flow have been conducted under pulsatile conditions, resulting in flow patterns and WSSs that were underestimated for otherwise Newtonian flow behavior.

As an emerging research tool, computational fluid dynamics (CFD) approach is progressively adopted by biofluid dynamics community as the preferred technique for numerical modeling of large artery hemodynamics. CFD simulations can offer numerous hemodynamic parameters such as WSS which remain difficult to access via in vivo and in vitro measurements. Quite a few researchers investigated the effect of wall compliance on arterial flow patterns. An experimental

study of compliant aortic bifurcation models[60] found that compliance reduced the shear rate at the outer walls and increased the shear rate at the inner walls.

Recently, computer simulations have been an excellent non-invasive method of studying flow within stenosed vessels. Computational simulations tend to have the benefit of being economical in comparison to experimental methods, which often require substantial investment in equipment. Initially, most of the simulations tended to make assumptions as to the geometry as well as on the fluid behavior to reduce computational time. With an increase in computational power, flow models of disease vessels now incorporate far more complicated simulations that increasingly approach the conditions as present within the body itself. Recent technological methods have allowed the scanning of arteries using angiography, which allows simulations to incorporate realistic artery geometries. The result is simulations which have geometries similar to that of real patients who have atherosclerosis

In recent years, FSI has been primary interest in modeling blood flow numerical simulations because of the arterial wall remodeling process. Fluid-structural interaction is a relatively new technique used in numerical problems to provide an understanding of the impact the flow has on structures, both within the flow and encompassing the flow. In recent years, the study of FSI effects in biomechanics has intensified, especially in the field of arterial blood flow. Other examples of the application of FSI analysis in cardiovascular research is the modeling of blood flow through the left ventricle[61] and the aortic valve[62]. This study aimed at investigating the hemodynamics of a compliant patient-specific femoral artery bifurcation model by a FSI scheme[63].

Despite the advances made in computing power and numerical algorithms, the high computational cost and the fundamental challenge of the FSI problem still restrict their use to a limited region, such as a bifurcation, the aortic arch or the examples listed above. This limitation motivates the adoption of 1D models, as they allow to compute the fluid dynamics in large part of the arterial tree at a reasonable computational cost[64,65].

As well as understanding many aspects of vascular physiology, clinical therapy such as the mechanism of disease, materials for treatment, matching of artificial vascular grafts to host vessels, assisting physicians in positively identifying individuals who exhibit the development of vascular disease, and accurate modeling of blood flow. Study of FSI effects in biomechanics has intensified, especially in the field of arterial blood flow. The FSI approach simultaneously models blood flow

(fluid) and arterial wall deformations (structure) and has received growing interest because of its potential impact in the medical field[66,67]. It has been implemented in modeling abdominal aorta[68], carotid bifurcation[69], and cerebral aneurysm[70]. Torii, Wood et al.[71] studied the effects of wall compliance on a patient-specific right coronary artery with a severe stenosis and found noticeable differences in the instantaneous WSS produced by the FSI and rigid wall models. Apart from the difference in geometrical properties, a significant diversity in mechanical properties of the vessel wall exists. The larger arteries are more elastic than, the smaller ones. Deformations up to 10% of the vessel radius are common in large arteries. This elasticity gives rise to the Windkessel effect (i.e., the distension of the large arteries during systole, functioning as a buffering reservoir for blood)[65] and provides a passive mechanism for smoothing the pulsatile blood flow from the heart.

Pulse waveforms carry information about the morphology and functionality of the cardiovascular system. Therefore, a good understanding of the mechanics of pulse wave propagation in normal conditions and the impact of disease and anatomical variations on the patterns of propagation can provide valuable information for clinical diagnosis and treatment. When arterial wall behavior is considered to simulate a wave propagation in the arterial tree, a heterogeneous composition of the cardiovascular models can be triggered featuring different assumptions on the spatial degrees of freedom.

On one hand, the heterogeneity of the circulatory system requires the use of different models in its various compartments, featuring different assumptions on the spatial degrees of freedom. On the other hand, the mutual interactions between its compartments imply that these models should preferably not be considered separately. These requirements have led to the concept of geometrical multiscale modeling, where the main idea is to couple 3D models with reduced 1D and 0D models. Recently, the coupling and integration of models with different DOF have been analyzed by Quarteroni et al.[72,64,73–75], linking together reduced 1D model with 3D models of the arterial tree. This task is very cumbersome since this problem involves deformable domains (compliant arterial walls) as well as other non-linearities in the governing equations such as convective terms, FSIs and also, regions of various dimensionality and the coupling conditions between them. This research proposed an alternative approach for coupling models of non-matching dimensionality and used it to implement a model of an aneurysm in the common carotid artery bifurcation.

Geometric multiscale FSI models have received considerable attention in recent years is the key component of hemodynamic modeling. 1D and 3D formulations have been used extensively to simulate arterial hemodynamics. Landmark contributions in 1D modeling include the works of Hughes and Lubliner[76], Stergiopoulos et al.[77], Olufsen et al.[78], Formaggia et al.[79], Sherwin et al.[80], Bessems et al.[81], and Mynard and Nithiarasu[82]. 1D methods have been used to improve our theoretical understanding of hemodynamics, in particular, to study the mechanisms underlying pulse wave propagation and also clinically in applications such as wave intensity analysis. Several comparisons against *in vivo*[78,83] and *in vitro*[84,85] data have shown the ability of the nonlinear 1D equations of blood flow in compliant vessels to capture the main features of pressure and flow waveforms in large arteries. Indeed, arterial pulse wavelengths are sufficiently long compared to arterial diameters to justify the use of a 1D rather than a three-dimensional 3D approach when a global and sectionally averaged assessment of blood flow in the arterial system is required.

Accurate predictions can be made when the flow is predominantly unidirectional, and there are no sudden changes in cross-sectional area. However, 1D models require the introduction of additional empirical laws to account for recirculation and pressure losses in the presence of vessel curvatures, stenosis, aneurysms, etc[86]. These geometric complexities are intrinsically captured with 3D models, which can provide localized hemodynamic quantities such as WSS, particle residence time, etc. Nan Xiao et al.[86], studied a systematic comparison between 1D and 3D compliant arterial models to exploit the advantages of both schemes: a computationally efficient 1-D model combined with a full 3D model sharing identical boundary condition and constitutive laws. This overlapping 3D-1D approach can potentially accelerate the solution turn-around time of complex 3D models, therefore improving their clinical applicability, and differs from previous efforts[75,87,88] where 3D and 1D models were coupled to represent spatially distinct parts of the arterial tree.

There are a few research groups in the United States that are currently working on cardiovascular hemodynamics modeling or related topics[89–91], such as a general approach to derive the FSI problem have been applied based on Hamilton’s variational principle[92,93]. Therefore, based on the statistical demonstrations on the importance of this issue, regarding health and economic aspects, a need for expanding the research effort on this subject in the United States seems to be necessary.

4 OBJECTIVES

This thesis presents a mathematical and numerical methodology that evaluates the CV parameters fields during an entire cardiac period in idealized 3D arterial units such as bifurcated branches and arterial aneurysm. The methodology uses robust algorithms to implement the geometrical multiscale modeling by coupling 3D Newtonian FSI models with quasi-1D FSI model that simulate the blood circulation in the circle of Willis. This approach will exploit the combination of two models, with different complexities, due to the fact that the current technology is not advanced enough to simulate the whole cardiovascular network using complex and accurate models, since this implies an elevated computational cost.

To reduce complexity of 3D geometry for the study, an idealized arterial model is taken into account. We use a quasi-1D as the reduced model, which resort to some simplifying assumptions in order to provide cross-sectionally averaged quantities for the pressure and velocity fields. The 3D model describes the blood flow using 3D equations for incompressible Newtonian fluids. Though it is well known that the mechanical interaction between the blood flow and the compliant vessel wall is relevant in the blood flow propagation phenomenon, the 3D model is constructed as a domain free in radial directions, considering the wall displacements.

This methodology solely focuses on simulating the multiscale interaction to overcome defective boundary conditions at coupling interface and studying local effects, while leveraging quasi-1D segment of the global in-house 1D algorithm demonstrated in application of Hamilton's variational method by A.S.Liberson et al. [92-94]. Available software packages for solving the governing fluid and structural equations and parsing boundary parameters between 3D & 1D models are employed. The main objectives of the present research are summarized as follows:

- To model an idealized large arterial bifurcation and perform 3D FSI pulsatile flow simulation, using isotropic compliant structure and artificial boundary conditions.
- To develop a scheme to implement an in-house coupling formulation at 3D-1D interface using commercially available tools. In this case, a validated 1D model acts as an absorbing downstream boundary condition to 3D.
- To determine the extent of local 3D FSI effects in a 3D & 1D multiscale coupled systems.

5 METHODOLOGY

Governing equations developed are independent of the material characteristics. A constitutive relation (material model) is required to relate the stress state of the body to its motion or state of strain. We are interested in Newtonian behavior for fluids and elastic behavior for solids.

5.1 Fluid Domain: Newtonian Blood

The most appropriate set of equations to simulate the blood flow in the arterial network is the time-dependent fluid equations *Navier-Stokes* expressing the balance of linear momentum derived from the underlying physical principles of *conservation of the momentum and mass*, Eq. 4 & 5 respectively. These describe blood flow in arteries as a homogeneous, unsteady, and incompressible fluid, in terms of the velocity and the pressure fields. In an open bounded domain, the system of equations representing blood is given by:

$$\rho \frac{\partial u}{\partial t} + \rho(u \cdot \nabla)u - \text{div } \sigma(P, u) = 0 \quad (4)$$

$$\text{div } u = 0 \quad (5)$$

$$\sigma(P, u) = pI + \tau(u) \quad (6)$$

where ρ is the fluid constant density, and the Cauchy stress tensor $\sigma(P, u)$ depends on the fluid velocity u and P is the Lagrange multiplier connected to the incompressibility constraint, which defines the mechanical pressure for incompressible fluids, identified by $P = P(x, t)$ and I is the unitary tensor. $\sigma(P, u)$ holds the assumption that the stress tensor only depends on the velocity gradient and the fluid mass density at a particular time, and is independent upon the previous history of the fluid deformations. $\tau(u) = \tau(\mu, D(u))$ is also called the extra stress tensor, with $D(u)$ denoting the symmetric part of the velocity gradient (strain rate tensor),

$$\tau(u) = 2\mu \frac{1}{2}(\nabla u + \nabla^T u) = 2\mu D(u) \quad (7)$$

Conservation of momentum now is,

$$\rho \frac{\partial u}{\partial t} + \rho(u \cdot \nabla)u + \nabla P - \text{div } \tau(u) = 0 \quad (8)$$

with u and P are the unknown fluid velocity and pressure, respectively.

The *Newtonian fluid model* is a good approximation for many fluids and assumes that the stress is proportional to the rate of deformation:

$$\sigma = 2\mu D(u) + \lambda \text{tr}(D(u))I \quad (9)$$

Here μ is the coefficient of shear viscosity or dynamic viscosity. The second constant of proportionality λ is termed the second viscosity which relates stress to volumetric deformation. In the incompressible limit $\lambda \rightarrow \infty$ and $\text{tr}(d) = 0$, to account for the unknown hydrostatic pressure $\lambda \text{tr}(d)$ is replaced so that the Cauchy stress is given by

$$\sigma = 2\mu D(u) - pI \quad (10)$$

Applying the constitutive fluid equation, *the Navier-Stokes* equations for incompressible Newtonian fluids becomes,

$$\rho \frac{\partial u}{\partial t} + \rho(u \cdot \nabla)u + \nabla P - \text{div}(2\mu D(u)) = 0 \quad (11)$$

$$\text{div } u = 0 \quad (12)$$

The *Reynolds number*, Eq 14, is used to predict transitions from laminar to turbulent flow. It is a similarity parameter for viscosity and expresses the ratio of steady inertial forces to viscous forces within the fluid. And Eq 11 can be written as Eq 13,

$$\rho \frac{\partial u}{\partial t} + \rho(u \cdot \nabla)u + \nabla P - \frac{1}{Re} (2\mu \text{div } D(u)) = 0 \quad (13)$$

$$Re = \frac{\rho|u|D}{\mu} \quad (14)$$

A low Reynolds number ($Re \ll 1$) reflects the high viscous forces over inertial ones, meaning that the local boundary highly controls the flow pattern. For a Reynolds number much less than one, which is the case of the smaller arteries (arterioles), it is reasonable to neglect convective acceleration terms. On the other hand, a high Reynolds number ($Re \gg 1$) reveals the turbulence in the flow pattern, resultant from the inertial dominance. An increased Reynolds number seems to increase the WSS and to decrease the pressure [95]. Typically, viscous stresses ($Re \ll 1$) tend to stabilize and organize the flow, and excessive inertial forces ($Re \gg 1$) tend to disrupt the organized flow, leading to spontaneous flow irregularity and eventually to turbulent behavior.

Another non-dimensional *Womersley number*, Eq 15, which governs the relationship between unsteady inertial forces and viscous forces [96], and is given by,

$$\alpha \propto \frac{D}{\sqrt{\mu T}} \quad (15)$$

where D is the artery diameter, T is the pulse period. physically, the Womersley number is assumed to be the ratio between the tube diameter to the laminar boundary layer growth over the pulse period, since this growth can be considered proportional to $\sqrt{\mu T}$. For very small Womersley values, the velocity reaches a parabolic profile, as predicted by the Poiseuille because of the low frequency of pulsations. In fact, in some situations, even unsteady flows are reasonable treated as quasi-static [97]. For high Womersley number greater than 10, the velocity profile tends to flatten. Besides obtaining the velocity and pressure fields, it is also relevant to get information about mechanical parameters. The most common indicators related to arterial diseases are defined, due to their believed influence in the origin and aggravation of many pathologies, including aneurysms, on or near the wall [98]. The most sought *hemodynamic indicator is the WSS*. The WSS is the shear stress vector at the wall, including direction, can be obtained by subtracting the normal component of the viscous stress vector from the total viscous stress vector, Eq 16, on the wall, and is given by

$$\tau_t \cdot t = \tau - \tau_n \cdot n \quad (16)$$

Where t is the unit tangent to the wall, n is the outward normal to the wall surface, τ_t & τ_n are the tangential and normal components of the viscous stress vector, respectively. The WSS is not easily measured for pulsatile flows, but for laminar steady flows it is calculated as Eq 17, where Q is the cross-sectional flow rate.

$$WSS = \frac{32\mu Q}{\pi d^3} \quad (17)$$

A numerical simulation is an excellent tool, to gather information on hemodynamic indicators, since having the velocity flow field it is extremely feasible to compute the WSS or its derived measures, contrary to in vitro or in vivo experiments. The prescription of proper initial and *boundary conditions* is a crucial step in the mathematical modeling and the numerical formulation of the arterial region of interest. After defining the initial condition, $u = u_0$, for $t = 0$ in the fluid equations are mathematically well defined and prepared to be solved by numerical methods only when the appropriate set of boundary conditions is imposed on the limits of the bounded domain. The classical conditions that we can prescribe on the boundary are the *Dirichlet and the Neumann, or natural, boundary conditions*, Eq 18 & 19 respectively. For the fluid equations, the former corresponds to impose the velocity field, while the latter consists in imposing the normal stresses.

$$u(x, t) = \bar{u} \quad (18)$$

$$\sigma(x, t) \cdot n = \bar{t} \quad (19)$$

Besides the Dirichlet and Neumann boundary conditions, it is also possible to prescribe an appropriate combination of these two, called Robin boundary conditions.

5.2 Structure Domain: The Artery Wall

Arteries exhibit non-linear elastic behavior, where the material does not follow Hooke's Law Fig.5.2.1(b). Due to the properties of its constituents, the arterial wall exhibits a non-isotropic nonlinear response to cyclic pressure loads Fig.5.2.1(a). The relationship is non-linear showing that as the stress in an artery increases, the material becomes stiffer and resists the strain. Moreover, the arteries are tethered mainly longitudinal by the surrounding tissue observed using a change in the geometrical ratio between the diameter and thickness of the arterial wall. Due to these complex properties, it formally is not possible to define Young's modulus as done in linear elastic theory. Still, in order to obtain a global idea of the elastic behavior, it is possible to lump all properties together as if the arterial wall was homogeneous and measure the stress-strain relationship. In such cases, we define Young's modulus as the slope of the curve at a given stress-strain point as shown in Fig 5.2.1(c), linearized about an equilibrium state, for instance, the mean or diastolic pressure yields an incremental effective Young's modulus, defined as

$$E = \frac{d\sigma}{d\varepsilon} \quad (20)$$

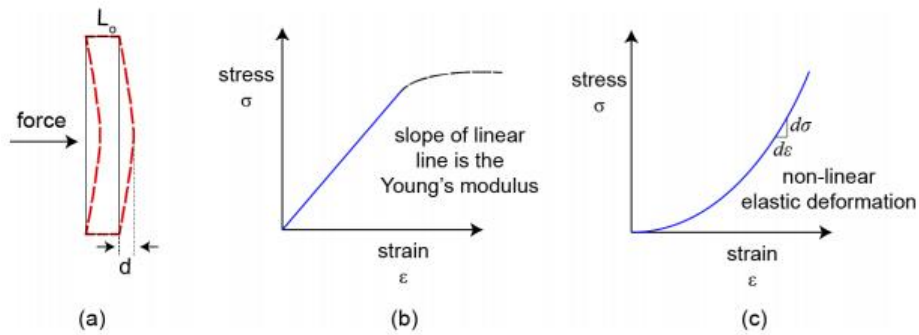


Figure 5.2.1 Non-linear elastic response due to cyclic pressure loads

Small displacements, for FSI problems that involve small displacements, the fluid-flow field can be solved assuming that the structural displacement does not affect the flow field. As a result, steady-state FSI problems with small displacements involve only a one-way coupling between

fluid and structure. That is, displacements (and stresses) of the structure are affected by the flow field, but the flow field is not affected by the structure.

Large displacements, for FSI problems that involve large displacements, the flow field is affected by structural deformations. As a result, the fluid and structure exhibit a two-way coupling, and it is necessary to resolve the fluid flow problem after each update of the structural configuration. In this sense, the FSI problem can be considered a moving-boundary problem. An additional level of nonlinearity is introduced in such problems because the fluid and the structural problem must be solved iteratively.

Following are the structural equations following Tube's law,

$$P(\eta) = (1 + \nabla_0)S(\eta) \quad (21)$$

$$S(\eta) = 2\mu E + \lambda \text{tr}(E)I \quad (22)$$

$$E = \frac{1}{2}(\nabla_0\eta + \nabla_0^T\eta + \nabla_0^T\eta\nabla_0\eta) \quad (23)$$

Where, $\lambda = \frac{E\varepsilon}{(1+\varepsilon)(1-2\varepsilon)}$ $\mu = \frac{E}{2(1+\varepsilon)}$ are Lamé constants

$$\rho_w \frac{\partial^2 \eta}{\partial t^2} - \text{div}(P) = 0 \quad (24)$$

where ρ_w is wall density, η is wall displacement, E is Young's modulus of elasticity & ε is Poisson's ratio ($\varepsilon = 0.5 \rightarrow$ incompressible material). Differences in the flow field due to structural deformation are primarily caused by the effect of such deformation on the mesh. Therefore, in problems that involve large displacements, the fluid mesh must be adjusted after each update of the structural configuration. When the structural displacements are of the same order of magnitude as a characteristic length of the flow domain, the re-meshing problem becomes extremely complex and is likely to constitute the most challenging step in the simulation.

The Dirichlet boundary condition imposes displacements, and the Neumann boundary condition imposes tractions. A Robin boundary condition is a weighted combination of Dirichlet and Neumann boundary conditions and acts to impede displacements and changes in displacement of the boundary.

$$u(x, t) = \bar{u} \quad (25)$$

$$\sigma(x, t) \cdot n = \bar{t} \quad (26)$$

The most basic form of Robin boundary condition essentially states that the surface traction is proportional to the displacement on the boundary and is given by

$$\sigma(x, t)n = -ku \tag{27}$$

where k is the spring constant or foundation stiffness.

5.3 Fluid-Structure Interaction Theory

Fluid-structure interaction scenarios are those that involve the coupling of fluid mechanics and structural mechanics. In an FSI problem, the stresses and deformations of a given structure are computed simultaneously with the flow parameters that surround the structure. That is, the deformations of the structure are due to the pressure gradients of the fluid, and likewise, the pressure and velocities depend upon the deformation of the structure illustrated in Fig 5.3.1.

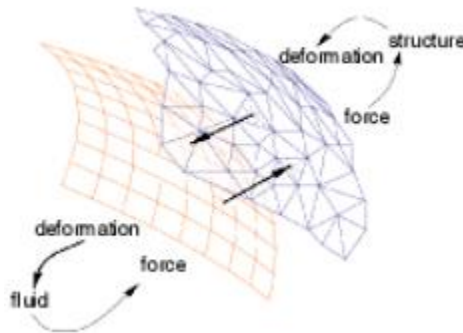


Figure 5.3.1 Transfer of forces & displacements between an arbitrary mapped fluid & structural mesh faces

Fluid-structure interaction problems can be simple or complex. For example, the computation of stresses for a given flow field and fixed structural configuration represents a simple problem. Complex problems are those that involve large structural deformations, changes in topology, contact problems, and geometric and material nonlinearities. The complexity of any given FSI problem is determined, in large part, by the extent to which the structural component is displaced. Simple FSI problems typically involve structures that do not undergo large displacements. Conversely, problems that involve large structural displacements tend to be complicated. Concerning structural displacements in FSI problems, the terms "small" and "large" are relative and problem-specific. In some problems, displacements on the order of a few millimeters can significantly affect the flow field. As a general rule, however, displacements are considered

significant only if they are of the same order of magnitude of the smallest length scale that is relevant in the simulation.

5.4 Arbitrary Lagrangian-Eulerian (ALE) Method

The motion of fluids and solids can be described in two ways, Lagrangian and Eulerian. In the Lagrangian formulation, the motion of particles is tracked in space, whereas in the Eulerian formulation, particles move through a controlled fixed volume. For finite element analysis, in the Lagrangian formulation, material points are fixed to the mesh, while in the Eulerian formulation, material points move through a fixed mesh [99]. For this reason, the Lagrangian formulation is typically used for solids, while the Eulerian formulation is for fluids.

A problem arises, however, in the use of a purely Eulerian formulation for a fluid model containing moving boundaries, since the fixed mesh through which the particles move is also moving. In this case, a hybrid formulation known as the ALE method is appropriate. In this method, the Eulerian formulation is used at fixed boundaries, the Lagrangian formulation is used at moving boundaries, and the ALE formulation is used at the fluid-structure interface. In the governing equations of the ALE formulation, the actual fluid velocity concerning a fixed mesh is replaced by a relative velocity relating the actual fluid velocity to the mesh velocity. In doing so, the conservation equations for fluid, structure and at the interface are modified as represented in Fig 5.4.1,

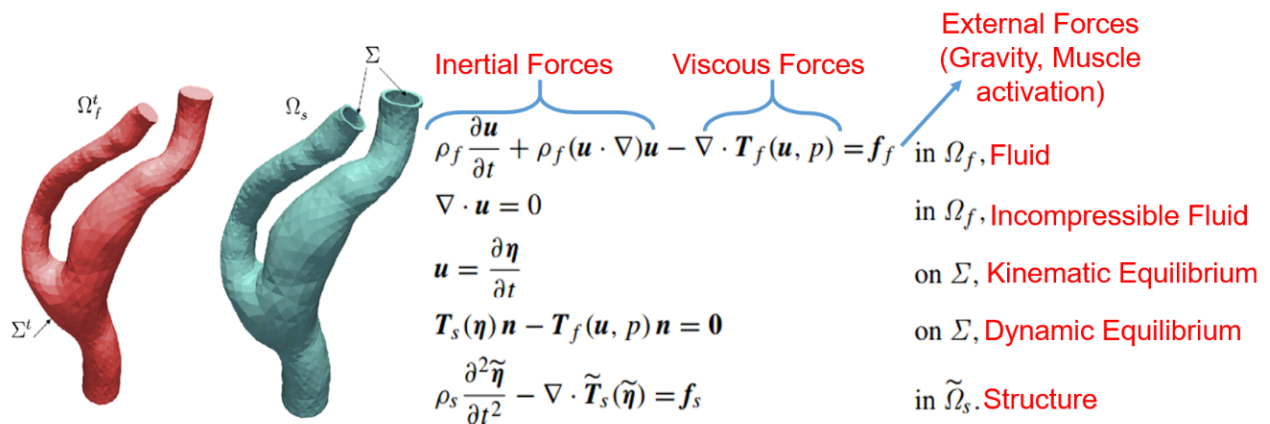


Figure 5.4.1 FSI governing equations

5.5 FSI Modeling

In industry and research, the finite element method (FEM) is primarily used for structural modeling while the finite volume method (FVM), often referred to as CFD is used for fluid modeling. Coupling these two methods is a common approach to FSI modeling and the one used in this project. Under FEM, a set of equations nonlinear in velocity are linearized to be numerically approximated using time & spatial discretization techniques. Resulting equations are solved for finding the current position at each time-step in an iterative procedure until the convergence criteria are met. FVM discretizes the conservative form of transport equations over a region of control volumes to form a set of coupled equations. Several methods can solve these algebraic equations determined towards the end of FEM and FVM. The ANSYS Academic Research is used to simulate the entire FSI system. The ANSYS Workbench System Coupling component is used to couple ANSYS® Mechanical™ software, FEM code, with ANSYS Fluent software, the FVM solver, in an implicit manner.

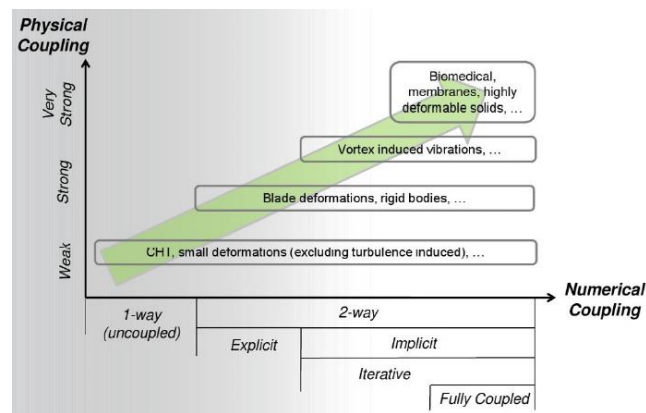


Figure 11 Biomedical computational models demand a fully coupled FSI

For FSI simulation of blood flow, a structural model of the artery needs to be coupled with a fluid model of the blood flow. Two dominant methods of FSI coupling exist as shown in Fig 5.5.1. First is a monolithic approach, where the coupling forms a single set of equations so that the fluid and structure models are solved simultaneously. Alternatively, in a staggered approach, the fluid and structure are solved as two separate systems (partitioned) sequentially. For strongly-coupled FSI problems, an implicit coupling scheme and relaxation techniques are required to mitigate the numerical instability inherent in partitioned FSI algorithms known as the artificial added-mass

effect. The monolithic coupling approach does not suffer from the added mass effect; however, it is affected by a number of its numerical issues.

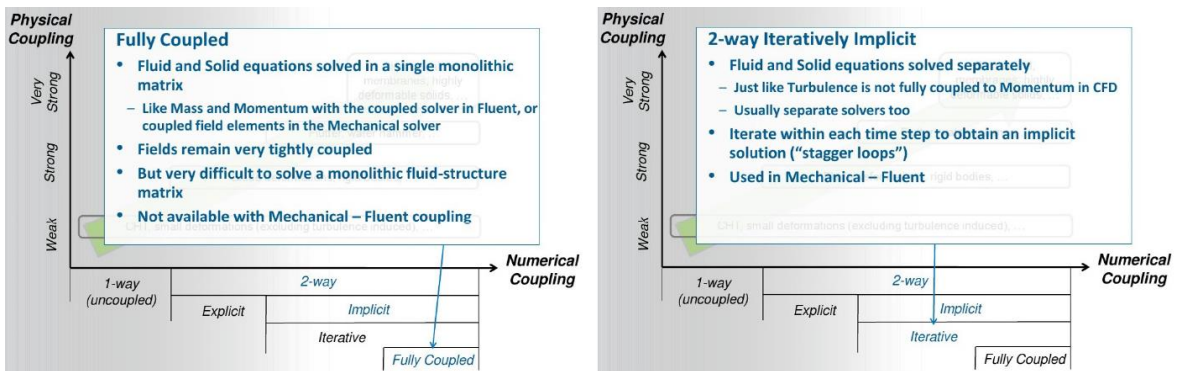


Figure 12.5.2 Advantages of two-way FSI

The sequential-staggered approach solves the system in coupling steps where each model is solved once, and the solutions on the interface boundary are exchanged between the subsystems described in Fig 5.5.2. For the problem, where the pressure forces on the structure are solely dependent on the fluid solution, the fluid model should be solved first each coupling iteration.

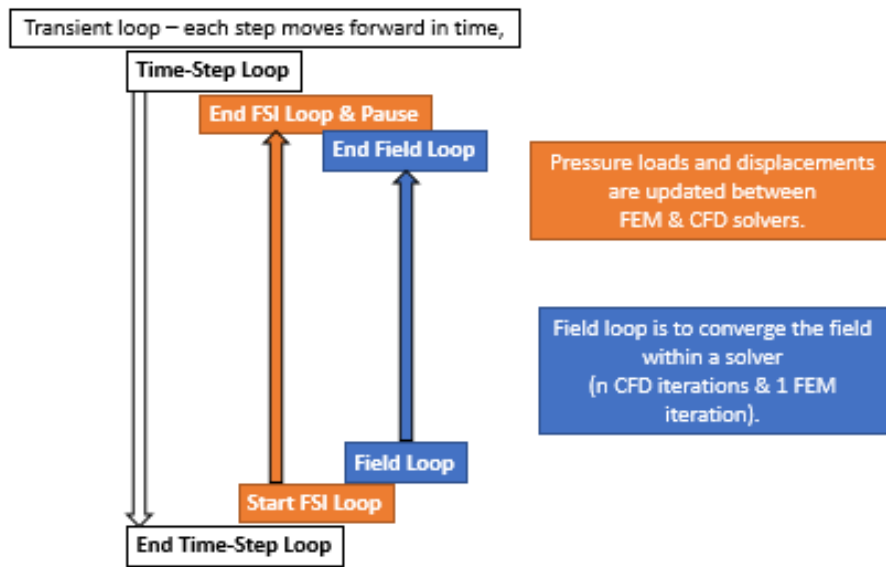


Figure 5.5.3 FSI iterative loops

The General Grid Interface (GGI) algorithm [100] implements a scheme in transferring the fluid model boundary solution (the pressure) as the conservative variable force, from the fluid boundary mesh to the structure boundary nodes. To transfer the non-conservative structure boundary solution (the displacement) the Smart Bucket (SB) algorithm [101] is executed. Once the fluid model

receives a boundary displacement solution update from the structure model a dynamic mesh is smoothing operation is performed to deform and maintain a mesh quality as the process illustrated in Fig 5.5.4. The convergence of the FSI model is achieved when each of the solvers is converged, and the change in each of the boundary solution transfers between coupling steps is considered negligible.

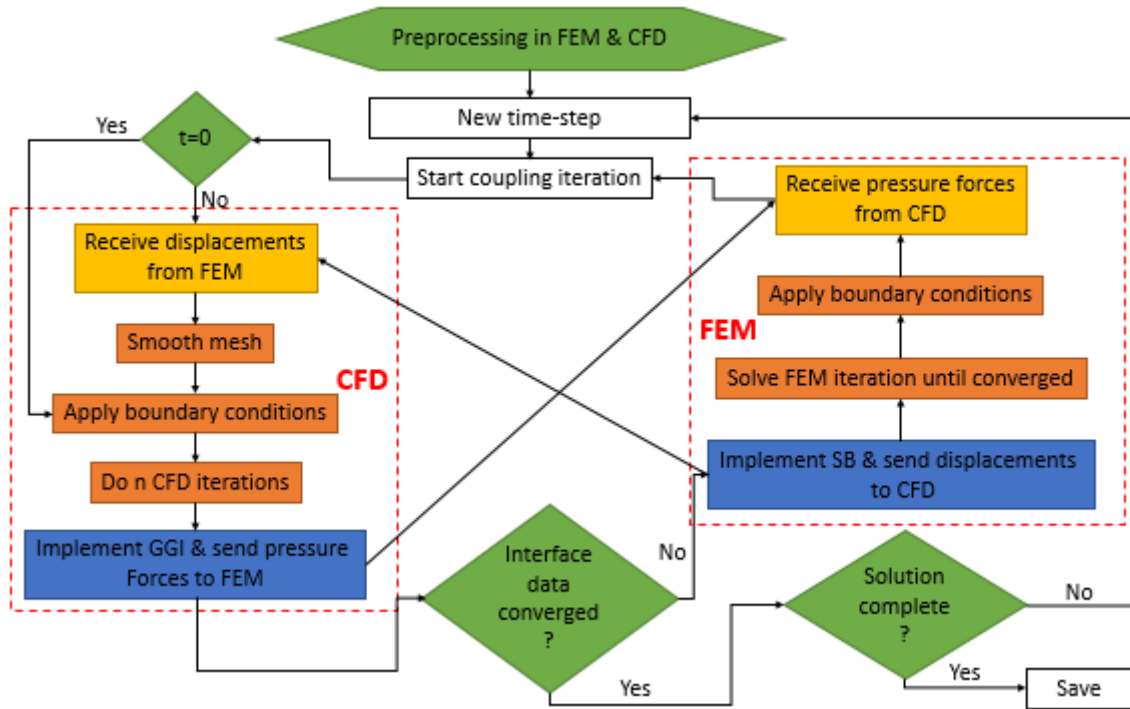


Figure 5.5.4 FSI process

FSI system is converged when the change in the solution transfers between coupling steps have both converged along with the CFD iterations. The FEM model converges fully during each coupling step. The fluid model is required to solve at the end of each time step, regardless of if the staggered sequence starts with the fluid, so that the FSI boundaries are conformal at the end, and start, of each time-step. Coupled FSI convergence is determined at the end of each coupling step from the normalized root mean square of the change in the solution transfer which is given by

$$RMS_{change} = \sqrt{\left(\frac{\Phi_i^n - \Phi_i^{n-1}}{1/2(\max|\Phi| - \min|\Phi| + |\Phi|)}\right)^2} \quad (28)$$

To overcome the added-mass effect instability in FSI coupling specific relaxation techniques are required. However, these techniques slow the convergence rate of the FSI simulation increasing its computational expense. Modeling the blood flow through the artery walls at each coupling step,

make FSI models of strongly coupled cardiovascular systems take many times longer to simulate than the corresponding fluid model alone [102-104]. Numerical instabilities under certain combinations of physiological parameters are caused for a given geometry, as soon as the density of the structure is lower than a certain threshold or for a given structure density, as soon as the length of the domain is greater than a certain threshold.

Added-mass is the inertia added to a system because an accelerating or decelerating body must move some volume of surrounding fluid as it moves through (incompressibility constraint). A significant issue with this is that it increases as the time-step size decreases. The oscillation will develop in the first time step. The case may fail within the first few coupling iterations, or it may make it to the second or third time-step, with oscillation growing in magnitude. The stronger the physics coupling between structure and fluid, the more unstable the added mass-effect becomes. The following criteria set a stronger coupling between the fluid and structure: a lower stiffness or a thinner structure geometry, a higher viscosity fluid, a higher pressure changes within the fluid, and the closer the fluid-structure density ratio is to unity. A useful technique in very strongly coupled FSI problems is to modify the FVM (CFD) continuity equation so that the diagonal entries of the linear matrix system are rescaled by,

$$a_{ij} = a_{ij} + KV\delta_{ij} \quad (29)$$

For all $i, j \in 1, 2, \dots, n$ where n is the number of cells adjacent to the FSI boundary, K is the scaling factor and, V is the volume of the cell adjacent to the boundary. The Kroenecker delta function δ_{ij} is defined as

$$\delta_{ij} = \begin{cases} 0 & \text{if } i \neq j \\ 1 & \text{if } i = j \end{cases} \quad (30)$$

Increasing the scaling factor K improves the diagonal dominance of the cells adjacent to the coupling interface. This slows the convergence rate of the fluid such that the force transfer changes are more smooth. The effect is similar to that of under-relaxation but is applied only to the solution on the boundary. The strength of the boundary source coefficient stabilization method is that it slows the rate of convergence primarily on the boundary so that less overall efficiency is lost in modelling the FSI problem.

5.6 In-house 1D Code

A 1D model of the human artery was initially proposed by Euler in 1755 [105] and resulted in a primary system of two non-linear partial differential equations for the conservation of mass and momentum for inviscid flow. Nevertheless, only in the 1970s, the first solution of the linearized 1D model was provided. Since then, 1D models for blood flow have been widely applied [106, 107]. They provide a fair description of the flow motion in arteries and the mechanics of its interaction with the wall displacement.

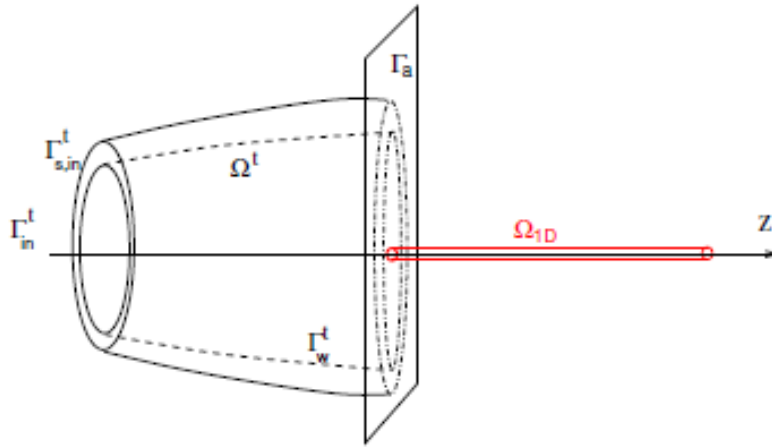


Figure 5.6.1 Sectional view of coupling a 3D model exit (downstream) with a reduced 1D model. In this work, we will adopt the approach proposed in [107], where the 1D model is obtained using a simplification of the 3D incompressible Navier-Stokes equations coupled with a structural model for the artery wall as shown in Fig 5.6.1. More precisely, the 1D model accounts for the evolution, in time and the artery axial direction, of the mean quantities: flow rate, mean pressure, and area. This model has been successfully implemented in MATLAB [93] in an in-house research study. There, the evolution in time and the axial coordinate of the mean quantities over the major the arteries of the human circulatory system was analyzed. Namely, the wave propagation of blood from the heart to the circle of Willis was studied. The computational algorithm can simulate the fluid-structure interaction in pulsatile blood flow in the arterial system and is validated against well-known numerical, in-vitro and in vivo data from different cases of human arterial trees [84,85]. The feasibility of tracking variations of cardiovascular markers, such as the blood pressure or stroke volume, have been previously studied experimentally by measurement of the pulse transit time. Governing partial differential equations,

Mass Conservation

$$\frac{\partial A}{\partial t} + \frac{\partial Au}{\partial x} = 0 \quad (31)$$

Momentum Conservation

$$\frac{\partial u}{\partial t} + \frac{\partial}{\partial x} \left(\frac{u^2}{2} + \frac{P}{\rho} \right) = +K_r \frac{u}{\rho A} \quad (32)$$

Tube Law (FSI)

$$P = P_e + P_v \quad (33a)$$

$$p_e = 2\rho c_{mk}^2 \left(\sqrt{\frac{A}{A_0}} - 1 \right) \quad (33b)$$

$$p_v = \frac{\Gamma}{E} \frac{\rho c_{mk}^2}{2\sqrt{AA_0}} (VA)' \quad (33c)$$

5.7 Geometrical Multiscale Approach: 3D-1D Coupling

Developing a robust 3D fluid-structure interaction model to study the arterial tree and cardiovascular diseases (CVDs) is a highly desirable case. A common approach to handle dimensionally heterogeneous models is to decompose the global domain into subdomains where the partitioning takes place at the interfaces between the models. Prescribing the continuity of the flux and continuity of the normal stresses at the coupling interfaces, the interaction between the subdomains is induced through the transfer of interface boundary values. It is known as “geometrical multiscale approach,” one of the main advantages of coupling multiscale models, is the study of complex interactions between global and local scale hemodynamics in the arterial tree and specific arteries, respectively.

However, computation, cost and time limitation of a 3D approach prevents the researchers from building such complex and large models. Much more complicated than the assessment of conditions for the existent natural boundaries, is to set proper conditions on the artificial sections. In this case, they cannot be obtained from physical boundaries and can be a significant source of numerical inaccuracies during the resolution of the problem. Precisely, the issue relies on the fact that for those interfaces there is the need to account for the remaining parts of the arterial system, for which it is challenging to obtain appropriate boundary data.

5.8 Artificial Boundaries

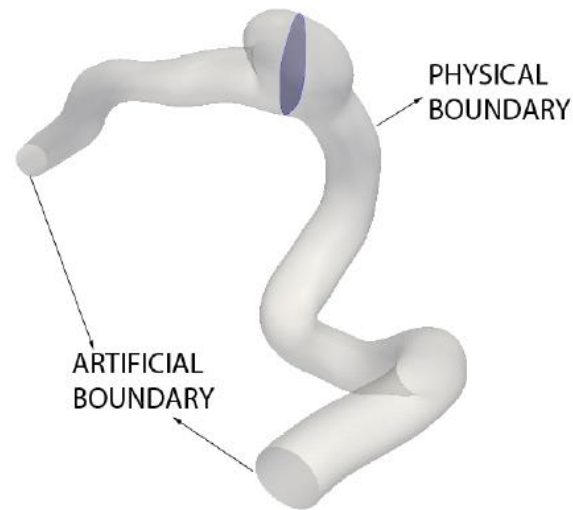


Figure 5.8.1 Artificial Boundaries

From a mathematical point of view, the 3D Navier–Stokes problem requires the scalars (such as the velocity components or the projection of the Cauchy stress tensor on the surface normal) at each point of the discretized boundaries. Very often the available data provided from medical measurements or reduced 1D models are expressed in terms of mean quantities such as the flow rate $Q(t)$ or mean pressure $P(t)$, rather than in pointwise quantities which are required for the 3D equations. In de Moura [108] continuity of the spatially averaged total (static + dynamic) pressure is preferred above continuity of the spatially averaged static pressure, as for this case conditional stability of the iterations between the 3D and 1D FSI models is proved analytically [109]. Nevertheless, whenever the dynamic pressure is small compared to the static pressure, both the continuity of pressure and total pressure work equally well in terms of a number of iterations between the 3D and 1D model and spurious wave reflections generated at the interface. On the other hand, clamping the vessel wall at the interface is unphysiological, since it generates spurious wave reflections at the interface. Still, the continuity of the flux and spatially averaged total pressure does not guarantee the continuity of the cross sectional area at the interface. One can impose a zero stress boundary condition on the structure interface. However, in curved geometries, this might result in undesired wall deformations. These conditions are referred to as defective boundary conditions, are insufficient to generate a well posed problem, since its solution is not unique. Several approaches have been advocated to well pose the flow rate and the mean pressure problems. For instance, in [110] the mean pressure problem is overcome by imposing the mean

pressure as constant normal stress on the artificial section Γ_i by means of the following Neumann boundary condition,

$$\sigma(u, p) \cdot n = P_i n \text{ on } \Gamma_i \quad (34)$$

A simple yet numerically most interesting case is the study of the propagation of a pressure pulse in an artery. This phenomenon illustrates the potential of the 1D model as an absorbing boundary condition, eliminating spurious wave reflections at the interface (inlet/outlet) of the 3D model [111]. Although this case is not physiological in terms of geometry and boundary conditions, it is beneficial for validation and to assess the characteristics of the coupling and, in particular, the reflections generated at the interface. The linear theory predicts that the pulse wave travels down the arterial system without change of shape, but with reflections from bifurcations, etc. Measurements show the pulse steepens and smoothens. Nonlinear effects give the characteristic directions in the form of Riemann invariants.

$$R_{\pm} = u \pm \frac{p}{\rho c} \quad (35)$$

Where u is velocity, p is pressure, c is pulse wave velocity (PWV) and quantities R_{\pm} are Riemann invariants, constant on the appropriate characteristics.

5.9 In-house 3D-1D Coupling Formulation

In this work, two arterial segments of the cardiovascular system are coupled using the geometrical multiscale approach. More precisely, the 3D model will be coupled with reduced, 1D models at the artificial boundaries in order to benefit from the higher accuracy of 3D while maintaining the computational speed offered by 1D models.

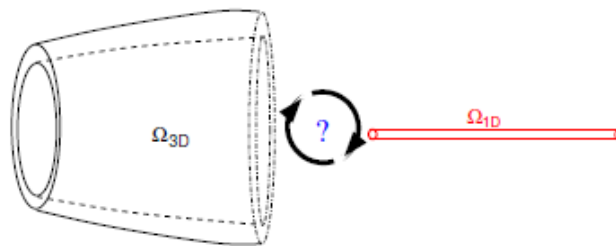


Figure 5.9.1 Coupling a 3D & a 1D model requires an interface formulation

Others usually develop their 3D and 1D code and couple them, such as Quarteroni *et al.* [75]. The idea behind these techniques is to reinterpret the original coupled problem as an interface problem

in terms of interface variables. Coupling interface formulation as needed in Fig 5.9.1, which communicates between for the two-way exchange of data in the 3D-1D interface. Following a set of coupling equations are employed at the coupling interface,

Continuity, where A , u are cross-sectional area and velocity

$$u_1 A_1 = u_2 A_2 \quad (36)$$

Conservation of momentum, where P is Pressure

$$\frac{p_1}{\rho} + \frac{1}{2} u_1^2 = \frac{p_2}{\rho} + \frac{1}{2} u_2^2 \quad (37)$$

Forward propagating linearized characteristic wave R_+

$$u_1 + \frac{p_1}{\rho c} = R_+ \quad (38a)$$

Backward propagating linearized characteristic wave R_-

$$u_2 - \frac{p_2}{\rho c} = R_- \quad (38b)$$

5.10 Coupling Implementation using ANSYS & MATLAB

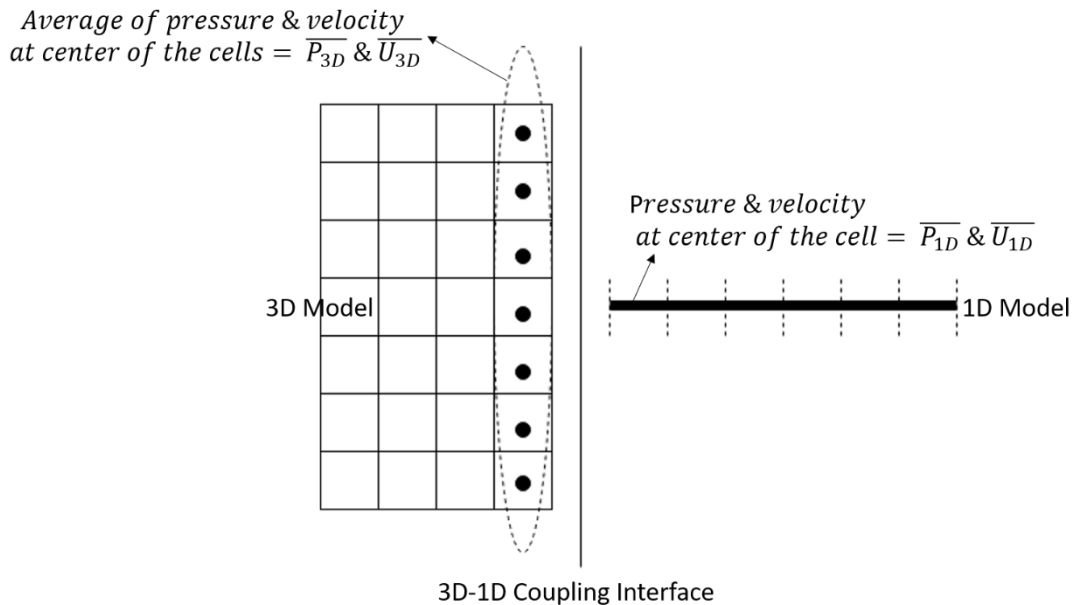


Figure 5.10.1 Variables needed to facilitate coupling

As mentioned in Fig 5.10.1, variables needed for implementing the in-house coupling formulation are average values of pressure & velocity at the center of the cells on 3D boundary face at the

interface and averaged values of pressure and velocity at the cell of the 1D boundary node at the interface.

In the implicit coupling, sub-iterations between the 3D and 1D models are performed at each time step. A solution of the coupled problem is approximated iteratively, by resorting to a splitting strategy, i.e., each model is solved separately and yields the resultant information to the other model.

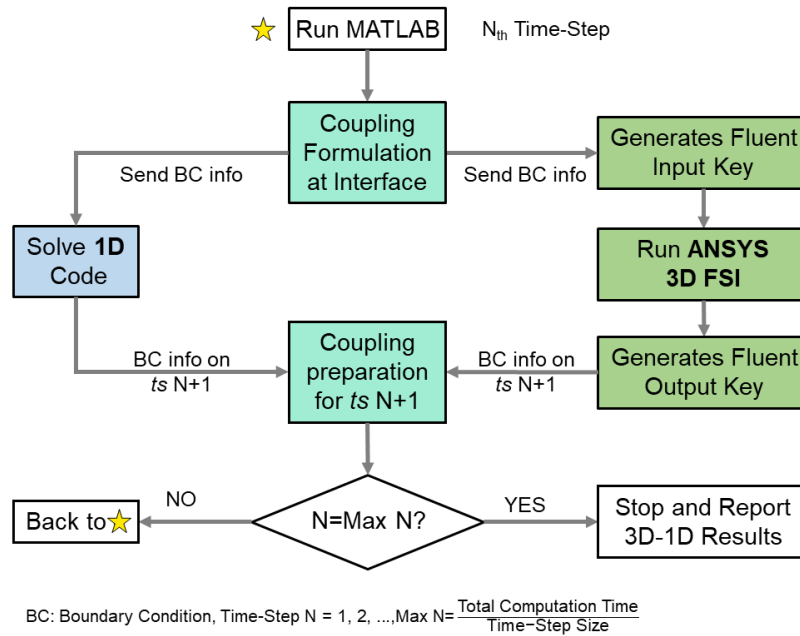


Figure 5.10.2 Coupling implementation scheme

Here is the sequence of operations executed within each time-step or 3D-1D coupling step also represented in Fig 5.10.2,

- At first time-step, an Input m-code (MATLAB), transfers initial boundary conditions (velocity and pressure) to the 1D m-code and a Coupling Interface m-code generates an ANSYS Fluent input key with initial boundary information (velocity or total pressure).
- 1D m-code solves for mean velocity and means total pressure and pauses.
- ANSYS 3D FSI retrieves input key, a *read-key* User Defined Function (UDF) in Fluent reads the input key to apply either a velocity profile or total pressure on the 3D as Navier-Stokes solves for the other. A *write-key* UDF in Fluent generates a Fluent output key with boundary information of pointwise area-weighted average of velocity and pressure in the 3D and pauses.

- At the end of first time-step, Coupling Interface m-code reads both Fluent output key and 1D solution to obtain the averaged data at the coupling boundary and solves using conditions described in formulation then moving forward to the next time step. This process is repeated for every time step.

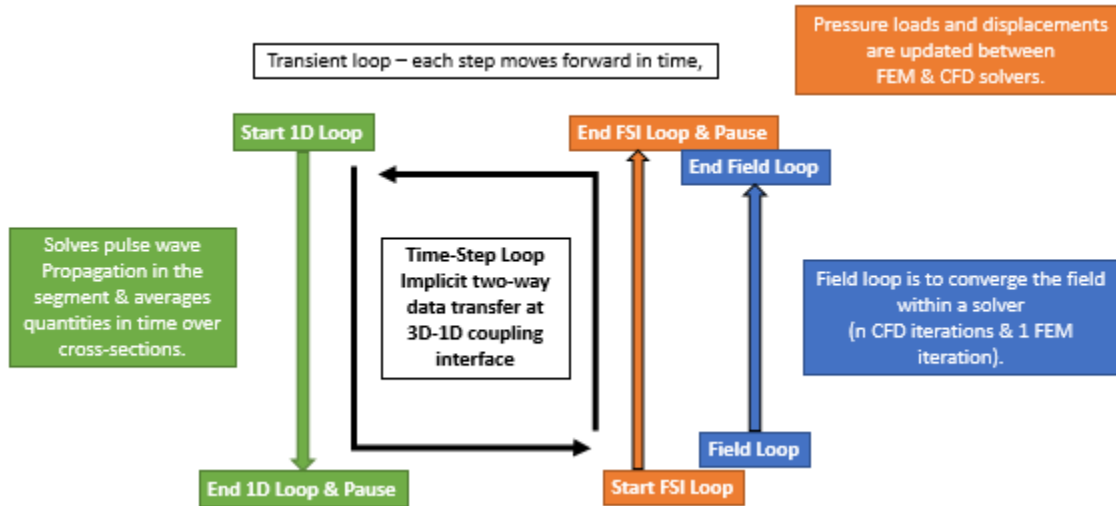


Figure 5.10.3 A multiscale coupling process employing ANSYS & MATLAB

6 IMPLEMENTATION & RESULTS

A computational modeling and coupling methodology between the 3D and the 1D code in the respective interfaces is required, is the objective of numerous authors. Here, we employ commercial tools to investigate 3D FSI (ANSYS) problem. Then intertwine it with 1D numerical (MATLAB) code. The computational model is configured and simulated in ANSYS Workbench software. The blood model mesh and vessel wall geometry and mesh constructed from the blood model are implemented in Workbench modules ANSYS Fluent for CFD solvers & Mechanical for FEM solvers. These two models are coupled in Workbench using the System Coupling module to form the 3D FSI model. For a more detailed description of the approach used in this project, please refer to the ANSYS Fluent User's Guide and the ANSYS System Coupling User's Guide.

Ansys Fluent is written in the computer language C and makes use of the flexibility and variety offered by the language. User defined functions (UDF) written in C may also be appended to Fluent, thus increasing its versatility.

MATLAB is a high-level language and interactive environment for numerical computation, visualization, and programming. Using MATLAB, one can analyze data, develop algorithms, and create models and applications. The language, tools, and built-in math functions enable one to explore multiple approaches and reach a solution faster than with spreadsheets or traditional programming languages, such as C/C++ or Java.

6.1 3D FSI Model

6.1.1 Blood Domain: Geometry

The carotid artery is shown in Fig 6.1.1 a blood vessel highly susceptible to the anatomical pathologies due to bifurcation, high turbulence/reverse flow, etc., causing the formation of atherosclerosis as it can influence the blood flow to the brain which leads to the stroke. Blood flows in a pulsatile manner from the common carotid artery (CCA) inlet toward the bifurcation junction of the carotid. While the blood continues along the external proportion carotid artery (ECA) artery flows toward the face and the neck. The internal carotid artery (ICA) part supplies the blood to the brain. A center-line & spline geometry as listed in Table 1 is developed using SolidWorks for the specifications outlined in the literature.

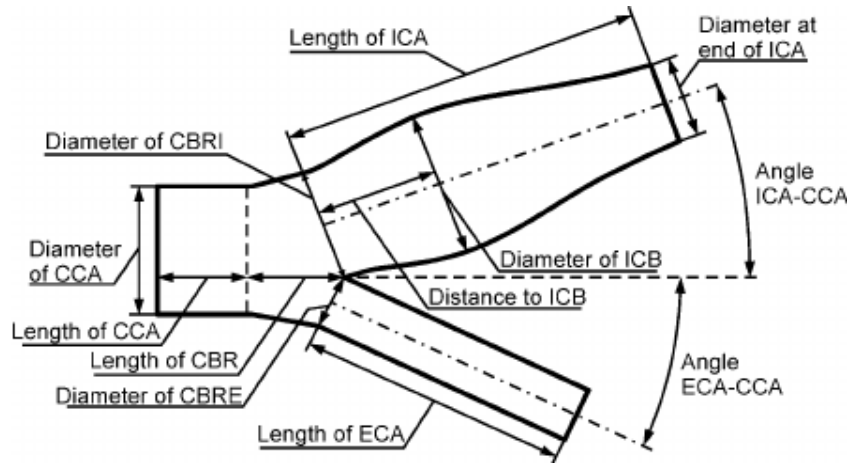


Figure 6.1.1. Carotid artery bifurcation Perktold et al. [49,51]

Table 4 Geometry Specifications

GEOMETRY SPECIFICATION	DIMENSION (MM)
DIAMETER OF THE CCA	6
LENGTH OF THE CCA	7
DIAMETER OF THE ICA	6.5
LENGTH OF THE ICA	26
DIAMETER OF THE ECA	3.6
LENGTH OF THE ECA	18
DIAMETER OF ICB	6.5
DISTANCE TO ICB	5.3
DIAMETER AT THE END OF ICA	4
ANGLE B/W ICA AND CCA	250
ANGLE B/W ECA AND CCA	250
WALL THICKNESS	0.2

Circular cross-sections were then created perpendicular to the axis at each point of the spline curvature bend. Cross-sections were then swept through the curves constituting the bifurcated artery. These surfaces were blended with rounding to follow the shape of the carotid artery bifurcation best to enclose the blood domain. This surface model, shown in Figure, was then exported to ANSYS DesignModeler component of the Fluent to ensure its compatibility with ANSYS Fluent software for final editing. The ends of the domain were extended to varying degrees in DesignModeler to ensure that the inlet and outlet lengths were sufficiently long for the blood model.

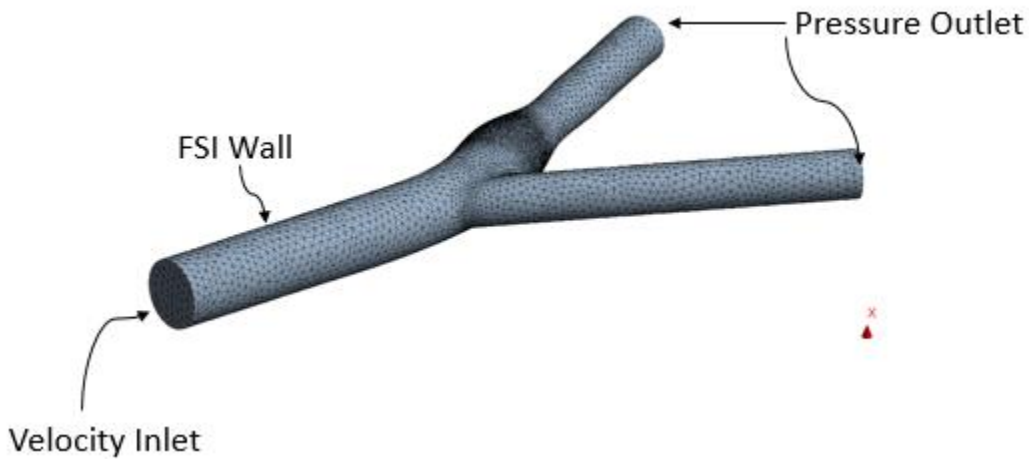


Figure 13 Blood domain boundaries

6.1.2 Blood Domain: Material behavior and boundary conditions

Blood is modeled as a Newtonian blood while the upstream, and downstream behavior, is replicated with inlet velocity profile and a uniform pressure outlet boundary conditions (BC) respectively as shown in Fig 6.1.2. In the arterial system, blood ordinarily demonstrates Newtonian behavior, where the viscosity remains relatively constant, as a result of high shear rates above 100 s^{-1}). Although studies have found that WSS in the arteries are underpredicted by a Newtonian model, we decided to model it as such and limit the complexity of the blood model to focus on creating an optimally stable FSI model. We thus assume blood to be an isotropic, homogeneous, and incompressible Newtonian blood with a density of 1060 kgm^{-3} and a viscosity of $3.5 \text{ Pa}\cdot\text{s}$.

A standard approach in CFD modeling is to prescribe a velocity BC at the inlet of a domain and pressure at the outlets, for a well-posed and robust numerical system. An inlet flow boundary condition is imposed on the inlet of each model using a velocity profile. This produces a time-

varying and spatially constant velocity profile across the inlet that mimics the left common carotid artery flow profile illustrated in Fig 6.1.3 [105] over each cardiac cycle.

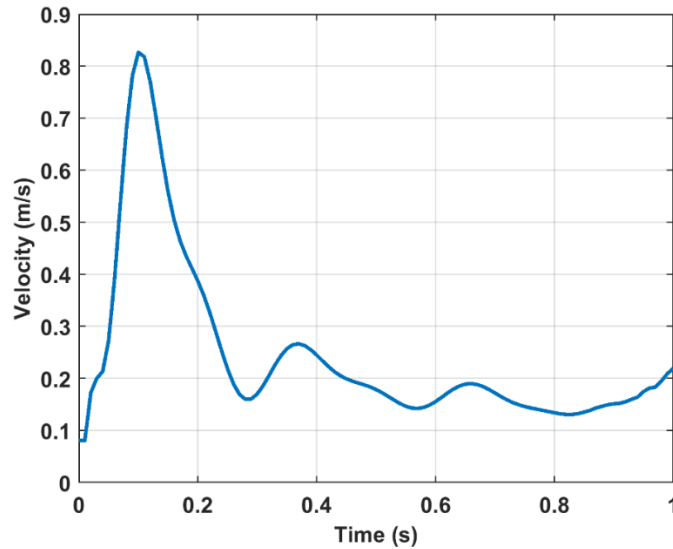


Figure 6.1.3 Inlet Velocity Jasanova et al. [105]

Though prescribing a uniform velocity distribution is unphysical; however, this is admissible provided that the inlet is far enough upstream for the physically accurate flow profile to develop before reaching the region of interest, the bifurcation in our case. Prescribing a parabolic velocity at the inlet would likely have allowed the use of a shorter inlet length, decreasing the computation time for the blood and FSI models. The pressure outlet BCs are imposed by constant pressure of 0 or 13,332 Pa, while a no-slip boundary condition is imposed on the walls of the vessel. Vessel porosity is also ignored; therefore blood is considered not to penetrate through the walls as it flows through the vessel.

The ability to apply time-varying profile BCs is not a standard feature in ANSYS Fluent. However, its features can be enhanced and customized by writing a User-Defined Function (UDF), which is compiled and then implemented by the blood solver each blood iterations. The solver executes specific DEFINE Macros at different stages of the solution process to carry out functions that the user defines. The details of the DEFINE Macros we implemented in the UDF are summarised in Table 2.

Table 5 ANSYS Fluent UDF Macros

DEFINE MACRO	EXECUTED AT	SOURCE CODE
Profile	Each Iteration	Applies the time-varying velocity uniformly over all cell faces of the inlet
execute_at_end	End of time-step	Sets $h^t = h^{t+\Delta t}$

6.1.3 Blood Domain: Mesh Generation

Domain discretization is necessary in order to facilitate the numerical solution of partial differential equations. Most common meshing techniques use either hexahedral or tetrahedral elements. Hexahedral ensures that the mesh scales well, so that grid quality is maintained as the is refined and also been structured to minimize the amount of numerical diffusion by aligning the cells with the general direction of flow through the domain. Though hexahedral meshing is a simple method, it causes highly skewed cells to form. Furthermore, the quality of these cells deteriorates further as the mesh is refined. The boundary layers created to capture the velocity gradient near to the wall accurately and to gradually build curvature into the mesh as it reaches the outer circular shaped walls of the domain.

While this applies well for a rigid domain CFD problems, the mesh deformation that takes place in the FSI simulation is prone to developing skew cells, and in some cases cell inversion. This is issue grows further as the quality of the mesh decreases. Additionally, the displacements of the FSI boundary mesh are predominantly perpendicular to the boundary itself; our strategy thus inhibits mesh deterioration further by ensuring that the cells are principally orthogonal to the outer walls of the blood domain (the FSI boundary). Triangular prisms can be used with a tetrahedral mesh to accomplishes this to a degree, provided that the boundary layer thickness is large enough or excluded and the internal tetrahedral mesh is of sufficient quality. The current dominance of tetrahedral meshing can be attributed most notably to its ability to robustly mesh arbitrary, complex geometries. Also, the use of tetrahedral elements often simplifies the process of adapting the mesh during the simulation. Hence the domain of the problem is discretized into a tetrahedral volumetric mesh using CFD mesh methods.

6.1.4 Blood Domain: Solver settings and solution behavior

Since the momentum and continuity equations are coupled through the velocity terms, and the convective term in each of the momentum equations introduces a non-linearity, an iterative solution strategy is used in pressure-based solvers to converge to the true solution. A segregated approach is often used in CFD where the coupled equations are corrected one after another giving a robust and efficient method. The SIMPLE segregated algorithm or one of its derivatives can be used to update the velocity and pressure fields progressively.

An extensive array of solver schemes and settings were assessed to find the fastest convergence rate while maintaining accuracy. A time-step size of 0.005s was used for its temporal accuracy, convergence rate, and solution accuracy. The PISO pressure-velocity coupling scheme, a revision of the SIMPLE algorithm, is the preferred solver in ANSYS Fluent software for transient problems. This scheme did perform best in our model particularly with Skewness Correction, and Skewness-Neighbour Coupling deactivated. The critical solver settings we have used are summarised in Table 3. For larger time-step sizes the URFs need to be reduced to ensure stability and to attain an optimal, but slower, convergence rate.

Table 6 ANSYS Fluent Solver Settings

PISO Scheme Settings	
Skewness Correction	0
Neighbor Correction	1
Skewness-Neighbor Coupling	Off
Discretization	
Pressure	2 nd order upwind
Momentum	2 nd order
time	2 nd order implicit
URFs	
Pressure	0.2
Momentum	0.5

The opposite is true if the time-step size is decreased with a URF upper limit of around 0.4 for pressure. A necessary quantity in this regard is the Courant number which gives the approximate number of cells the blood passes through in one time-step. Courant number is calculated from

$$C = \frac{u_c \Delta t}{L_c} \quad (39)$$

where u_c and L_c are the characteristic flow velocity and cell length respectively. The stability of a typical blood solution is inversely proportional to the Courant number. To ensure that the model converges correctly for each time-step we monitored the scaled residuals, and the convergence of the velocity, pressure and WSS solutions over their respective domains. We note that the maximum values and integrals converged more than sufficiently if the scaled continuity residual decreased to a value of $1 * 10^{-4}$, hence this was chosen as the convergence criterion for our problem in both the FSI model. The residuals for the segregated x, y, and z momentum equations reduced to values between $1 * 10^{-5}$ and $1 * 10^{-6}$ at convergence, depending on the time-step size. With the optimal solver settings 90 iterations on average were required to converge within each time-step. A single cardiac cycle (pulse) requires less than 18-20 minutes to complete on an Intel®Xeon(R) E5 workstation with 20 cores (12 used) and 128 GB RAM.

6.1.5 Structural Domain: Geometry & Mesh

Shell elements can be used to generate an efficient structure. However, the use of shell elements requires the inlet and outlet extremities to be fixed in space, which is unphysical and likely to lead to significant error if the inlet and outlet lengths are short as in our model. A Robin BC is applied on the outer surfaces of the vessel walls to mimic the behavior of the tissue surrounding the vessel walls. This constrains the model adequately while allowing it to deform more naturally. At present, a Robin BC cannot be applied to shell elements in ANSYS Mechanical module.

To incorporate the Robin BC the blood boundary mesh is extruded to generate the geometry of the vessel walls. The blood artery wall was extruded to form the artery vessel walls. The arterial thickness is set to 1/10th of the lumen diameter, the approximate ratio according to and meshed with a combination of triangular and quad elements.

6.1.6 Structural Domain: Material

The vessel walls are made up of a complex set of layers of tissue with helically distributed collagen fibers. Increased tensile stress and deformation cause these fibers to reorient in the direction of the

principal strain so that the tensile strength of the vessel increases in this direction. Anisotropic hyperelastic material models can model this tissue and fiber behavior. However, in our case, we have assumed that the vessel walls follow the linearly elastic model described with Young's modulus of 0.24 MPa . The assumed Young's modulus corresponded to the mean (intima, media, and adventitia layers) Young's modulus of the aorta. The Poisson's ratio was set to 0.5. Arterial wall density was also specified as 1050 kgm^{-3} .

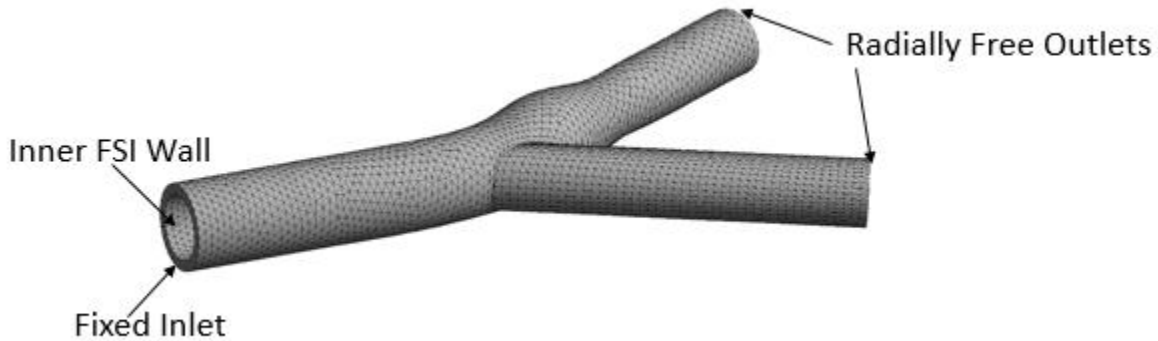


Figure 6.1.4 Structural boundaries

6.1.7 Structural Domain: Boundary and initial conditions

The model is constrained at the ends of the domain, at the inlet and outlet by Dirichlet BCs. The inlet is fixed in place fully to aid in stabilizing the FSI model where the pressure, and pressure changes, are highest. This BC has a negligible effect on the overall solution, especially in the region of interest, since it is far from the bifurcation. At the outlets, nodes are prevented from displacing axially and tangentially but are free to displace radially from the center-line made by each outlet.

6.1.8 Structural Domain: Solution method

A direct solver with a full Newton-Raphson method is used to iterate toward the solution. It is found that the use of multiple substeps to ramp the pressure BC in each time-step is not necessary. This only increased the solution time showing that Newton iterations alone were enough to converge efficiently to the solution at each time-step meaning one substep per time-step.

6.1.9 FSI set-up & analysis

To run, stabilize, and optimize an FSI simulation a few of the key features are required. The implicit FSI algorithm used follows the approach described in the methodology section. For mesh

update at every time-step in the FSI simulation, Fluent employs Dynamic Meshing feature. Dynamic Meshing allows a variety of smoothing methods, dynamic layering, and local meshing methods. The spring-based smoothing method is a very efficient mesh smoothing technique which maintained the initial blood mesh quality throughout the simulation. An adjustment of the Laplace Node Relaxation parameter was necessary to avoid cell deterioration, however. The spring-based method performs well for a tetrahedral mesh and when the boundary deformation is largely normal to that of the boundary surface itself, as it is in our case. The Laplace node relaxation parameter needs to be increased from its default value to 1 to ensure that the internal blood mesh nodes follow the boundary nodes correctly. This ensures that cell inversion and solution divergence do not take place. It is expected that values below unity could be used as long as they are close enough to 1; this has not been tested, however. The artery outlet faces require a dynamic mesh zone geometry with a faceted definition, blood domain as deforming and FSI boundary as system coupling with boundary stabilization parameter for the mesh motion to function correctly. Only the local remeshing method was used with designated minimum and maximum length scales and maximum cell skewness. To maintain wall refinement as the vessel wall expands, the maximum length scale is twice the minimum length scale with a maximum cell skewness is 0.6-0.7.

The time-stepping of FSI simulation is driven by the System Coupling component of the ANSYS Workbench. Since the blood solves iteratively, the changes in forces that are sent to the structure can be controlled to a degree by only fractionally solving the blood each coupling step. This is the mechanism by which the FSI model is stabilized. The structure model, on the other hand, converges fully (with a direct solver) each coupling step. The following simple changes have stabilizing effect on the FSI coupling:

- decreasing the number of blood iterations per coupling step,
- decreasing the blood URFs,
- increasing time-step size.

Increasing the time-step size can adversely affect the convergence rate of the FSI model, however. This is as a result of the increased time-step size decreasing the rate of convergence of the blood. This means that more blood iterations can be taken each coupling step while maintaining the FSI coupling stability. However, more coupling steps will be required to converge to the blood and overall FSI solutions. The effect is that the overall FSI convergence rate decreases if the time-step

is increased. Although the convergence rate of the FSI solution is negatively affected by an increased time-step size, the overall computational expense is decreased since fewer timesteps need to be taken to complete a simulation. The time required to simulate an FSI simulation of a single cardiac-cycle for each time-step.

Table 4 Computation time for an FSI case

Time-step size	No. of time-steps	Coupling iteration per time-step	Total CPU time per cardiac cycle
0.01 s	100	25	6 hrs
0.005 s	200	20	11 hrs
0.002 s	500	15	18 hrs

This table also shows the number of coupling steps required to converge each time step and the number of time-steps required to complete a simulation of a cardiac cycle. The computational time maintains a linear indirectly proportional relationship to the time-step size over the range of models tested. The FSI models were run on a Xeon(R) E5 workstation with 20 cores and 128 GB RAM; the blood model was run on 12 of the cores and the structure on 4.

A parameter that affects the FSI stability the most is the number of blood iterations carried out each coupling step. The fewer iterations the blood solution converges each coupling step, the more stable the FSI model is, this is easily achieved by carrying out fewer fluent iterations per coupling step. Another method is to lower the blood Under Relaxation Factors (URFs), this, however, has less of an effect on stability, and the effect diminishes further as the URFs are lowered. Excessively lowering URFs is a very inefficient method in decreasing the rate of convergence and increasing the stability of the blood.

The changes described above affect how much the blood solution converges each coupling step globally. This is not optimal since the FSI instability is caused purely by the changes in the solution at the FSI boundary. The boundary solution stabilization by coefficient-based method slows the convergence rate primarily on the FSI boundary. This method increases the stability of the FSI coupling while the blood convergence rate is not affected to the same degree as it is when URFs or number of blood iterations are decreased.

In weakly-coupled FSI problems, it is sometimes possible to achieve stability by ramping up the pressure solution that is transferred to the structure over a number of the coupling steps (as opposed to applying any of the changes above); this is implemented in the ANSYS Workbench software's System Coupling component. In strongly coupled problems, however, this will only delay the onset of the growth of the instability. Once the instability takes to hold the solutions to both models oscillate with an increasing degree until negative cells form, causing the FSI simulation to fail.

A combination of all of the above methods was required to stabilise the model optimally. The number of iterations needs to be decreased drastically, in our case to 4 iterations per time-step. We were able to stabilize the added-mass effect with a coefficient-based scale factor of 0.5 at the FSI boundary. The parameters that ensured optimal damping and simulation efficiency for a sufficiently small time-step size of 0.005 s are given in Table 5.

Table 5 Dynamic Mesh & System Coupling Settings

Stabilization setting	Value
Pressure URF	0.1
Momentum URF	0.2
Boundary stabilization method	Coefficient-based
Boundary stabilization scale factor	0.5
No. of the Fluent iteration per coupling iteration	4
No. of the pressure ramping coupling iterations (if required)	6
No. of the coupling iterations within a time-step	15

6.1.10 Results

Following results are plotted at four different time point comprising a range of conditions within a cardiac cycle to account flow acceleration and deceleration phases. These time points are shown in Fig 6.1.5, at 0.08s, 0.15s, 0.2s and 0.4s. Axial velocity contours are plotted at various cross-sections (axial slices) along the length of the artery.

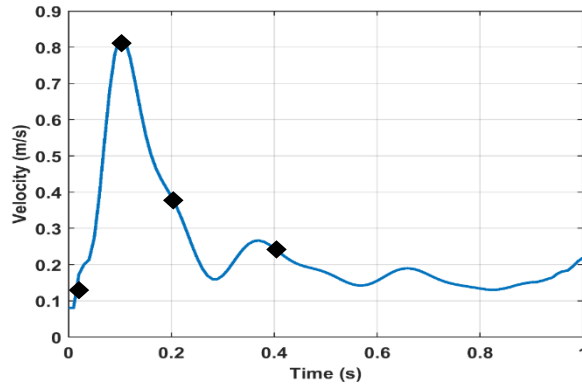


Figure 6.1.5 Acceleration & deceleration phases in a cardiac cycle

The flow in the CCA follows the curvature of the vessel and is slightly skewed towards the outer wall of the artery. Downstream of the bifurcation, a strong skewing towards the flow divider walls occurs as a result of branching for both ICA and ECA. The flow during the deceleration phase was more disturbed, and the region of reversed or low-velocity zones was larger than during the acceleration phase.

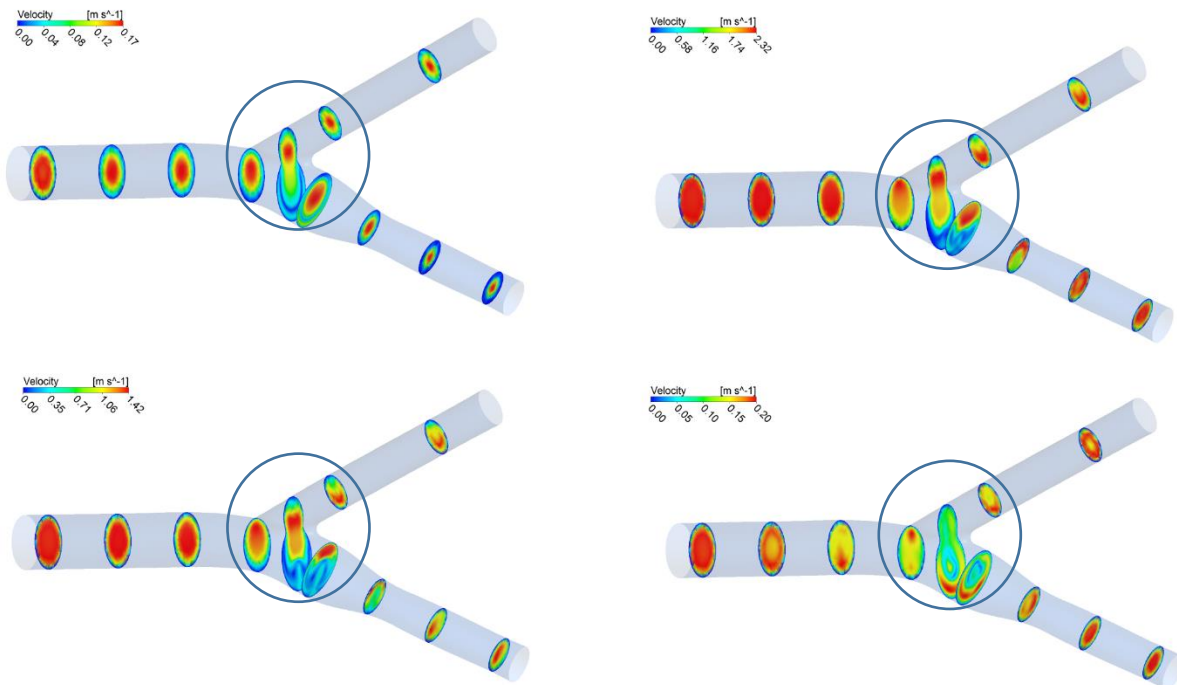


Figure 6.1.6 Axial velocity on axial slices

Areas of interest are circled in Fig 6.1.6, at bifurcation level and the sinus maximum diameter location. In Fig 6.1.7 & Fig 6.1.8, it can be seen that the reversed flow zones partially extend up

to the center of the cross section. Lower axial velocities can be observed on carotid sinus slices, especially during peak systole and diastole descend which implies that blood is recirculating around this area. Note that the velocities in the artery of the FSI model are lower than the respective velocity in the CFD model throughout the cardiac cycle. This should not be the case since the models are based on the same geometry and should agree at some stage of the cardiac-cycle. This is as a result of the large initial deformation in the FSI model. Because the initial configuration of the structure model is unstressed, the initial pressure causes the FSI model to deform initially while the blood model in Perktold et al. maintains its form.

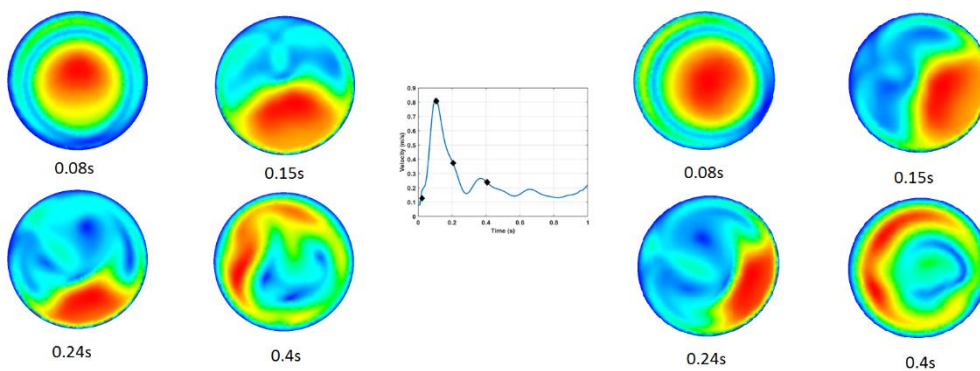


Figure 6.1.7 Axial velocity contours in normal plane view for CFD on the left and FSI on the right slightly tilted towards left

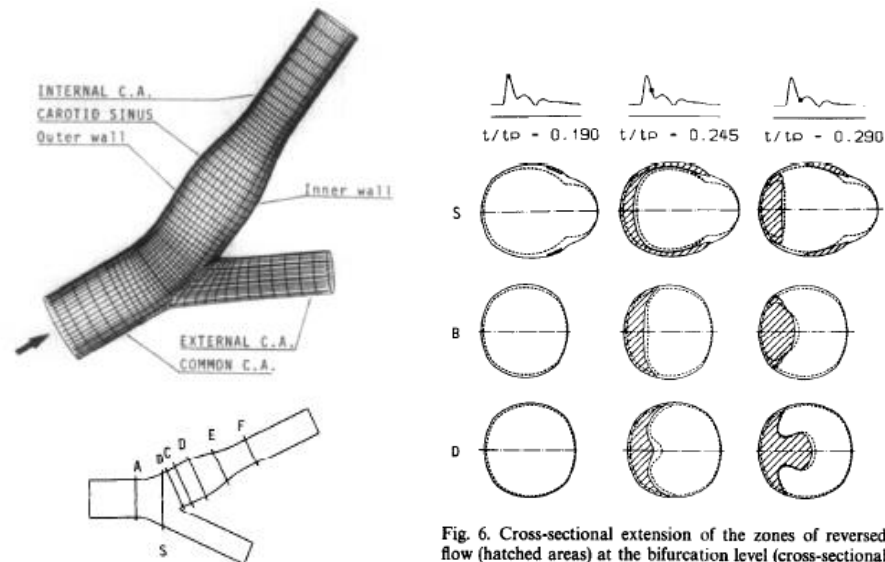


Fig. 2. Carotid artery bifurcation model. A, B, C, D, E, F; S indicate flow cross-section levels where numerical results are displayed.

Fig. 6. Cross-sectional extension of the zones of reversed flow (hatched areas) at the bifurcation level (cross-sectional cut S), at the proximal sinus location (cut B) and at the sinus maximum diameter location (cut D) at peak flow rate, during systolic deceleration and at minimum flow rate: solid line, distensible model; dashed line, rigid model.

Figure 6.1.8 Perktold et al. [49,51]

Regardless of the above, the relative velocity distributions and flow features predicted by both models are almost identical. Recirculation zones can also be observed in the following plot Fig 6.1.9. During systole, reverse flows are high in the carotid sinus which with low shear rates, these regions are highly susceptible to lesion formations. Recirculation is not observed in B & D section of the blood only model by Perktold et al. until 0.24s as arterial compliance is neglected in their model, this observation complements CFD results presented in Fig 6.1.7 as reverse start to intensify whereas in FSI model stromal recirculations zones are formed at peak systole.

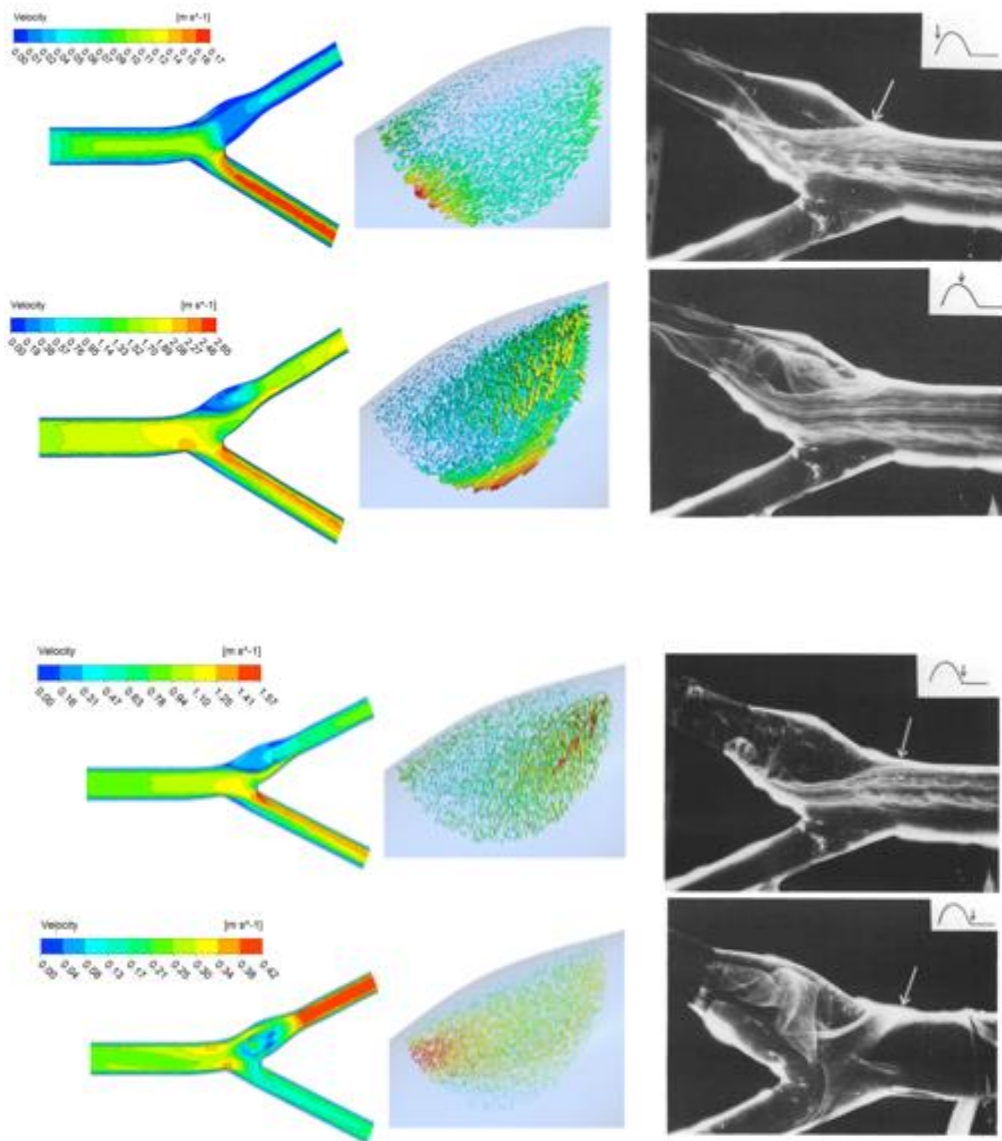


Figure 6.1.9 Velocity magnitude contours and recirculation zones in carotid sinus 0.08s-0.4s(top-bottom) verified with experiments conducted by Ku. et al [30]

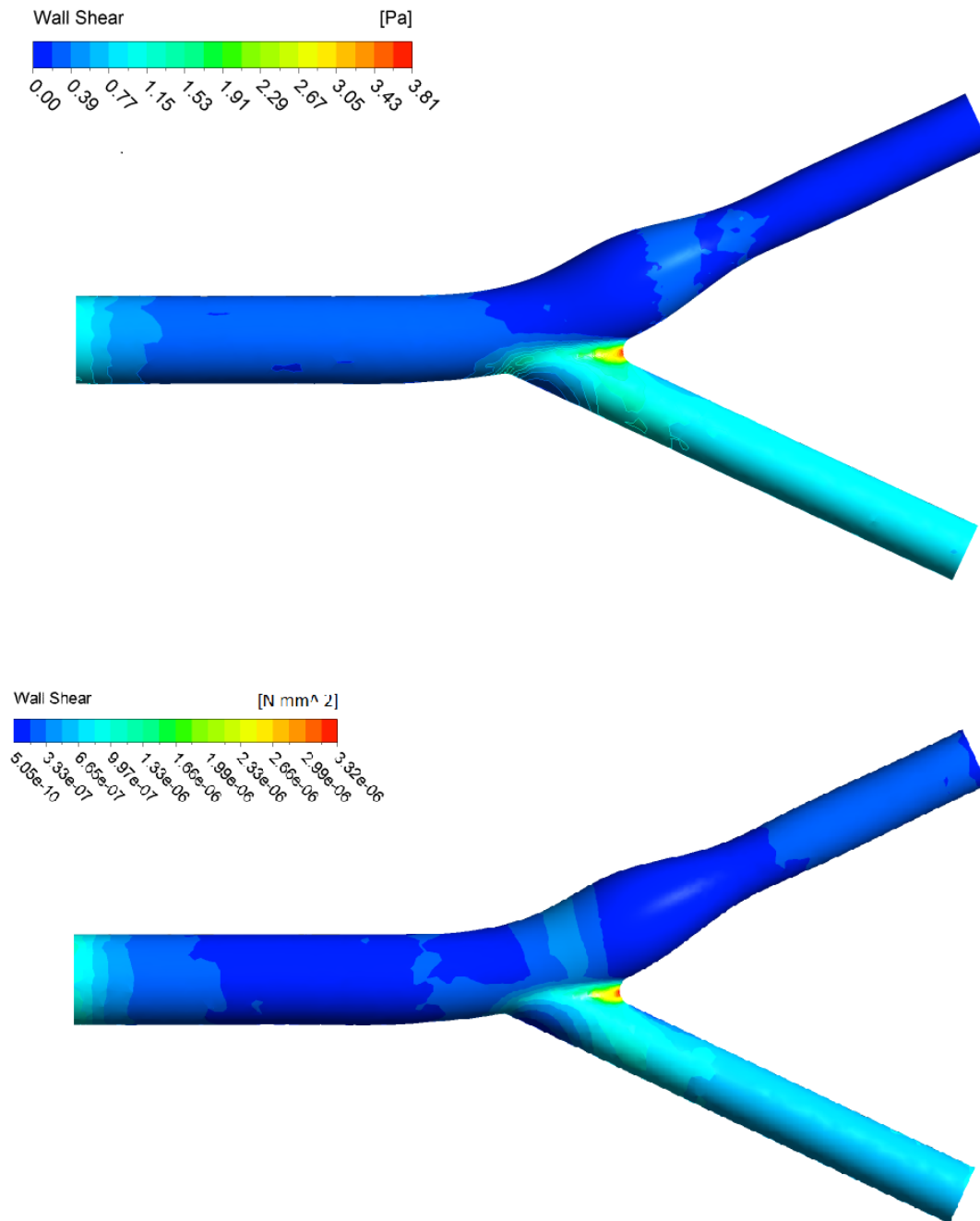


Figure 6.1.10 Peak systole wall shear stress (WSS); CFD on the top in Pa & FSI in the bottom in N/mm^2

The WSS distributions of the fluid and FSI models at peak flow rate are shown in Fig 6.1.10. The peak WSS in our CFD model is overestimated by approximately 14% this is in comparison with the corresponding WSS overestimation of 15% by Decorato et al. bifurcation comparison [112]. The wall shear stress magnitude revealed peak values at the bifurcation and moderately elevated

values around the ICA from the inner wall. The lowest average wall shear was seen primarily at the inner wall of the ICA and ECA. WSS oscillated in both magnitude and direction during the systolic phase. At the inner wall of the internal carotid sinus and in the region of the flow divider, wall shear stress was highest during systole. It can be assumed that arterial thickening in this location is likely to be minimal. At the outer wall of the carotid sinus where intimal plaques can be thickest, mean shear stress was low 0.7 Pa but the instantaneous shear stress oscillated as shown in Fig 6.1.11. Along the side walls of the sinus, intimal plaque thickness was greater than in the region of the flow divider, and circumferential oscillations of shear stress were prominent. Interestingly, near the carotid sinus, notable lower wall shear stress is observed, probably due to flow recirculation with low-velocity gradient.

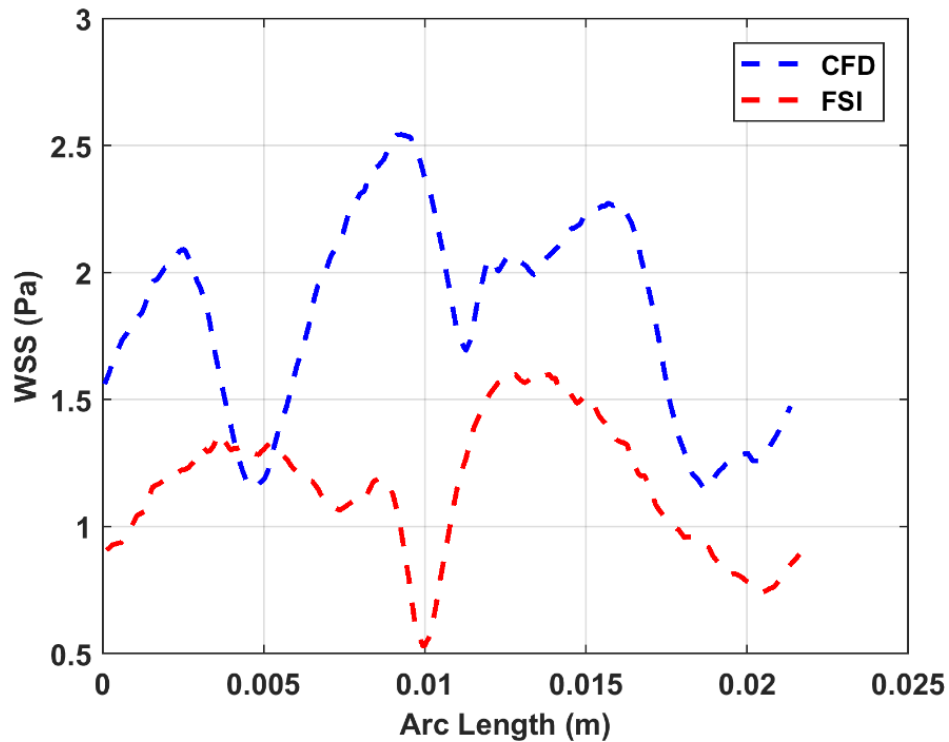


Figure 6.1.11 WSS on Carotid sinus curvature at maximum diameter

Plotted in the same Fig 6.1.11 & Fig 6.1.12 are the amount by which the CFD model overestimates the WSS over the carotid sinus and bifurcation boundary when compared with the FSI model.

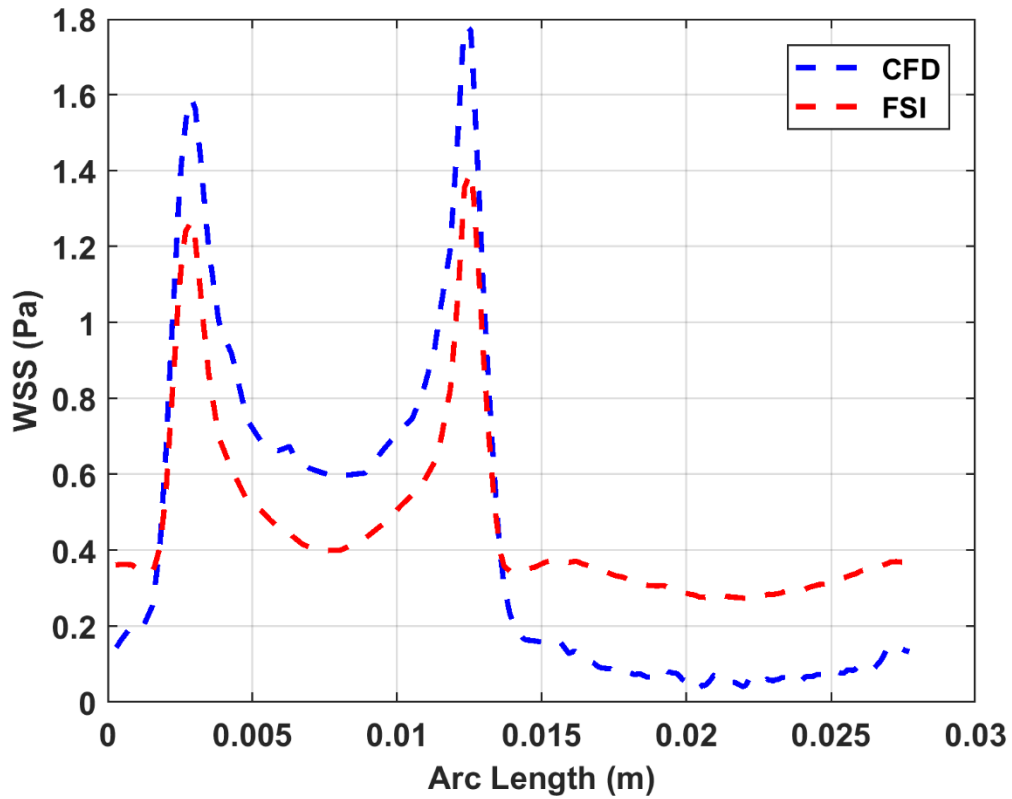


Figure 6.1.12 WSS on bifurcation curvature

The instantaneous wall shear stress oscillates from 0.4 to 1.4 Pa at the flow divider. Mean wall shear stress, from max systole to max diastole, experiences a 70.0% increase at the main bifurcation flow divider plotted in Fig 6.1.12. These findings confirm that plaques tend to form in areas of low, rather than high, shear stress, but indicate also that marked oscillations in the direction of wall shear may enhance atherogenesis.

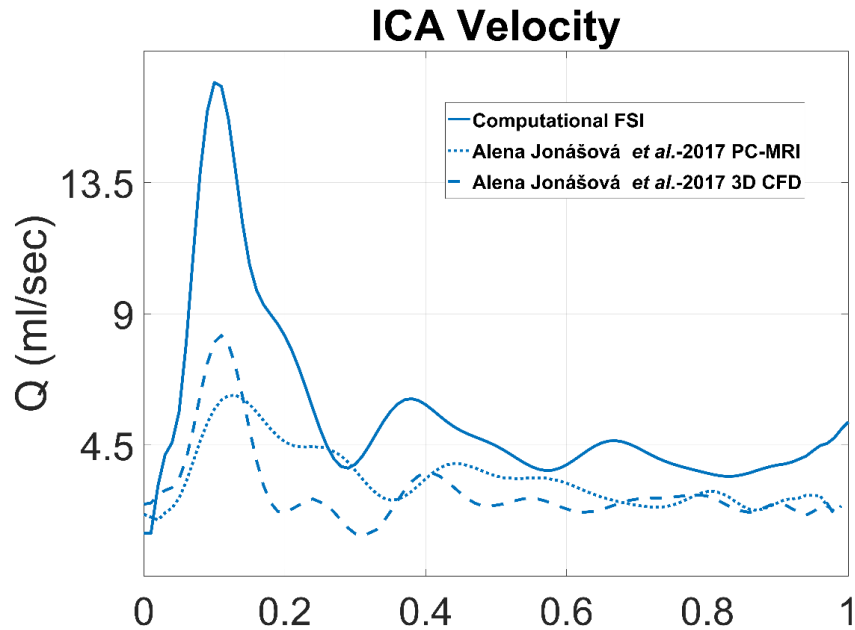


Figure 6.1.13 Velocity is the internal carotid artery compared to Josanova et al. [105]

It must be taken into account that very small differences upstream in a blood model can change the positioning of streamlines downstream to a large degree. With prescribed inlet velocity from Alena Jonasova et al., the velocity profile in the ICA follows the peaks and shape of the validated CFD model Fig 6.1.13. The WSS are the important criteria here however, and since the WSS are dependant on the velocities, an accurate solution to the velocity distribution is crucial. Prestressing is therefore vital to accurately predicting the WSS solution in FSI modelling of artery. As the boundary conditions considered in blood and structural domain are assumptions, merely artificial. Boundaries that represent the accurate upstream and downstream behavior are needed. Coupling a 3D model with a reduced model will make it possible to establish absorbing or non-reflective boundary conditions are applied to account the neighbor arterial effects.

6.2 3D-1D Coupling

Coupling between these two models at the interface of 3D model outlet and 1D segment inlet is carried out using a coupling algorithm discussed in the methodology section. The simulations were carried out using a fixed time step of 0.00005s for the 3D model and the 1D model. Also in the 1D model, a non-reflective boundary condition was considered at the downstream section of the segment, i.e., zero resistance is applied for stagnating pressure variations.

An idealized symmetrical aneurysm model is extracted from Mix et al. [112] using SolidWorks spline geometry and revolving the geometry around its centerline as shown in Fig 6.2.1.

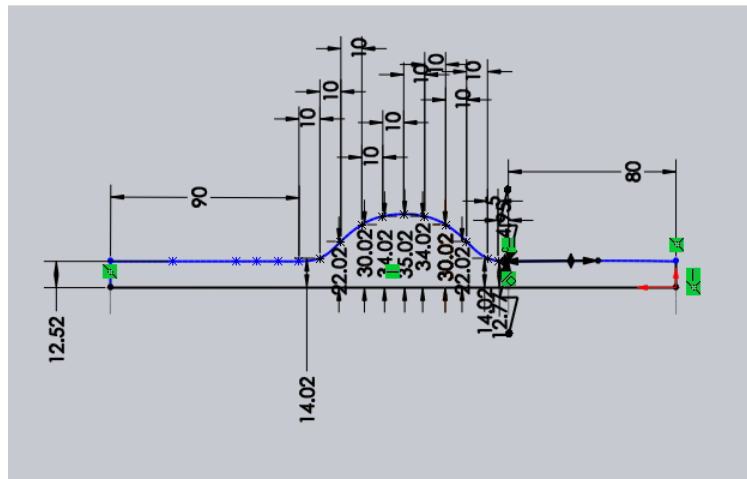


Figure 6.2.1 Aneurysm geometry (Units in mm) extracted from Mix et al. [113]

Adapting to learnings from modeling an FSI problem as discussed in 3D FSI model section, the current the model is set-up using similar blood and structural domain parameters except for blood outlet boundary conditions shown in Fig 6.2.2.

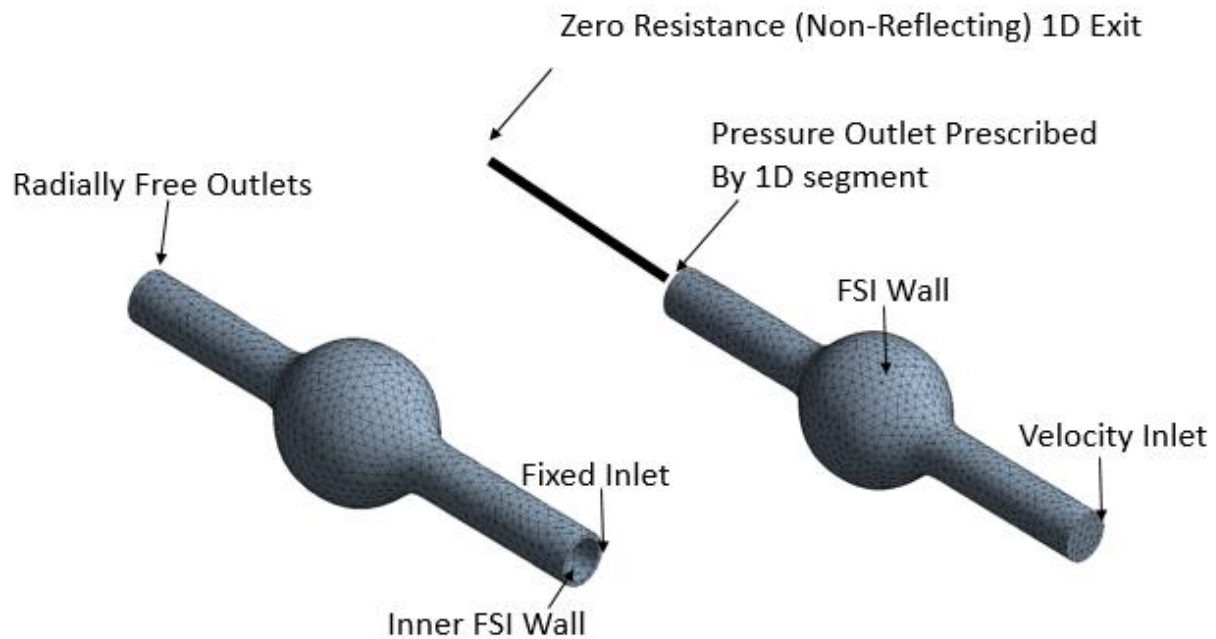


Figure 6.2.2 3D & 1D boundaries (3D Structural on the left & 3D Blood on the right)

To simplify the problem, a sin wave depicted in Fig 6.2.3 is considered as the velocity inlet boundary condition on the blood domain.

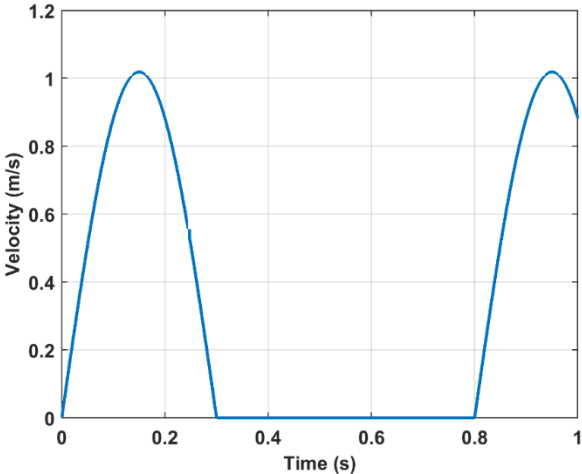


Figure 6.2.3 Inlet velocity at 3D inlet

At the outlet of the blood domain, at $t=0$, the pressure is defined as 0 Pa using another DEFINE_PROFILE UDF. As the FSI iterations march forward, ANSYS is updating pressure and velocity across the blood domain. At the end of each time-step, DEFINE_EXECUTE_AT_END UDF attached as APPENDIX: UDF 3 hooked to the ANSYS Fluent solver extracts pressure and velocity values at the center of the cells on outlet face. UDF then writes these arrays to an output text file and pauses for 5 sec to receive new pressure boundary value from the 1D model calculated at the 3D-1D interface.

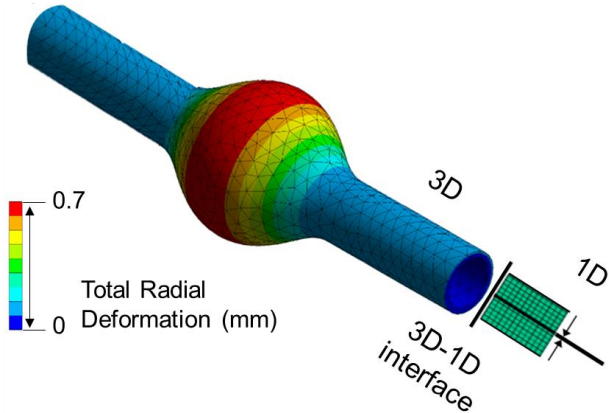


Figure 14 3D-1D coupling representation

A MATLAB script named as READWRITE_ANSYS.m is developed based on 3D-1D coupling implementation discussed in the Methodology section.

READWRITE_ANSYS.m receives the output text files from ANSYS Fluent, read the pressure and velocity arrays, calculates average values, and transfers to the in-house coupling & 1D FSI code which calculates a new pressure and velocity boundary data for each model. READWRITE_ANSYS.m now writes the new pressure boundary data into an input text file and pauses to receive next output text file. 3D FSI now executes the DEFINE_PROFILE UDF at 3D outlet, reads and applies the new pressure boundary data onto outlet face. thus completing one time-step and marching into next.

As discussed in Table 5, 3D FSI simulations alone are computationally intensive and time-consuming as controlled by a variety of stabilization techniques mentioned in 3D FSI section. Here, as the 3D FSI in boundary dependent of coupling interface and 1D code, fixed time-step is imperative. 1D code is non-linear solver with faster solution time as it runs an adaptive time-stepping method which sees a range of time-step sizes smaller being 1e-6s to larger 1e-3s. However, time-step can be fixed to match that of 3D FSI case to maintain the coupling implementation consistent.

Note that a smaller fixed time-stepping coupling will drastically increase computation hours adding to an existing disadvantage of 3D FSI simulation. Additionally, the pause commands in DEFINE_EXECUTE_AT_END UDF and READWRITE_ANSYS.m add hours which varies with a time-step size. Typically, a 3D-1D coupled simulation **takes approximately 250 hours** when running on a Xeon(R) E5 workstation with 20 cores and 128 GB RAM, the ANSYS utilizing 16 of the cores for blood and the structure, and leaving the rest for MATLAB 1D code and PC background process.

In this 3D model of an aneurysm coupled at the outlet to a 1D model of an artery. Given non-steady flow condition at 3D model inlet, velocity and pressure waveform results at interface ideally match as shown in Fig 6.2.5 & Fig 6.2.6, between 3D, 1D and 3D-1D coupling at the location of the interface. This results in a synchronous solution capturing the effect of the aneurysm on pulse wave propagation.

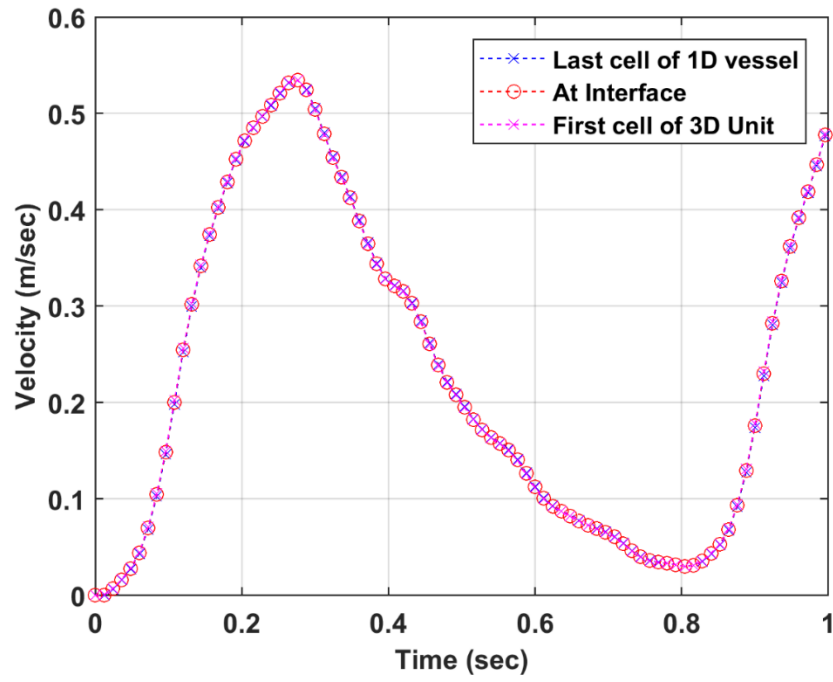


Figure 6.2.5 Velocity plot at the 3D-1D interface (3D outlet connected to 1D inlet)

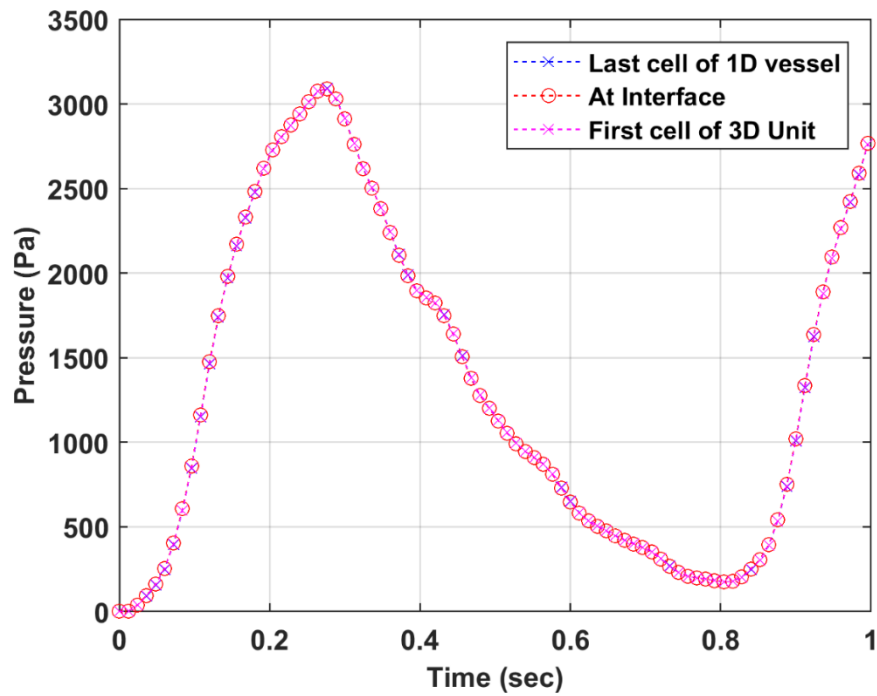


Figure 6.2.6 Pressure plot at the 3D-1D interface (3D outlet connected to 1D inlet)

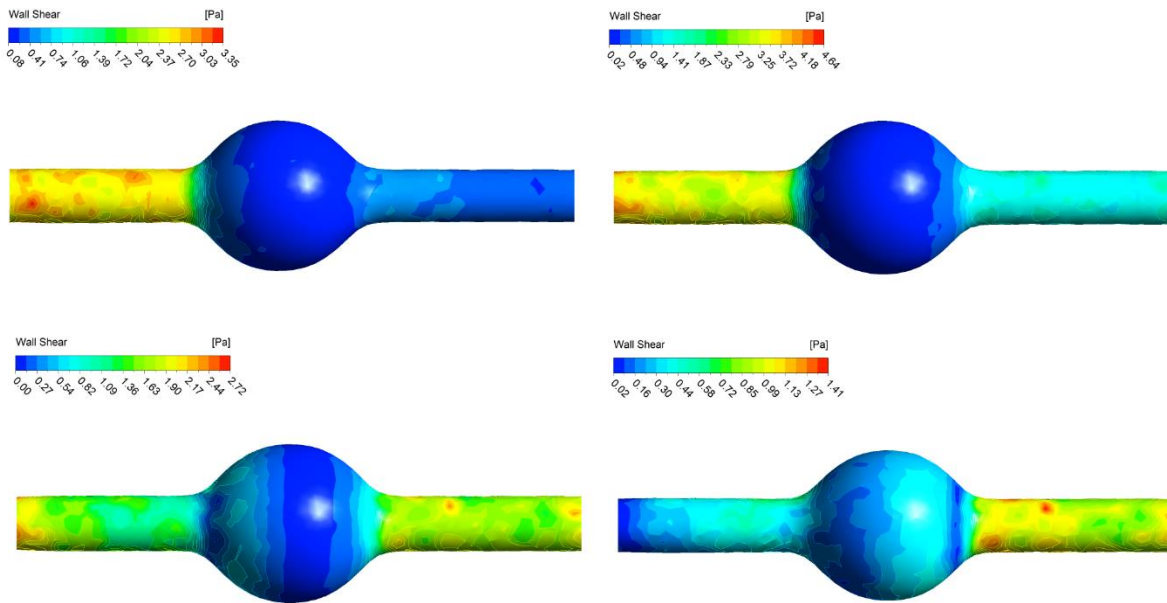


Figure 6.2.7 Wall shear stress (WSS)

The results for wall shear stress distributions at t 0.08s, 0.18s, 0.24s, and 0.4s are shown in Fig 6.2.7. The velocity magnitude distribution at the same temporal points is given in Fig 6.2.8. It can be seen that the velocities are low in the domain of the aneurysm, while the lower values of the wall shear stress are at the distal aneurysm zones. The flow patterns during peak systole change significantly. The abrupt expansion from the aneurysm neck induces a rapid decrease in the velocities followed by the formation of complex flow patterns and recirculation zones shown in Fig 6.2.8. During diastole, large and diffuse, recirculation zones are formed in the location of aneurysm. These are more pronounced as the aneurysmal sac widens and span almost the entire diameter of the aneurysmal bulge.

At regions of predicted flow recirculations, where low WSS and thrombus deposition predominated. These findings raise the possibility that this flow pattern may lead to thrombus deposition, which may elaborate arterial degeneration and eventual aneurysmal rupture.

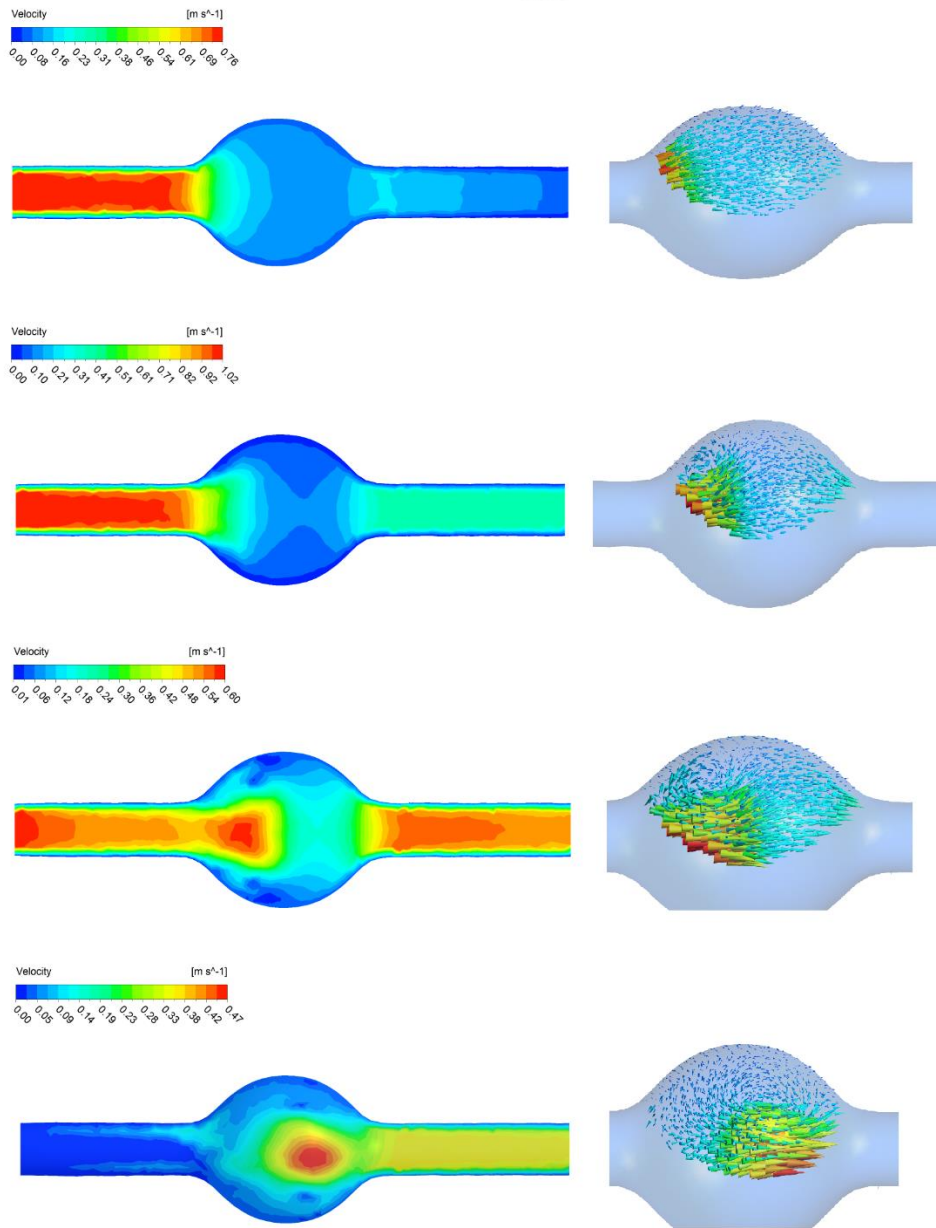


Figure 6.2.8 Velocity magnitude contours and recirculation zones in aneurysm

A velocity profile is plotted as Fig 6.2.9 at the cross-section of the aneurysm, in both 3D-1D and a total 3D case. A total 3D comprises of the 3D aneurysm with a downstream extension equivalent to the length of the 1D segment is the 3D-1D case. This establishes a simple validation of the 3D-1D model with a total 3D FSI performed using ANSYS alone.

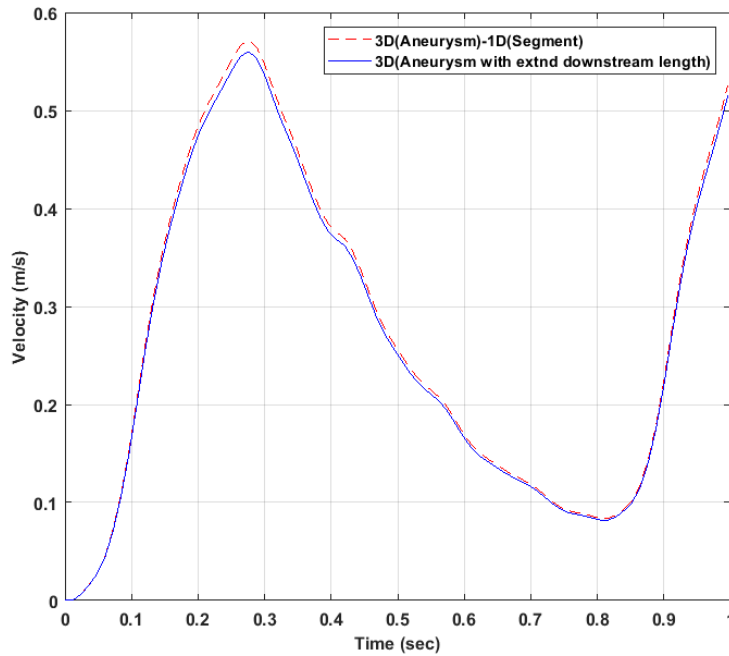


Figure 6.2.9 Validation on 3D-1D with total 3D model

In later models, DEFINE_EXECUTE_AT_END UDF is re-written to calculate the area-weighted average of velocity and pressure over a boundary face rather than extracting cell values.

6.3 1D-3D-1D Coupling

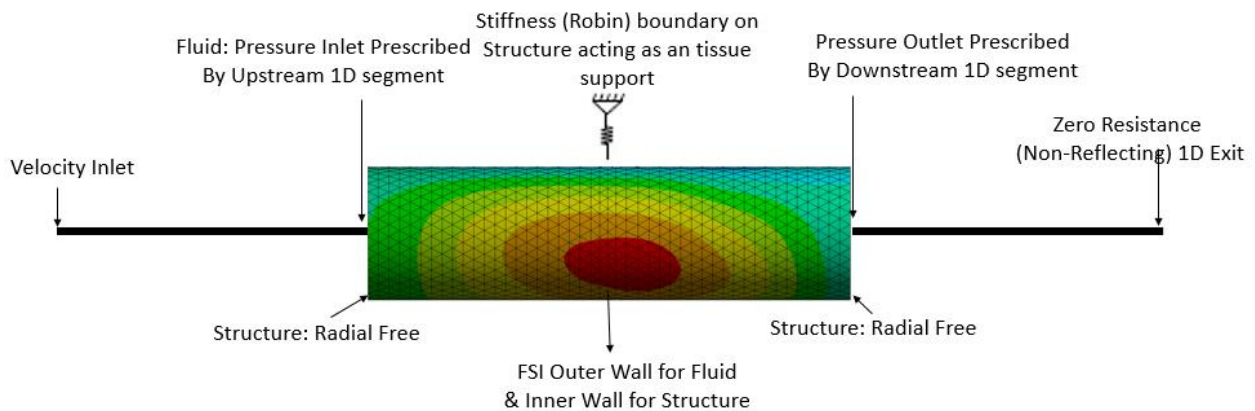


Figure 6.3.1 Two 1D segments connected to a 3D cylinder model

In this simulation, we consider a cylinder geometry for 3D FSI. A 1D segment is added to 3D inlet creating another coupling interface between 1D last cell and 3D inlet face cells. However, 3D upstream structural inlet was fixed in the above cases, which is unphysiological. Inlet has to displace freely in a radial direction to have close to physiological behavior for the pulse to move

through the inlet. Robin BC has thus been applied to constrain the model so that it does not deform excessively when the boundaries. This case has been tested for an assumption of stiffness of the tissue support surrounding the artery. Stiffness of the Robin BC was thus set at 0.01 Nmm^{-3} to constrain the model sufficiently but have negligible effect on the strain in the vessel walls. Final model boundaries as shown in Fig 6.3.1.

Boundary conditions in ANSYS Fluent are controlled by DEFINE_PROFILE macros at inlet and outlet to apply a pressure boundary data on their respective & coupling implementation by READWRITE_ANSYS_1D3D1D.m

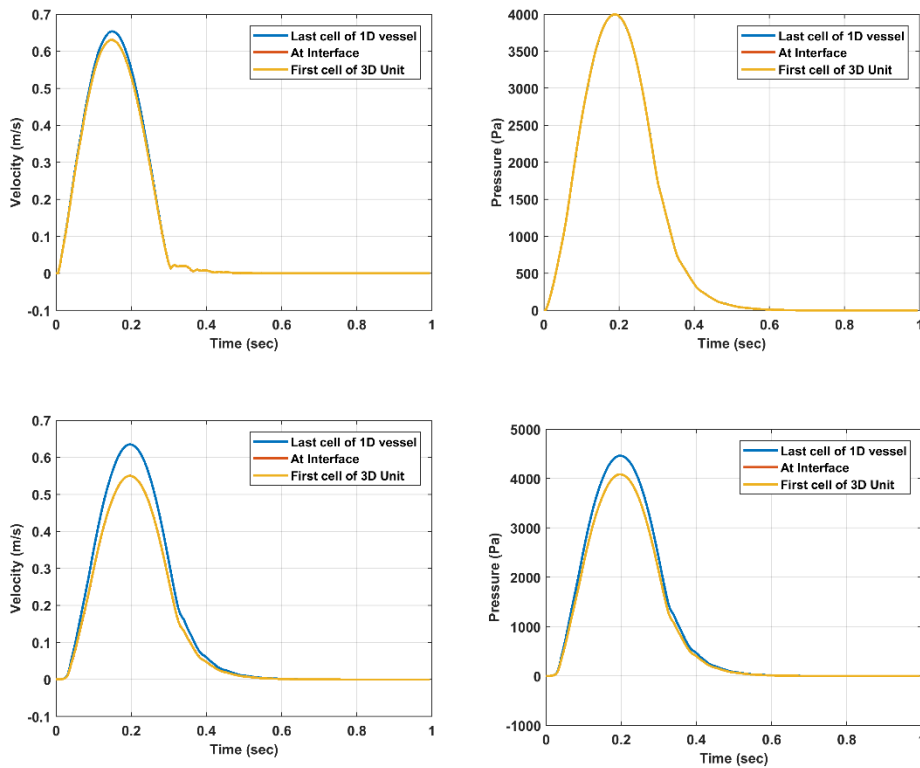


Figure 6.3.2 Velocity & Pressure plots at the 1D-3D interface on top and 3D-1D interface in the bottom

In Fig 6.3.2, Velocity values are decreased by 26% in the 3D model when compared to 1D; this can be due to the new Robin boundary condition applied on the structure wall. As stiffness analysis of the tissue support is not in the scope of the work, results plotted are realized as is. Velocities and pressure match fairly well at upstream and downstream interfaces. And similar velocity

profiles are plotted as intra model validation in Fig 6.3.3 at center (dashed line) of a total 3D, total 1D and, a 1D-3D-1D model.

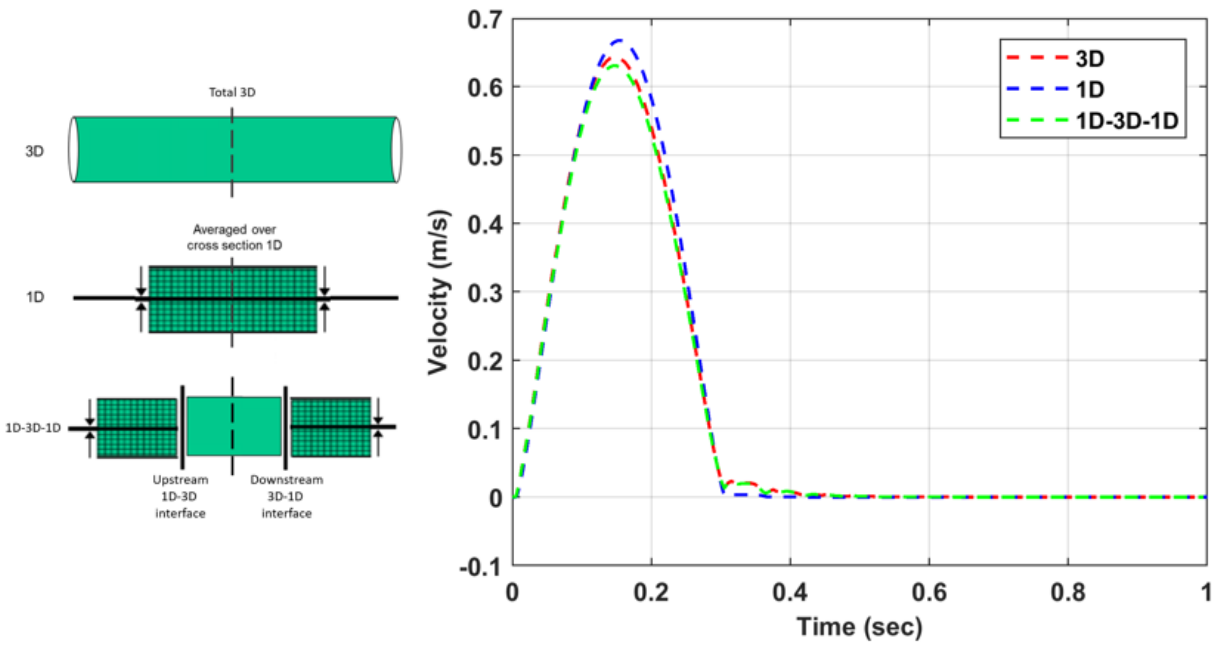


Figure 6.3.3 Time varying velocity plots at center cross-section in three models

7 CONCLUSION & FUTURE WORK

This thesis has presented the development and solution of an FSI simulation of idealized geometries. The approach has made use of ANSYS Fluent and ANSYS Mechanical software, implemented in ANSYS Workbench software, that solves the fluid and structure problems consecutively. The fluid is solved iteratively, providing the principal stabilization features to the FSI model, while the direct structure solver converges fully. It was found the FSI model could be optimally stabilized by combining several solution damping techniques within the iterative fluid solver, including FSI boundary stabilization, together with a boundary transfer ramping, and URFs.

To model more accurately the flow of blood in the vessel, where shear-thinning is likely to occur, non-Newtonian fluid models such as the Casson, or Carreau-Yusada models, should be used for the blood. A more efficient FSI model could be developed by prescribing a parabolic velocity inlet condition, in place of the uniform boundary condition we have used. This would allow the inlet length to be shortened to reduce the number of elements while still maintaining accuracy in the region of interest.

The Robin boundary condition used in the final model could also be enhanced with additional modeling techniques as it may replicate the effect of the surrounding tissue more accurately. No tissue stiffness or less model deforms excessively if it is not prestressed, resulting in an underapproximation of the velocity and WSS solutions, particularly in the artery. It has been shown that the model is able to predict flow features, such as recirculation, that may lead to arterial failure. It would be important in future studies to extend the model by accounting for prestressing in a manner that makes use of medically imaged data.

This work mostly focused on developing an implementation scheme to perform multiscale simulations like 3D-1D & 1D-3D-1D. While flow profiles at interface seemed to match reasonably well, computational expenses were drastic and unforeseen. Also, the presented multiscale coupling only couples fluid domain with 1D neglecting area change at the interface and 3D structural domain. Researchers at the in-house lab developed a unique Hamiltonian based coupling technique to benefit from the higher accuracy of the 3D while maintaining the computational speed offered by 1D models which accounts for area variation.

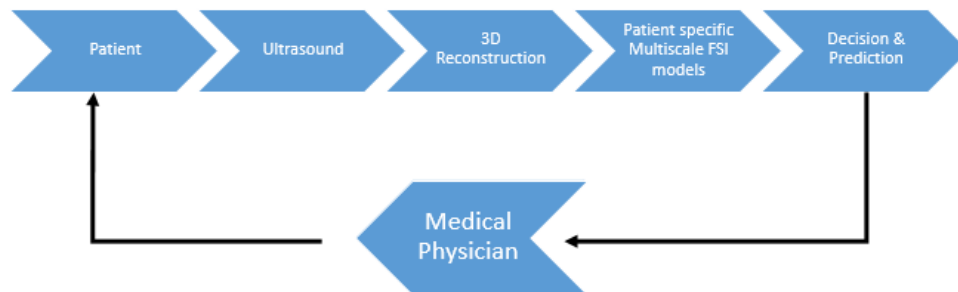
$$a_1 \frac{\overline{P_{1D}}}{\rho} + a_2 \overline{V_{1D}}^2 = \int r f(r) \left(\frac{P_{3D}}{\rho} + V^2 \right) dr$$

Where a_1, a_2 are coefficients, P and V - pressure and velocity, respectively. r - radius and $f(r)$ - the shape profile of velocity.

8 SOCIETAL CONTEXT

A geometrical multiscale approach incorporating computational FEM, CFD & FSI like tools are widely applied for exploratory research of fluid flow in complex geometries with the flexibility to incorporate user-defined properties. It has immense potential in biomedical applications. Current medical angiographic techniques permit fairly accurate detection of the arterial disease once clinical symptoms suggestive of the existence of thrombosis/aneurysmal risk/stenotic disease are found. However, minor symptoms are usually difficult to identify, and significant symptoms often would not develop (especially at rest) until the late stage of the disease due to inherent cardiovascular compensatory responses.

In this sense, patient-specific treatment strategies can be developed by providing design-algorithms, using such data thus developing new techniques of clinical practice for computer-aided diagnosis planning in a grid-supported virtual environment. Analyzing arterial pulses may potentially provide additional insight. Data from patients with different diseases using non-invasive techniques such as intravascular ultrasound can be used to validate relevant hemodynamic flow quantities and generate metrics of the disease state. So it is crucial to develop accurate simulation tools to understand the hemodynamics, especially at the location of diseased arteries. A reliable simulation technique enables the creation of an experimental environment. This facilitates training for virtual invasive techniques like angioplasty and stenting. This study explores methods in calculating wall shear stress intensity to prognosticate the life of a tissue or pulse transit time in local regions of large arteries in order to detect the presence of cause.



9 REFERENCES

1. “Cardiovascular diseases (CVDs)”, World Health Organization.
2. Heart Disease and Stroke Statistics-2019 At-a-Glance <https://healthmetrics.heart.org/wp-content/uploads/2019/02/At-A-Glance-Heart-Disease-and-Stroke-Statistics-%E2%80%93-2019.pdf>
3. Tortora, G. J., *Principles of Human Anatomy*, 9th ed., John Wiley & Sons, New York, NY, 2002.
4. D.N. Ku. Blood flow in arteries. *Annual Review of Fluid Mechanics*, 29(1):399–434, 1997.
5. JR Womersley. Method for the calculation of velocity, rate of flow and viscous drag in arteries when the pressure gradient is known. *The Journal of Physiology*, 127(3):553–563, 1955.
6. C.A. Taylor, T.J.R. Hughes, and C.K. Zarins. Finite element modeling of blood flow in arteries. *Computer Methods in Applied Mechanics and Engineering*, 158(1-2):155–196, 1998.
7. W.G. Bradley Jr, V. Waluch, K.S. Lai, E.J. Fernandez, and C. Spalter. The appearance of rapidly flowing blood on magnetic resonance images. *American Journal of Roentgenology*, 143(6):1167, 1984
8. H. Baek, MV Jayaraman, PD Richardson, and GE Karniadakis. Flow instability and wall shear stress variation in intracranial aneurysms. *Journal of The Royal Society Interface*, 7(47):967, 2010.
9. G.J. Hademenos and T.F. Massoud. *The physics of Cerebrovascular Diseases: Biophysical Mechanisms of Development, Diagnosis, and Therapy*. Springer Verlag, 1998.
10. Fung, Y. C., *Biomechanics: Motion, Flow, Stress, and Growth*, Springer-Verlag, New York, NY, 1990.
11. Fung, Y.C., *Mechanical Properties of Living Tissues*, 2nd edition, Springer Verlag, New York, 1993.
12. Caro, C.G., Pedley, T.J., Schroter, R.C., and Seed, W.A., *The Mechanics of Circulation*, Oxford University Press, New York, NY, 1978.
13. E.F. Goljan. *Rapid review pathology*. Mosby/Elsevier, 2010.
14. X. He and D.N. Ku. Pulsatile flow in the human left coronary artery bifurcation: average conditions. *Journal of Biomechanical Engineering*, 118:74–82, 1996
15. H. Zakaria, A.M. Robertson, and C.W. Kerber. A parametric model for studies of flow in arterial bifurcations. *Annals of Biomedical Engineering*, 36(9):1515–1530, 2008.

16. S. Juvela, M. Porras, K. Poussa, et al. Natural history of unruptured intracranial aneurysms: probability of and risk factors for aneurysm rupture. *Journal of Neurosurgery*, 96(1):57–57, 2002.
17. D.M. Sforza, C.M. Putman, and J.R. Cebral. Hemodynamics of cerebral aneurysms. *Annu Rev Fluid Mech*, 41:91–107, 2009.
18. B.R. Blackman, G. García-Cardeña, and M.A. Gimbrone Jr. A new in vitro model to evaluate differential responses of endothelial cells to simulated arterial shear stress waveforms. *Journal of biomechanical engineering*, 124:397, 2002.
19. J.T. Flaherty, J.E. Pierce, V.J. Ferrans, D.J. Patel, W.K. Tucker, and D.L. Fry. Endothelial nuclear patterns in the canine arterial tree with particular reference to hemodynamic events. *Circulation Research*, 30(1):23, 1972.
20. Deserranno, D., Popovic, Z. B., Greenberg, N. L., Kassemi, M., and Thomas, J. D., “Axisymmetric Fluid-Structure Interaction Model of the Left Ventricle,” *Second MIT Conference on Computational Fluid and Solid Mechanics*, Elsevier Science Ltd., Oxford, UK, 2003, pp.1669-1672.
21. De Hart, J., Baaijens, F. P. T., Peters, G. W. M., and Schreurs, P. J. G, “A Computational Fluid-Structure Interaction Analysis of a Fiber-Reinforced Stentless Aortic Valve,” *Journal of Biomechanics*, Vol. 36, 2003, pp. 699-712.
22. Peskin, C. S., and McQueen, D. M., *Fluid Dynamics of the Heart and its Valves*, Englewood Cliffs, NJ, Prentice-Hall, Inc. 1996, pp. 309-337.
23. Taelman, L., Degroote, J., Verdonck, P., Vierendeels, J., and Segers, P., 2013, “Modeling Hemodynamics in Vascular Networks Using a Geometrical Multiscale Approach: Numerical Aspects,” *Ann. Biomed. Eng.*, 41(7), pp. 1445–1458.
24. Formaggia, L., Quarteroni, A., and Vergara, C., 2013, “On the Physical Consistency between Three-Dimensional and One-Dimensional Models in Haemodynamics,” *J. Comput. Phys.*, **244**(Supplement C), pp. 97–112.
25. Benjamin, E. J., Blaha, M. J., Chiuve, S. E., Cushman, M., Das, S. R., Deo, R., Ferranti, S. D. de, Floyd, J., Fornage, M., Gillespie, C., Isasi, C. R., Jiménez, M. C., Jordan, L. C., Judd, S. E., Lackland, D., Lichtman, J. H., Lisabeth, L., Liu, S., Longenecker, C. T., Mackey, R. H., Matsushita, K., Mozaffarian, D., Mussolino, M. E., Nasir, K., Neumar, R. W., Palaniappan, L., Pandey, D. K., Thiagarajan, R. R., Reeves, M. J., Ritchey, M., Rodriguez, C. J., Roth, G. A.,

- Rosamond, W. D., Sasson, C., Towfighi, A., Tsao, C. W., Turner, M. B., Virani, S. S., Voeks, J. H., Willey, J. Z., Wilkins, J. T., Wu, J. H., Alger, H. M., Wong, S. S., Muntner, P., and Subcommittee, O. behalf of the A. H. A. S. C. and S. S., 2017, “Heart and Related Therapeutic Implications,” *Nat. Clin. Pract. Cardiovasc. Med.*, **2**(9), pp. 456–464.
26. Zarins, C. K., Giddens, D. P., Bharadvaj, B. K., Sottiurai, V. S., Mabon, R. F., and Glagov, S., 1983, “Carotid Bifurcation Atherosclerosis. Quantitative Correlation of Plaque Localization with Flow Velocity Profiles and Wall Shear Stress,” *Circ. Res.*, **53**(4), pp. 502–514.
27. Ku, D. N., Biancheri, C. L., Pettigrew, R. I., Peifer, J. W., Markou, C. P., and Engels, H., 1990, “Evaluation of Magnetic Resonance Velocimetry for Steady Flow,” *J. Biomech. Eng.*, **112**(4), pp. 464–472.
28. Schettler, G., Nerem, R. M., Schmid-Schönbein, H., Mörl, H., and Diehm, C., eds., 1983, *Fluid Dynamics as a Localizing Factor for Atherosclerosis*, Springer Berlin Heidelberg, Berlin, Heidelberg.
29. Friedman, M. H., Deters, O. J., Mark, F. F., Brent Barger, C., and Hutchins, G. M., 1983, “Arterial Geometry Affects Hemodynamics: A Potential Risk Factor for Atherosclerosis,” *Atherosclerosis*, **46**(2), pp. 225–231.
30. Ku, D. N., Giddens, D. P., Zarins, C. K., and Glagov, S., 1985, “Pulsatile Flow and Atherosclerosis in the Human Carotid Bifurcation. Positive Correlation between Plaque Location and Low Oscillating Shear Stress,” *Arterioscler. Dallas Tex.*, **5**(3), pp. 293–302.
31. Cecchi, E., Giglioli, C., Valente, S., Lazzeri, C., Gensini, G. F., Abbate, R., and Mannini, L., 2011, “Role of Hemodynamic Shear Stress in Cardiovascular Disease,” *Atherosclerosis*, **214**(2), pp. 249–256.
32. Dokunin, A. V., 1958, “A Modification of the Method of Differential Manometry for Registration of the Volume Velocity of the Blood Flow,” *Bull. Exp. Biol. Med.*, **46**(5), pp. 1414–1417.
33. Bitterman, H., Brod, V., Weisz, G., Kushnir, D., and Bitterman, N., 1996, “Effects of Oxygen on Regional Hemodynamics in Hemorrhagic Shock,” *Am. J. Physiol. - Heart Circ. Physiol.*, **271**(1), pp. H203–H211.
34. Barfod, C., Akgören, N., Fabricius, M., Dirnagl, U., and Lauritzen, M., 1997, “Laser-Doppler Measurements of Concentration and Velocity of Moving Blood Cells in Rat Cerebral Circulation,” *Acta Physiol. Scand.*, **160**(2), pp. 123–132.

35. Urdzik, J., Bjerner, T., Wanders, A., Duraj, F., Haglund, U., and Norén, A., 2013, “Magnetic Resonance Imaging Flowmetry Demonstrates Portal Vein Dilatation Subsequent to Oxaliplatin Therapy in Patients with Colorectal Liver Metastasis,” *HPB*, **15**(4), pp. 265–272.
36. Elhawary, A. M., and Pang, C. C., 1995, “Renal Vascular and Tubular Actions of Calcitonin Gene-Related Peptide: Effect of NG-Nitro-L-Arginine Methyl Ester,” *J. Pharmacol. Exp. Ther.*, **273**(1), pp. 56–63.
37. Chen, Z., Milner, T. E., Srinivas, S., Wang, X., Malekafzali, A., Gemert, M. J. C. van, and Nelson, J. S., 1997, “Noninvasive Imaging of in Vivo Blood Flow Velocity Using Optical Doppler Tomography,” *Opt. Lett.*, **22**(14), pp. 1119–1121.
38. Decking, U. K. M., Pai, V. M., Bennett, E., Taylor, J. L., Fingas, C. D., Zanger, K., Wen, H., and Balaban, R. S., 2004, “High-Resolution Imaging Reveals a Limit in Spatial Resolution of Blood Flow Measurements by Microspheres,” *Am. J. Physiol. Heart Circ. Physiol.*, **287**(3), pp. H1132-1140.
39. Stone, P. H., Coskun, A. U., Kinlay, S., Popma, J. J., Sonka, M., Wahle, A., Yeghiazarians, Y., Maynard, C., Kuntz, R. E., and Feldman, C. L., 2007, “Regions of Low Endothelial Shear Stress Are the Sites Where Coronary Plaque Progresses and Vascular Remodelling Occurs in Humans: An in Vivo Serial Study,” *Eur. Heart J.*, **28**(6), pp. 705–710.
40. Vennemann, P., Lindken, R., and Westerweel, J., 2007, “In Vivo Whole-Field Blood Velocity Measurement Techniques,” *Exp. Fluids*, **42**(4), pp. 495–511.
41. Day, S. W., and McDaniel, J. C., 2005, “PIV Measurements of Flow in a Centrifugal Blood Pump: Steady Flow,” *J. Biomech. Eng.*, **127**(2), pp. 244–253.
42. Lim, W. L., Chew, Y. T., Chew, T. C., and Low, H. T., 2001, “Pulsatile Flow Studies of a Porcine Bioprosthetic Aortic Valve in Vitro: PIV Measurements and Shear-Induced Blood Damage,” *J. Biomech.*, **34**(11), pp. 1417–1427.
43. Liepsch, D., Pflugbeil, G., Matsuo, T., and Lesniak, B., 1998, “Flow Visualization and 1- and 3-D Laser-Doppler-Anemometer Measurements in Models of Human Carotid Arteries,” *Clin. Hemorheol. Microcirc.*, **18**(1), pp. 1–30.
44. Buchmann, N. A., Atkinson, C., Jeremy, M. C., and Soria, J., 2011, “Tomographic Particle Image Velocimetry Investigation of the Flow in a Modeled Human Carotid Artery Bifurcation,” *Exp. Fluids*, **50**(4), pp. 1131–1151.

45. Bharadvaj, B. K., Mabon, R. F., and Giddens, D. P., 1982, "Steady Flow in a Model of the Human Carotid Bifurcation. Part I--Flow Visualization," *J. Biomech.*, **15**(5), pp. 349–362.
46. Bharadvaj, B. K., Mabon, R. F., and Giddens, D. P., 1982, "Steady Flow in a Model of the Human Carotid Bifurcation. Part II--Laser-Doppler Anemometer Measurements," *J. Biomech.*, **15**(5), pp. 363–378.
47. Rindt, C. C. M., Steenhoven, A. A. van, Janssen, J. D., Reneman, R. S., and Segal, A., 1990, "A Numerical Analysis of Steady Flow in a Three-Dimensional Model of the Carotid Artery Bifurcation," *J. Biomech.*, **23**(5), pp. 461–473.
48. Anayiotos, A. S., Jones, S. A., Giddens, D. P., Glagov, S., and Zarins, C. K., 1994, "Shear Stress at a Compliant Model of the Human Carotid Bifurcation," *J. Biomech. Eng.*, **116**(1), pp. 98–106.
49. Perktold, K., and Rappitsch, G., 1995, "Computer Simulation of Local Blood Flow and Vessel Mechanics in a Compliant Carotid Artery Bifurcation Model," *J. Biomech.*, **28**(7), pp. 845–856.
50. Slager, C. J., Wentzel, J. J., Gijssen, F. J. H., Thury, A., van der Wal, A. C., Schaar, J. A., and Serruys, P. W., 2005, "The Role of Shear Stress in the Destabilization of Vulnerable Plaques
51. Perktold, K., and Resch, M., 1990, "Numerical Flow Studies in Human Carotid Artery Bifurcations: Basic Discussion of the Geometric Factor in Atherogenesis," *J. Biomed. Eng.*, **12**(2), pp. 111–123.
52. Myers, J. G., Moore, J. A., Ojha, M., Johnston, K. W., and Ethier, C. R., 2001, "Factors Influencing Blood Flow Patterns in the Human Right Coronary Artery," *Ann. Biomed. Eng.*, **29**(2), pp. 109–120.
53. Lee, B. K., Kwon, H. M., Hong, B. K., Park, B. E., Suh, S. H., Cho, M. T., Lee, C. S., Kim, M. C., Kim, C. J., Yoo, S. S., and Kim, H. S., 2001, "Hemodynamic Effects on Atherosclerosis-Prone Coronary Artery: Wall Shear Stress/Rate Distribution and Impedance Phase Angle in Coronary and Aortic Circulation," *Yonsei Med. J.*, **42**(4), pp. 375–383.
54. He, X., and Ku, D. N., 1996, "Pulsatile Flow in the Human Left Coronary Artery Bifurcation: Average Conditions," *J. Biomech. Eng.*, **118**(1), pp. 74–82.
55. Lei, M., Kleinstreuer, C., and Truskey, G. A., 1995, "Numerical Investigation and Prediction of Atherogenic Sites in Branching Arteries," *J. Biomech. Eng.*, **117**(3), pp. 350–357.

56. Lee, S.-W., Antiga, L., and Steinman, D. A., 2009, "Correlations among Indicators of Disturbed Flow at the Normal Carotid Bifurcation," *J. Biomech. Eng.*, **131**(6), p. 061013.
57. Wille, S. Ø., 1981, "Pulsatile Pressure and Flow in an Arterial Aneurysm Simulated in a Mathematical Model," *J. Biomed. Eng.*, **3**(2), pp. 153–158.
58. Perktold, K., Gruber, K., Kenner, T., and Florian, H., 1984, "Calculation of Pulsatile Flow and Particle Paths in an Aneurysm-Model," *Basic Res. Cardiol.*, **79**(3), pp. 253–261.
59. Finol, E. A., and Amon, C. H., 2001, "Blood Flow in Abdominal Aortic Aneurysms: Pulsatile Flow Hemodynamics," *Trans.-Am. Soc. Mech. Eng. J. Biomech. Eng.*, **123**(5), pp. 474–484.
60. Duncan, D. D., Barger, C. B., Borchardt, S. E., Deters, O. J., Gearhart, S. A., Mark, F. F., and Friedman, M. H., 1990, "The Effect of Compliance on Wall Shear in Casts of a Human Aortic Bifurcation," *J. Biomech. Eng.*, **112**(2), pp. 183–188.
61. Deserranno, D., Popovic, Z. B., Greenberg, N. L., Kassemi, M., and Thomas, J. D., 2003, "Axisymmetric Fluid-Structure Interaction Model of the Left Ventricle."
62. De Hart, J., Baaijens, F. P. T., Peters, G. W. M., and Schreurs, P. J. G., 2003, "A Computational Fluid-Structure Interaction Analysis of a Fiber-Reinforced Stentless Aortic Valve," *J. Biomech.*, **36**(5), pp. 699–712.
63. Kim, Y.-H., Kim, J.-E., Ito, Y., Shih, A. M., Brott, B., and Anayiotos, A., 2008, "Hemodynamic Analysis of a Compliant Femoral Artery Bifurcation Model Using a Fluid Structure Interaction Framework," *Ann. Biomed. Eng.*, **36**(11), p. 1753.
64. Formaggia, L., Nobile, F., Quarteroni, A., and Veneziani, A., 1999, "Multiscale Modelling of the Circulatory System: A Preliminary Analysis," *Comput. Vis. Sci.*, **2**(2–3), pp. 75–83.
65. Taelman, L., Degroote, J., Verdonck, P., Vierendeels, J., and Segers, P., 2013, "Modeling Hemodynamics in Vascular Networks Using a Geometrical Multiscale Approach: Numerical Aspects," *Ann. Biomed. Eng.*, **41**(7), pp. 1445–1458.
66. Vigmostad, S. C., Udaykumar, H. S., Lu, J., and Chandran, K. B., 2010, "Fluid–structure Interaction Methods in Biological Flows with Special Emphasis on Heart Valve Dynamics," *Int. J. Numer. Methods Biomed. Eng.*, **26**(3–4), pp. 435–470.
67. Heil, M., and Hazel, A. L., 2011, "Fluid-Structure Interaction in Internal Physiological Flows," *Annu. Rev. Fluid Mech.*, **43**(1), pp. 141–162.

68. Scotti, C. M., Shkolnik, A. D., Muluk, S. C., and Finol, E. A., 2005, “Fluid-Structure Interaction in Abdominal Aortic Aneurysms: Effects of Asymmetry and Wall Thickness,” *Biomed. Eng. OnLine*, **4**, p. 64.
69. Tada, S., and Tarbell, J. M., 2005, “A Computational Study of Flow in a Compliant Carotid Bifurcation—Stress Phase Angle Correlation with Shear Stress,” *Ann. Biomed. Eng.*, **33**(9), pp. 1202–1212.
70. Tezduyar, T. E., Takizawa, K., Brummer, T., and Chen, P. R., 2011, “Space–time Fluid–structure Interaction Modeling of Patient-Specific Cerebral Aneurysms,” *Int. J. Numer. Methods Biomed. Eng.*, **27**(11), pp. 1665–1710.
71. Torii, R., Wood, N. B., Hadjiloizou, N., Dowsey, A. W., Wright, A. R., Hughes, A. D., Davies, J., Francis, D. P., Mayet, J., Yang, G.-Z., Thom, S. A. M., and Xu, X. Y., 2009, “Fluid–structure Interaction Analysis of a Patient-Specific Right Coronary Artery with Physiological Velocity and Pressure Waveforms,” *Commun. Numer. Methods Eng.*, **25**(5), pp. 565–580.
72. Formaggia, L., Gerbeau, J.-F., Nobile, F., and Quarteroni, A., 2001, “On the Coupling of 3D and 1D Navier–Stokes Equations for Flow Problems in Compliant Vessels,” *Comput. Methods Appl. Mech. Eng.*, **191**(6), pp. 561–582.
73. Quarteroni, A., 2001, “Modeling the Cardiovascular System: A Mathematical Challenge,” *Mathematics Unlimited — 2001 and Beyond*, Springer, Berlin, Heidelberg, pp. 961–970.
74. Formaggia, L., Gerbeau, J., Nobile, F., and Quarteroni, A., 2002, “Numerical Treatment of Defective Boundary Conditions for the Navier--Stokes Equations,” *SIAM J. Numer. Anal.*, **40**(1), pp. 376–401.
75. Quarteroni, A., Tuveri, M., and Veneziani, A., 2000, “Computational Vascular Fluid Dynamics: Problems, Models and Methods,” *Comput. Vis. Sci.*, **2**(4), pp. 163–197.
76. Hughes, T. J. R., and Lubliner, J., 1973, “On the One-Dimensional Theory of Blood Flow in the Larger Vessels,” *Math. Biosci.*, **18**(1), pp. 161–170.
77. Reymond, P., Bohraus, Y., Perren, F., Lazeyras, F., and Stergiopoulos, N., 2011, “Validation of a Patient-Specific One-Dimensional Model of the Systemic Arterial Tree,” *Am. J. Physiol. Heart Circ. Physiol.*, **301**(3), pp. H1173-1182.
78. Olufsen, M. S., Peskin, C. S., Kim, W. Y., Pedersen, E. M., Nadim, A., and Larsen, J., 2000, “Numerical Simulation and Experimental Validation of Blood Flow in Arteries with Structured-Tree Outflow Conditions,” *Ann. Biomed. Eng.*, **28**(11), pp. 1281–1299.

79. Formaggia, L., Lamponi, D., and Quarteroni, A., 2003, "One-Dimensional Models for Blood Flow in Arteries," *J. Eng. Math.*, **47**(3–4), pp. 251–276.
80. Sherwin, S. J., Franke, V., Peiró, J., and Parker, K., 2003, "One-Dimensional Modelling of a Vascular Network in Space-Time Variables," *J. Eng. Math.*, **47**(3–4), pp. 217–250.
81. Bessems, D., Rutten, M., and Vosse, F. V. D., 2007, "A Wave Propagation Model of Blood Flow in Large Vessels Using an Approximate Velocity Profile Function," *J. Fluid Mech.*, **580**, pp. 145–168.
82. Mynard, J. P., and Nithiarasu, P., 2008, "A 1D Arterial Blood Flow Model Incorporating Ventricular Pressure, Aortic Valve and Regional Coronary Flow Using the Locally Conservative Galerkin (LCG) Method," *Commun. Numer. Methods Eng.*, **24**(5), pp. 367–417.
83. Steele, B. N., Wan, J., Ku, J. P., Hughes, T. J. R., and Taylor, C. A., 2003, "In Vivo Validation of a One-Dimensional Finite-Element Method for Predicting Blood Flow in Cardiovascular Bypass Grafts," *IEEE Trans. Biomed. Eng.*, **50**(6), pp. 649–656.
84. Alastruey, J., 2006, "Numerical Modelling of Pulse Wave Propagation in the Cardiovascular System: Development, Validation and Clinical Applications."
85. Matthys, K. S., Alastruey, J., Peiró, J., Khir, A. W., Segers, P., Verdonck, P. R., Parker, K. H., and Sherwin, S. J., 2007, "Pulse Wave Propagation in a Model Human Arterial Network: Assessment of 1-D Numerical Simulations against in Vitro Measurements," *J. Biomech.*, **40**(15), pp. 3476–3486.
86. Xiao, N., Alastruey, J., and Figueroa, C. A., 2014, "A Systematic Comparison between 1-D and 3-D Hemodynamics in Compliant Arterial Models," *Int. J. Numer. Methods Biomed. Eng.*, **30**(2), pp. 204–231.
87. Passerini, T., Luca, M. de, Formaggia, L., Quarteroni, A., and Veneziani, A., 2009, "A 3D/1D Geometrical Multiscale Model of Cerebral Vasculature," *J. Eng. Math.*, **64**(4), p. 319.
88. Formaggia, L., Quarteroni, A., and Vergara, C., 2013, "On the Physical Consistency between Three-Dimensional and One-Dimensional Models in Haemodynamics," *J. Comput. Phys.*, **244**(Supplement C), pp. 97–112.
89. Humphrey, J. D., and Taylor, C. A., 2008, "Intracranial and Abdominal Aortic Aneurysms: Similarities, Differences, and Need for a New Class of Computational Models," *Annu. Rev. Biomed. Eng.*, **10**, pp. 221–246.

90. Lillie, J. S., Liberson, A. S., Mix, D., Schwarz, K. Q., Chandra, A., Phillips, D. B., Day, S. W., and Borkholder, D. A., 2015, "Pulse Wave Velocity Prediction and Compliance Assessment in Elastic Arterial Segments," *Cardiovasc. Eng. Technol.*, **6**(1), pp. 49–58.
91. Lillie, J. S., Liberson, A. S., and Borkholder, D. A., 2016, "Quantification of Hemodynamic Pulse Wave Velocity Based on a Thick Wall Multi-Layer Model for Blood Vessels," *J. Fluid Flow Heat Mass Transf. JFFHMT*, **3**(1), pp. 54–61.
92. Liberson, A., Seyed Vahedein, Y., and Borkholder, D., 2017, "Variational Approach of Constructing Reduced Fluid-Structure Interaction Models in Bifurcated Networks."
93. Liberson, A., Seyed Vahedein, Y., and Borkholder, D., 2017, "Application of Variational Principle to Form Reduced Fluid-Structure Interaction Models in Bifurcated Networks," *J. Fluid Flow Heat Mass Transf.*, **4**, pp. 1–9.
94. Seyed Vahedein, Yashar & Karnam, Yogesh & Liberson, Alexander. (2018). Predictive Multiscale Approach (3D-1D) for Blood Flow Simulations in Cardiovascular Networks. 10.13140/RG.2.2.14993.07526/1.
95. B.V. Rathish Kumar. A space time analysis of blood flow in a 3D vessel with multiple aneurysms. *Computational Mechanics*, 32(1):16-28, 2003.
96. JRWomersley. Method for the calculation of velocity, rate of flow and viscous drag in arteries when the pressure gradient is known. *The Journal of Physiology*, 127(3):553-563, 1955.
97. A.M. Robertson, A. Sequeira, and M.V. Kameneva. Hemorheology. In G.P. Galdi, R. Rannacher, A.M. Robertson, and S. Turek, editors, *Hemodynamical Flows: Modeling, Analysis and Simulation*, pages 63-120. Birkhauser, 2008.
98. D.M. Sforza, C.M. Putman, and J.R. Cebral. Hemodynamics of cerebral aneurysms. *Annual Rev Fluid Mech*, 41:91-107, 2009.
99. Bathe, K. J., *Finite element procedures*, Prentice Hall, Englewood Cliffs, NJ, 1996.
100. Galpin PF, Broberg RB, Hutchinson BR. Three-dimensional navier stokes predictions of steady-state rotor/stator interaction with pitch change. *Proceedings of 3rd Annual Conference of the CFD Society of Canada, Banff, AB, Canada, vol. 3rd Annual Conference of the CFD, Advanced Scientific Computing Ltd: Society of Canada, Banff, Alberta, Canada, 1995.*
101. Jansen KE, Shakib F, Hughes TJR. Fast projection algorithm for unstructured meshes. *Computational Nonlinear Mechanics in Aerospace Engineering 1992*; 146:175.

102. Decorato I, Kharboutly Z, Vassallo T, Penrose J, Legallais C, Salsac AV. Numerical simulation of the fluid structure interactions in a compliant patient-specific arteriovenous fistula. *International Journal for Numerical Methods in Biomedical Engineering* 2014; 30(2):143–159.
103. Ngoepe MN, Reddy BD, Kahn D, Meyer C, Zilla P, Franz T. A numerical tool for the coupled mechanical assessment of anastomoses of PTFE arterio-venous access grafts. *Cardiovascular Engineering and Technology* 2011; 2(3):160–172.
104. Degroote J, Bruggeman P, Haelterman R, Vierendeels J. Stability of a coupling technique for partitioned solvers in FSI applications. *Computers & Structures* 2008; 86(23-24):2224–2234.
105. Jonášová, A., and Vimmr, J., 2017, “Noninvasive Assessment of Carotid Artery Stenoses by the Principle of Multiscale Modelling of Non-Newtonian Blood Flow in Patient-Specific Models,” *Appl. Math. Comput.*
106. J. Alastruey, KH Parker, J. Peiro, SM Byrd, and SJ Sherwin. Modelling the circle of Willis to assess the effects of anatomical variations and occlusions on cerebral flows. *Journal of Biomechanics*, 40(8):1794–1805, 2007.
107. L. Formaggia and A. Veneziani. Reduced and multiscale models for the human cardiovascular system. *Lecture Notes VKI Lecture Series*, 7, 2003.
108. de Moura, A. The geometrical multiscale modelling of the cardiovascular system: coupling 3D FSI and 1D models. Ph.D. Thesis, Politecnico di Milano, Milan, 136 pp, 2007.
109. Formaggia, L., A. de Moura, and F. Nobile. On the stability of the coupling of 3D and 1D fluid-structure interaction models for blood flow simulations. *ESAIM—Math. Model. Numer. Anal. (Modelisation Mathematique Et Analyse Numerique)* 41:743–769, 2007.
110. J.G. Heywood, R. Rannacher, and S. Turek. Artificial boundaries and flux and pressure conditions for the incompressible Navier-Stokes equations. *International Journal for Numerical Methods in Fluids*, 22(5):325–352, 1996.
111. Nobile, F. Coupling strategies for the numerical simulation of blood flow in deformable arteries by 3D and 1D models. *Math. Comput. Model.* 49:2152–2160, 2009.
112. Decorato, Z Kharboutly, T Vassallo, J Penrose, C Legallais, and AV Salsac. Numerical simulation of the fluid structure interactions in a compliant patient-specific arteriovenous

fistula. *International Journal for Numerical Methods in Biomedical Engineering*, 30(2):143-159, 2014.

113. Mix et al. - 2017 - Detecting Regional Stiffness Changes in Aortic Aneurysmal Geometries Using Pressure-Normalized Strain.

